

**THE ROLE OF THE ARYL HYDROCARBON RECEPTOR IN 2,3,7,8-  
TETRACHLORODIBENZO-*p*-DIOXIN-INDUCED MITOCHONDRIAL DYSFUNCTION  
IN MOUSE HEPATOMA CELLS**

**By**

**Hye Jin Hwang**

**A DISSERTATION**

**Submitted to  
Michigan State University  
in partial fulfillment of the requirements  
for the degree of**

**Biochemistry and Molecular Biology - Doctor of Philosophy**

**2015**

## **ABSTRACT**

### **THE ROLE OF THE ARYL HYDROCARBON RECEPTOR IN 2,3,7,8-TETRACHLORODIBENZO-p-DIOXIN-INDUCED MITOCHONDRIAL DYSFUNCTION IN MOUSE HEPATOMA CELLS**

**By**

**Hye Jin Hwang**

The aryl hydrocarbon receptor (AHR) is a Per-Arnt-Sim (PAS) domain family protein and ligand-activated transcription factor. The AHR directly regulates the expression of a large number of genes, including many that encode Phase I and Phase II drug metabolizing enzymes. Environmental contaminants such as polycyclic aromatic hydrocarbon or halogenated aryl hydrocarbon act as AHR ligands. The most potent AHR ligand, 2,3,7,8-tetrachlorodibenzo-p-dioxin (TCDD), causes various deleterious physiological effects, such as tumor promotion, chloracne, wasting syndrome, and hepatic steatosis. Over the last several decades, the AHR has been the focus of extensive research. Even with this depth of inquiry, there is a lack of understanding to the mechanism of action for AHR-mediated toxicity. Several possibilities have been proposed. For example, since the AHR is a transcription factor, it has been proposed that one, or more, of the genes that is regulated by the AHR leads to toxicity. The cytochrome P450 monooxygenases (CYPs) and TCDD-inducible poly (ADP-ribose) polymerase (TiPARP) are primary targets of AHR-regulated expression and are capable of promoting oxidative stress. In addition, the AHR can participate in crosstalk with other signaling pathways related to proliferation, development, differentiation, immune suppression, lipid metabolism and apoptosis. Several of these pathways are also involved in mediating the cellular response to oxidative stress. Given that oxidative stress is central to multiple pathways involved in AHR-mediated TCDD-induced toxicity and that the mitochondria, which consume most of cellular oxygen, are the main site generating oxidative stress, the role of the mitochondria in AHR signaling and toxicity was explored.

Using the protease protection assay with digitonin extraction, the AHR was localized to

the inter-membrane space (IMS) of the mitochondria. TCDD exposure induced a degradation of mitochondrial AHR similar to that of cytosolic AHR. Using siRNA in mouse hepatoma hepa1c1c7 cells, TOM20 and AHR-interacting protein (AIP) knockdown revealed that these two proteins are involved in the import of AHR into the mitochondria. The inhibition of heat shock protein-90kDa (HSP90) activity using an ATPase inhibitor, geldanamycin, also suggested that activity of HSP90 decided the level of mitochondrial AHR. TCDD altered the metabolic rate of cells in an AHR-dependent manner as measured by oxygen consumption rate (OCR) using the XF24 Extracellular Flux Analyzer. 30 nM TCDD exposure in hepa1c1c7 cells caused a significant AHR-dependent decrease in the OCR, but no change in the respiratory control ratio and the enzyme activities in ETC and ATP synthase. On the other hand, 30 nM TCDD exposure in AHR-deficient hepac12 cells caused no significant changes but the increased the respiratory control ratio and the activity of complex I. The mitochondria proteome was investigated using stable isotope labeling by amino acids in cell culture (SILAC). SILAC identified a battery of proteins that were influenced by TCDD in an AHR-dependent manner. The proteomic data suggested TCDD-induced AHR-mediated regulation in heme metabolism, lipid metabolism, redox potential, and mitochondrial biogenesis.

Collectively, the data suggest the model 1) mitochondrial AHR in the IMS binds to components in the inner-membrane (IM), 2) TCDD induces the loss of interaction of AHR between a component in the IM, possibly causing an alteration in respiratory machinery, 3) AHR might help maintain homeostasis in respiratory efficiency against TCDD via regulating complex I or complex IV activity, and 4) AHR regulates the expression of genes that encode proteins that are important for various mitochondrial metabolic pathway and this regulation can be a result of mitochondrial retrograde signaling. This model supports a role for the mitochondria and possibly mitochondrial localized AHR in TCDD-induced toxicity, including metabolic dysfunction, wasting syndrome and hepatic steatosis.

## ACKNOWLEDGEMENTS

The graduate school life in the MSU brought me wonderful memories within my life. Those couldn't have been made without people whom I have had known, and I would never have achieved a PhD without them.

First, I would like to thank Dr. John LaPres, my PI, for his consistent support, encouragement, and patience. He is a good model of scientist. He has taught me how and what a scientist must think and consider. He was always accessible and provided valuable advice. His guidance made me get through tough challenges from experiments and endless learning.

Next, I would like to thank my committee members, for their precious time and supportive advice, Drs. Shelagh Ferguson-Miller, Kathy Gallo, Bill Henry, and Jeff MacKeigan. In every committee meeting, I got valuable guidance and insightful comments. I would especially like to thank Dr. Ferguson-Miller for providing a wealth of knowledge and collaboration regarding mitochondria and experimental techniques.

Also, I had luck to work with wonderful people, the members of LaPres lab. I thank Drs. Scott Lynn, Dorothy Tappenden, and Ajith Vengellur for being exceptional colleagues, scientific mentors, and friends. I also thank Dr. Steve Proper for help and friendship. Finally, I want to thank the current members, Peter Dornbos and Michelle Steidemann, and the past graduate rotation students and undergraduate students, Taylor, Sarah, Mike, Larissa, Kai, for their huge efforts and help in the project.

I would like to thank the Biochemistry & Molecular Biology program, and RTSF facility for their assistance. In addition, I also want to thank Dr. Laurie Kaguni for giving me the opportunity to attend the mitochondria summer schools.

Lastly, I would like to thank my family for their love, supports and being there. Without you, I could not have done all of mine here. I love you and thank you.

## TABLE OF CONTENTS

LIST OF TABLES .....	vii
LIST OF FIGURES .....	viii
KEY TO SYMBOLS AND ABBREVIATIONS.....	x
CHAPTER 1. LITERATURE REVIEW .....	1
PER-ARNT-SIM (PAS) DOMAIN PROTEINS.....	2
ARYL HYDROCARBON RECEPTOR .....	3
Domains of AHR .....	4
Transactivation of AHR.....	8
Deactivation of AHR.....	9
AHR Chaperones.....	10
Ligands of AHR.....	11
Endogenous ligands .....	11
Xenobiotics .....	14
AHR Target Genes .....	17
Physiological Roles of AHR .....	20
MITOCHONDRIA.....	23
Structure of Mitochondria.....	23
Mitochondrial DNA (mtDNA).....	24
Synthesis of Mitochondrial Proteins.....	25
Synthesis of mitochondrial gene encoded proteins .....	25
Synthesis of nuclear gene encoded mitochondrial proteins.....	26
Nuclear-encoded Mitochondrial Protein Translocation .....	26
Nuclear Transcription Factors for Mitochondrial Biogenesis.....	28
Mitochondrial Respiration and Reactive Oxygen Species .....	29
TCA Cycle.....	33
Fatty Acid $\beta$ -oxidation and Ketogenesis .....	36
TCDD-INDUCED TOXICITIES AND METABOLIC DYSFUNCTION.....	37
CHAPTER 2. HYPOTHESIS AND SPECIFIC AIMS .....	43
HYPOTHESIS.....	44
SPECIFIC AIMS.....	45
CHAPTER 3. MATERIALS AND METHODS.....	46
CELL CULTURE.....	47
PREPERATION OF INTRACELLULAR FRACTIONS.....	47
TRYPSIN TREATMENT OF DIGITONIN EXTRACTED MITOCHONDRIA.....	48
siRNA KNOCKDOWN OF AIP OR TOM20 .....	48
HSP90 INHIBITION BY GELDANAMYCIN.....	49
WESTERN BLOTTING.....	49
OXYGEN CONSUMPTION RATE (OCR) MEASUREMENT.....	50

STATISTICAL ANALYSIS.....	51
ENZYMATIC ASSAY OF OXPHOS SYSTEM.....	51
Citrate Synthase Assay.....	52
Complex I Assay.....	52
Complex II assay.....	52
Complex II+III assay.....	53
Complex III assay.....	53
Complex IV Assay.....	53
Complex V Assay.....	54
STABLE ISOTOPIC LABELING BY AMINO ACIDS IN CELL CULTURE (SILAC) AND QUANTITATIVE PROTEOMIC ANALYSIS.....	54
Preparation of Mitochondrial Proteins.....	54
Mass Spectrometry (MS).....	55
Data Analysis.....	55
PROTEIN CONCENTRATION DETERMINATION.....	56
CHAPTER 4. RESULTS.....	58
CHARACTERIZATION OF MITOCHONDRIAL AHR IMPORT.....	59
Identification of a Mitochondrial Compartment of AHR Location.....	59
Prediction of MTS of AHR.....	62
Change in AHR Expression by AIP Knockdown.....	62
Change in AHR Expression by HSP90 Activity Inhibition.....	69
Change in AHR Expression by TOM20 Knockdown.....	69
AHR-MEDIATED TCDD-INDUCED MITOCHONDRIAL DYSFUNCTION.....	70
Cellular Respiration in Mouse Hepatoma Cells under TCDD Exposure.....	70
Change of OXPHOS Activity in Mouse Hepa Cells upon TCDD Exposure.....	75
Identification of Proteins Differently Expressed upon TCDD Exposure.....	75
Validation of Proteomic Results.....	76
CHAPTER 5. DISCUSSION.....	82
CHARACTERIZATION OF MITOCHONDRIAL AHR IMPORT.....	83
AHR-MEDIATED TCDD-INDUCED MITOCHONDRIAL DYSFUNCTION.....	89
CHAPTER 6. CONCLUSIONS AND FUTURE STUDIES.....	99
MITOCHONDRIAL AHR IN THE IMS.....	102
THE ROLE OF THE AHR IN MITOCHODNRIAL METABOLISM AND ITS ROLE IN TCDD- INDUCED TOXICITY.....	103
APPENDICES.....	105
APPENDIX A. SUPPLEMENTAL TABLES.....	106
APPENDIX B. HYPOXIA INDUCIBLE FACTORS (HIFs) MODULATE MITOCHONDRIAL OXYGEN CONSUMPTION AND TRANSCRIPTIONAL REGULATION OF NUCLEAR- ENCODED ELECTRON TRANSPORT CHAIN GENES.....	115
REFERENCES.....	146

## LIST OF TABLES

Table 4-1. The equations for mitochondrial stress parameters by XF mito stress test reporter generator. ....	71
Table 4-2. Identified proteins differentially regulated by 10 nM TCDD exposure for 72 h in an AHR-dependent manner. ....	78
Table 4-3. Relationship between MS quantification and Western blot quantification. ....	79
Table A-1. Identified mitochondrial proteins differentially regulated by 10 nM TCDD exposure for 72 h in an AHR-dependent manner. ....	106
Table A-2. Identified nonmitochondrial proteins differentially regulated by 10 nM TCDD exposure for 72 h in an AHR-dependent manner. ....	111
Table B-1. Primer pairs. ....	134
Table B-2. CcO enzyme activity. ....	138

## LIST OF FIGURES

Figure 1-1. Schematic of ligand-activated AHR transcription. ....	6
Figure 1-2. Schematic of ligand-activated AHR transcription. ....	7
Figure 1-3. Endogenous ligands of AHR. ....	13
Figure 1-4. Xenobiotics of AHR. ....	16
Figure 1-5. Schematic of Electron transport chain complexes and ATP synthase. ....	32
Figure 1-6. TCA cycle. ....	34
Figure 3. Experimental design for SILAC-based proteomic analysis of TCDD-induced changes to the mitochondrial proteome in mouse hepatoma cell. ....	57
Figure 4-1. Mitochondrial sub-compartment analysis. ....	60
Figure 4-2. The effects of ligand exposure on protease accessibility to digitonin extracted mitochondria. ....	61
Figure 4-3. The effect of AIP knockdown on the levels of the AHR in cellular fractions of hepa1c1c7 cells. ....	63
Figure 4-4. The effect of geldanamycin (GA)-induced HSP90 inhibition on the level of AHR protein within cellular fraction of hepa1c1c7. ....	65
Figure 4-5. The effect of TOM20 knockdown on the level of AHR protein in cellular fractions of hepa1c1c7 cells. ....	67
Figure 4-6. Measurement of oxygen consumption rate (OCR) from hepa1c1c7 cells. ....	72
Figure 4-7. Measurement of oxygen consumption rate (OCR) from hepac12 cells. ....	73
Figure 4-8. Activities of ETC complexes and ATP synthase. ....	74
Figure 4-9. SILAC analysis of differentially expressed proteins by TCDD. ....	77
Figure 4-10. Western blot analysis of differentially expressed proteins identified by SILAC in hepatoma 1c1c7 and c12 cells. ....	80

Figure 5-1. Suggested role of mitochondrial AHR. ....	88
Figure 5-2. AHR-mediated TCDD-induced regulation of protein expression in metabolic pathways.....	98
Figure 6. Summary of AHR-mediated TCDD-induced mitochondrial dysfunction. ....	101
Figure B-1. Genotype and protein comparisons of <i>Hif1α</i> WT and null cells. ....	139
Figure B-2. Measurement of oxygen consumption rate (OCR) from <i>Hif1α</i> WT and null cells. .	140
Figure B-3A. Dendrograms.....	141
Figure B-3B. Dendrograms.....	142
Figure B-4. Gene expression of control and select mitochondrial genes. ....	143
Figure B-5. Comparative amino acid sequences for COX7A1 and COX7A2 isoforms and a 3D representation of the COX monodimer. ....	145

## KEY TO SYMBOLS AND ABBREVIATIONS

ACOT2	acyl-CoA thioesterase 2
AHR	aryl hydrocarbon receptor
AIP	AHR-interacting protein
AHRR	AHR repressor
ARE	antioxidant response elements
ARNT	aryl hydrocarbon receptor nuclear translocator
ATP	adenosine triphosphate
BaP	benzo[a]pyrene
bHLH	basic helix-loop-helix
BSA	bovine serum albumin
CcO	cytochrome c oxidase
CO <sub>2</sub>	carbon dioxide
COX-2	cyclooxygenase-2
COX4	cytochrome c oxidase subunit 4
CoQ <sub>1</sub>	coenzyme Q <sub>1</sub>
CPOX	coproporphyrinogen-III oxidase
CYB5	cytochrome b5
CYP	cytochrome P450-dependent monooxygenase
cAMP	cyclic AMP
CCCP	carbonyl cyanide <i>m</i> -chlorophenyl hydrazone
DCPIP	2,6-Dichlorophenol Indophenol
DMEM	Dulbecco's modified Eagle's Medium
DMSO	dimethyl sulfoxide

DRE	dioxin-responsive element
DTNB	5,5'-dithiobis-(2-nitrobenzoic acid)
$\epsilon$	extinction coefficient
EDTA	ethylenediaminetetraacetic acid
EGTA	ethylene glycol tetraacetic acid
ENTPD2	ectonucleoside triphosphate diphosphohydrolase 2
ER	endoplasmic reticulum
ETC	electron transport chain
FAD	flavin adenine dinucleotide
FCCP	carbonyl cyanide-4-(trifluoromethoxy)phenylhydrazone
FDR	false discovery rate
FICZ	6-formylindolo(3,2-b)carbazole
GABP	nuclear respiratory factor 2
GST	glutathione S-transferase
H6PD	hexose-6-Phosphate Dehydrogenase
HAH	halogenated aromatic hydrocarbon
HEPES	2-[4-(2-hydroxyethyl)piperazin-1-yl] ethanesulfonic acid
HSP90	heat shock protein of 90 kDa
HDAC	histone deacetylase
HIF	hypoxia-inducible factor
HRE	hypoxia response element
HTP qPCR	high-throughput quantitative real-time polymerase chain reaction
IL	interleukin
IM	inner-membrane
IMS	inter-membrane space
KCl	potassium chloride

KCN	potassium cyanide
KPO <sub>4</sub>	potassium phosphate
MAPK	mitogen-activated protein kinase
MEF	mouse embryonic fibroblast
MgCl <sub>2</sub>	magnesium chloride
MPTP	mitochondrial permeability transition pore
MS	mass spectrometry
MTS	mitochondrial targeting signal
MRP	mitochondrial ribosomal protein
NaCl	sodium chloride
NAD	nicotinamide adenine dinucleotide
NES	nuclear export signal
NLS	nuclear localization signal
NRF1	nuclear respiratory factor 1
NRF2	NF-E2 p45-related factor 2
NQO1	NAD(P)H:quinone oxidoreductase 1
OCR	oxygen consumption rate
OM	outer-membrane
OXPHOS	oxidative phosphorylation
PAH	polycyclic aromatic hydrocarbon
PAS	Per-Arnt-Sim
PBS	phosphate buffered saline
PCB	polychlorinated biphenyl
PCB126	3,3',4,4',5-pentachlorobiphenyl
PDH	pyruvate dehydrogenase complex
PDK	pyruvate dehydrogenase kinase

PEPCK	phosphoenolpyruvate carboxykinase
PGC-1 $\alpha$	peroxisome proliferator-activated receptor- $\gamma$ coactivator-1 $\alpha$
PHD	prolyl hydroxylase domain-containing proteins
PMSF	phenylmethanesulfonyl fluoride
POLRMT	bacteriophage-related mtRNA polymerase
PPAR	peroxisome proliferator-activated receptor
QPCR	quantitative real-time polymerase chain reaction
ROS	reactive oxygen species
Scd1	stearoyl-CoA desaturase 1
SDS-PAGE	sodium dodecyl sulfate-polyacrylamide gel electrophoresis
SILAC	stable isotope labeling by amino acids in cell culture
SOD	superoxide dismutase
SULT	sulfotransferase
TAD	transcriptional activation domain
TCA	tricarboxylic acid
TCDD	2,3,7,8-tetrachlorodibenzo-p-dioxin
TIM	translocase of the inner membrane
TiPARP	TCDD-inducible poly (ADP-ribose) polymerase
TGF- $\beta$	transforming growth factor- $\beta$
TNF- $\alpha$	tumor necrosis factor- $\alpha$
TOM	translocase of the outer membrane
UGT	UDP-glucuronosyl transferase
VDAC	voltage-dependent anion channel
WT	wild-type
XAP2	hepatitis B viral X-protein interacting protein

## **CHAPTER 1. LITERATURE REVIEW**

## **PER-ARNT-SIM (PAS) DOMAIN PROTEINS**

Adaptation to environmental changes is important to maintain homeostasis of a living system. The Per-Arnt-Sim (PAS) domain family proteins are environmental sensors, which regulate physiological adaptive responses against stimuli such as xenobiotics, hypoxia, and light/dark cycles.<sup>1, 2</sup> The PAS domain proteins use different mechanisms to sense these stimuli and interact with partner proteins in order to regulate transcription. This transcriptional regulation is primarily geared towards coping with changing environment. For instance, in response to environmental toxicants, the aryl hydrocarbon receptor (AHR) regulates xenobiotic metabolic enzymes. Hypoxia, a state of decrease in available oxygen, which contributes to a development of physiological or pathological conditions such as angiogenesis, embryonic development and tumors, induces the hypoxia-inducible factors (HIFs) signaling pathway. Also, change in light cycling stimulates a circadian clock signal transduction, which is distributed throughout a whole organism, via activation of transcription factors such as CLOCK and BMAL1 and their repressors PER and CRYs.

The name, PAS, comes from three proteins, the clock gene period (Per), aryl hydrocarbon receptor nuclear translocator (Arnt), and single-minded (Sim). PAS domain proteins share three distinguished structural domains, PAS domain, basic helix-loop-helix (bHLH) domain, and transactivation domain (TAD). PAS domains consist of two subdomains, PAS-A and PAS-B and their role is interacting between partner proteins. The protein:protein interaction of PAS-A domain is homotypic while that of PAS-B is heterotypic. The bHLH resides in the N-terminal to the PAS domain. The bHLH domain interacts with partner proteins as well as a DNA target sequence. The N-terminal region of the PAS family proteins, containing bHLH and PAS domains, has highly conserved sequences through evolution. In contrast, the C-terminal region of the PAS proteins containing TAD has little sequence homology. As a

transcription factor, the PAS family protein recruits and binds transcription coactivators through TAD.

The most well-studied PAS family protein signaling pathways in higher eukaryotes also share common features in regulation mechanisms of those. Hypoxia and xenobiotic signaling have cytoplasmic regulation in the absence of stimuli. The levels of the HIF $\alpha$  isoforms are regulated by post-translational modification under normoxic state, and the AHR resides as a complex with chaperones in cytoplasm without ligand activation. The CLOCK and BMAL1 are translocated in nucleus constitutively, but nuclear translocation of their repressors is regulated by cytoplasmic proteasomal degradation. On the other hand, the response mechanisms mediated by these PAS family proteins are also required for developing organisms. Many studies indicate that AHR signaling pathways trigger physiological processes involved in proliferation, differentiation, inflammation, and endocrine disrupt. HIF signaling pathways also contribute to angiogenesis, proliferation, development and metabolic switches. Finally, circadian clock signaling pathways control not only sleeping time but also physiological rhythm such as temperature control, blood pressure, heart rate, and metabolic control through a whole body.

### **ARYL HYDROCARBON RECEPTOR**

Many industrial processes produce different kinds of persistent organic pollutants that accumulate in the environment.<sup>3, 4</sup> These pollutants can be biologically amplified as they are passed up the food chain. Among these, polycyclic aromatic hydrocarbons (PAHs) and halogenated aromatic hydrocarbons (HAHs) are present in many different areas of the United States and in many different kinds of animals. The hydrophobic nature of these makes them stored in fat tissues and readily bioaccumulated. Mammals exposed to PAHs or HAHs show pathological effects, such as endocrine disruption, aberrant neuronal development, hepatic

steatosis, immunosuppression, and tumor promotion. The environmental pollutant-induced toxicity is primarily mediated by the AHR, one of the PAS domain family members. The AHR is a ligand-activated transcription factor that mediates the toxic response to several prominent environmental pollutants, including halogenated biphenols, benzopyrenes and dioxins, such as 2,3,7,8-tetrachlorodibenzo-p-dioxin (TCDD). About 40 years have passed since Dr. Poland identified the AHR that has a high affinity of binding for TCDD.<sup>5</sup> Since then, many researchers have investigated properties of the AHR as a transcription factor. Previous studies provided evidence that AHR-mediated gene induction requires TCDD-AHR:ARNT complexes in the nucleus.<sup>6, 7</sup> The ligand-activated nuclear AHR heterodimerizes with the ARNT and forms a functional transcription factor. The AHR:ARNT heterodimer binds a specific nucleotide sequence in regulatory regions of DNA and the core sequence is now called as dioxin-responsive element (DRE) or xenobiotic-responsive element (XRE).<sup>8, 9</sup> Additional interacting partners of the AHR have also been identified, such as the heat shock protein of 90 kDa (HSP90) and the immunophilin-like protein, AHR-interacting protein (AIP, also known as ARA, or XAP2).<sup>10-12</sup> Since these initial characterizations, researches have revealed biochemical properties of the AHR, endogenous AHR-mediated physiological effects, as well as AHR-mediated environmental toxicity, upon exposure to ligands, such as TCDD.<sup>1, 13</sup>

### ***Domains of AHR***

The domain structure of mouse AHR protein (mAHR) has been described in many review articles (Figure 1-1).<sup>1, 14-16</sup> The N-terminus contains a nuclear localization signal (NLS), which has positively charged amino acids, and a basic helix-loop-helix (bHLH), which has two amphipathic  $\alpha$ -helices with conserved amino acids.<sup>2, 14</sup> The bHLH domain is the site for DNA binding, ARNT dimerization, and HSP90 binding.<sup>14</sup> Helix2 of the bHLH domain also has the leucine-rich nuclear export signal (NES) similar to other proteins.<sup>17</sup> The PAS domain is in the

central portion of the protein and is comprised of approximately 250 amino acids and contains two subdomains, PAS-A and PAS-B domains.<sup>2, 14</sup> The PAS-A domain is essential for AHR:ARNT interaction stability and PAS-B for ligand binding, and interaction with HSP90 and AIP.<sup>14</sup> In the absence of ligand, the AHR is found in the cytosol bound to AIP and a dimer of HSP90 (Figure 1-2). This complex stabilizes the AHR and enhances its ligand binding affinity.<sup>14</sup> In the presence of ligand, HSP90 is dissociated from PAS-B domain of the AHR in an ARNT-dependent manner and via structural coordination with PAS-A domain.<sup>18</sup> Subsequent change in bHLH structure also enhances stability of AHR:ARNT dimer and recognition of target DNA sequence.<sup>18</sup>

The C-terminus of the AHR has the glutamine-rich transcriptional activation domain (TAD).<sup>14, 19, 20</sup> Ligand binding to the AHR induces conformational changes in the TAD, which involves nuclear translocation of the AHR and maintaining AIP binding to a ligand-bound AHR complex.<sup>20-22</sup> For example, in the absence of ligand, human AHR (hAHR) localizes in the cytoplasm regardless of AIP expression level whereas mouse AHR (mAHR), which mainly localizes in nucleus in the absence of ligand, relocalizes to cytoplasm by AIP over-expression.<sup>20</sup> In the presence of ligand, mAHR-HSP90 complex unbound to AIP is translocated to the nucleus while hAHR-HSP90-AIP complex is translocated to the nucleus. Although molecular mechanisms of ligand-activated AHR conformational change to form AHR:ARNT dimer and association/dissociation of cytosolic chaperones have been revealed through *in vitro* studies, the molecular mechanisms of nuclear translocation of the AHR is obscure.<sup>10, 18</sup>

While the N-terminal sequences of the AHR are highly conserved among vertebrates, the C-terminal sequences of the protein are less conserved.<sup>20</sup> The studies on TCDD-toxicity in different species suggest that protein sequence variation within the C-terminal TAD of the AHR is a cause of different biochemical properties of the receptor, such as differences in the tertiary structure of the TAD in each species, affecting N-terminal structure for protein binding or

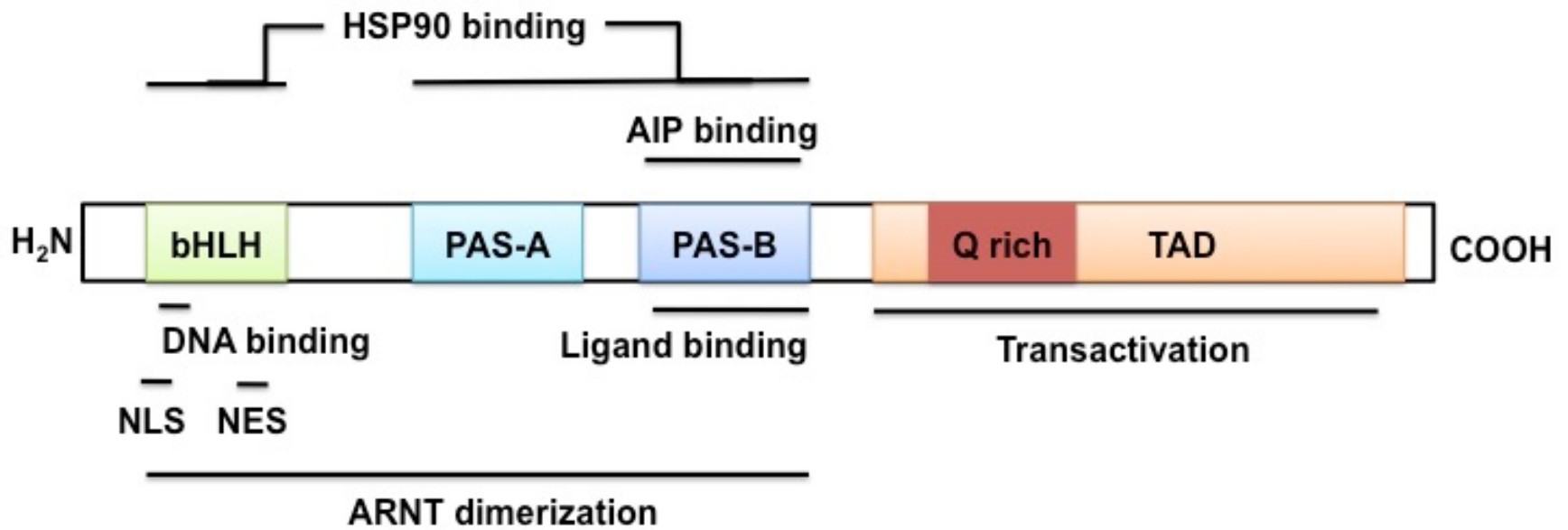


**Figure 1-1. Schematic of ligand-activated AHR transcription.**

Ligand and protein binding sites and specific target sequences are indicated as bars. bHLH: basic helix-loop-helix domain, PAS: Per-Arnt-Sim domain, TAD: transactivation domain, NLS: nuclear localization sequence, NES: nuclear export sequence.

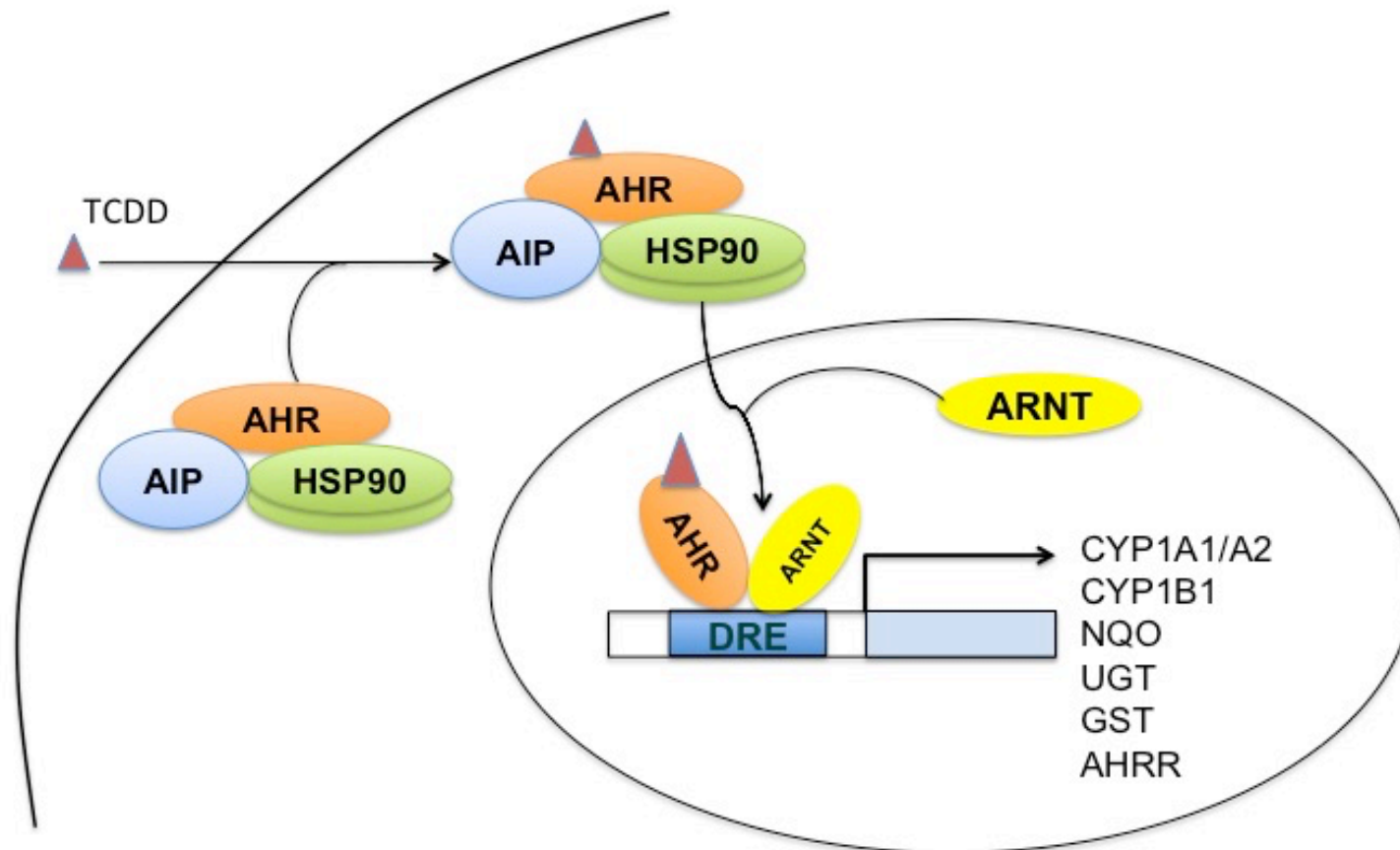


**Figure 1-2. Schematic of ligand-activated AHR transcription.**

Cytosolic AHR forms a complex with HSP90 and AIP. Ligand binding to AHR induces translocation of AHR into the nucleus, dissociation of AHR from chaperones, and heterodimerization of AHR with ARNT. The AHR:ARNT dimer binds to DRE of target genes and recruits transcriptional co-activators and general transcriptional machinery to initiate gene transcription.

NLS/NES exposure by ligand activation.<sup>20, 23</sup> Thus, diverse sequences of the TAD can be reflected in different sensitivity to TCDD-induced toxicity.<sup>23</sup>

### ***Transactivation of AHR***

Activation of the AHR depends on ligand-structure, tissue/cell specific contexts, and tissue/cell specific expression of nuclear cofactors.<sup>24</sup> The interaction of the ligand-bound AHR:ARNT dimer with a DRE, having a core sequence of 5'-T/GNGCGTG-3', accompanies chromatin remodeling complex, SWI/SNF, histone modifiers such as SRC-1, CARM-1, BRG-1, and HAT, and transcriptional coactivators, NCOA1-3 and p300/CBP, to target gene promoters.<sup>13, 14, 25, 26</sup> AHR:ARNT dimers also interact with general transcription factors, TATA-binding protein, TFIIB and TFIIF, which are required for RNA polymerase II reaction.<sup>19, 25</sup>

Comparison study with several AHR ligands suggests that structurally diverse chemicals are selective AHR modulators, inducing different surface topology of ligand-activated AHR complex.<sup>27, 28</sup> This selective receptor modulation may result in recruitments of different types of coactivators or repressors to DREs in a gene-, cell-, tissue-specific manner.<sup>27</sup> Also, different AHR structures between species can cause differential TCDD toxicity.<sup>29</sup> Analysis of multiple sequence alignment of AHRs in mammals reveals that ligand binding domain and TAD domain impact AHR function.<sup>29, 30</sup> For example, amino acid substitutions in the ligand binding domain of the AHR decreased the TCDD sensitivity in the DBA/2 mouse strain compared to C57BL/6 via steric effect.<sup>4</sup> As mentioned in the previous section, the low conservation in glutamine-rich portion of TAD of the AHR also impacts the median lethal doses of TCDD, leading to a decrease in sensitivity in the Han/Wistar (*Kuopio*) rat strain, which has alternative splicing in the TAD domain.<sup>4, 29</sup>

### ***Deactivation of AHR***

Because the AHR is a stress-responsive nuclear transcription factor, enhancing gene expression related to detoxification and physiology, the level of the AHR and AHR signaling pathway must be regulated. Post-translational modification is the primary mechanism to regulate intracellular AHR level and AHR transactivation. Upon export from the nucleus, the AHR is ubiquitinated and subsequently degraded in a proteasome-dependent manner.<sup>17, 31</sup> The C-terminal TAD of the AHR is essential for ubiquitination as a degron (i.e., specific structural element for degradation) and the DNA binding domain also contributes to AHR degradation in concert with heterodimer formation with ARNT.<sup>31</sup> Sumoylation on two lysine residues in the bHLH and TAD inhibits ubiquitination of AHR and consequently stabilizes AHR, but also represses transactivation of the receptor.<sup>32</sup> Phosphorylation is important for AHR binding to the DRE and transcription. Phosphorylation on two serine residues of NLS abolishes ligand-induced AHR import to nucleus. The AHR, when dephosphorylated in the NLS, can be transported into nucleus by importin.<sup>33</sup> However, dephosphorylation on both serine residues inhibits AHR binding to DRE. Phosphorylation on one serine residue of the NLS in the nucleus promotes accumulation of the AHR:ARNT dimer and transactivation.<sup>33</sup>

Negative feedback by AHR targets is another way to regulate AHR transactivation. The AHR repressor (AHRR) is an AHR target gene and a member of the bHLH/PAS family. AHRR is similar to the AHR at the amino acid sequence level, having N-terminal bHLH and PAS-A domain and a diverse C-terminal domain but is lacking a ligand-binding domain.<sup>34</sup> This suggests a model where AHRR might compete with the AHR to form a heterodimer with ARNT and AHRR:ARNT might bind to DRE through N-terminal region for feedback inhibition of AHR transactivation.<sup>35</sup> However, genetic modification of AHRR, AHR or ARNT in mammalian cells suggests a new model where AHRR:AHR interaction may be more important for repression of AHR.<sup>36, 37</sup>

TCDD-inducible poly (ADP-ribose) polymerase (TiPARP), a member of PARP family, is another AHR target gene.<sup>38</sup> Recent studies suggested a model where TiPARP acted as a negative feedback regulator of the AHR.<sup>36, 38</sup> In this model, TiPARP localized to the nucleus in order to bind to AHR target genes or the AHR itself. TiPARP promoted the ribosylations of the AHR or other unidentified factors involved AHR transactivation to repress AHR target gene transcription and induced the proteolysis of the receptor.<sup>38</sup>

G-protein signaling also regulates AHR transactivation. Activated  $G\alpha_{13}$  protein interacted with AIP and inhibited AHR:AIP interaction, resulting in AHR destabilization and loss of AHR transactivation.<sup>39</sup> Phosphodiesterase type 2A, which hydrolyzes cyclic AMP (cAMP), was found to bind to AIP to inhibit nuclear localization of the AHR induced by cAMP, as well as TCDD.<sup>40</sup> cAMP, a signaling molecule participating in many physiological responses, induced nuclear translocation of the AHR but this nuclear receptor did not form a heterodimer with ARNT.<sup>41</sup> cAMP also interfered with TCDD-induced gene expression in mouse hepa1 cells.<sup>41</sup> Considering the above studies, G-protein, phosphodiesterase type 2A and cAMP act as negative regulators of AHR target gene expression.<sup>40-42</sup>

### ***AHR Chaperones***

The HSP90 is an abundant cellular molecular chaperone and a co-chaperone of the AHR cytosolic complex. Many studies have demonstrated that HSP90 is required for the proper function of many different protein.<sup>21, 43-46</sup> The ATPase activity of HSP90 is essential for the interaction between the AHR ligand binding domain and the C terminus of AIP. The C-terminus of HSP90 binds to the TPR domains of AIP and the middle domain of HSP90 binds to the bHLH and PAS domains of AHR.<sup>21, 43</sup> Post-translational modification of the interacting proteins with AHR also affects receptor signaling. For instance, inhibition of histone deacetylase, HDAC6,

acting on HSP90, suppressed AHR transactivation and *Hdac6* null mice were resistant to PAH carcinogenic activation.<sup>47, 48</sup>

The AIP is a co-chaperone of nuclear receptors and viral proteins.<sup>49</sup> Seto's group identified hepatitis B viral X-protein interacting protein (XAP2), which interferes with X-protein transcriptional activation.<sup>50</sup> XAP2 was later characterized as a component of the AHR complex, AIP.<sup>51</sup> The AIP has an N-terminus that shares protein sequence similarity to FK506-binding proteins and a C-terminus that contains three tetratricopeptide repeat (TPR) domains. The AIP plays physiological roles in embryonic development and AHR stabilization.<sup>11, 12</sup> In fact, proteins that interact with the AIP are distributed in diverse biological processes, including nuclear hormone receptors, phosphodiesterases, transmembrane receptors, G proteins, hepatitis B viral X protein, and mitochondrial protein translocators.<sup>49</sup> The AIP has an evolutionarily conserved peptide sequence across species and this leads to a hypothesis that AIP may be essential for mammalian physiological function or associated with human diseases.<sup>49, 52</sup>

As mentioned in the previous section, a ligand-bound mAHR complex in the nucleus does not have the AIP. However, mouse AIP may be essential for binding of AHR to DRE within some AHR target genes. The gene expression of cytochrome P450 1b1 (*Cyp1b1*) and *Ahrr* were decreased under TCDD exposure in hepatic *Aip* null mice though the gene expression of other AHR targets, *Cyp1a1* and *Cyp1a2*, were not affected.<sup>53</sup> Hepatic *Aip* null mice also showed no TCDD-induced pathological changes, supporting the hypothesis that the AIP has an important role in TCDD-induced hepatotoxicity.<sup>53</sup>

## ***Ligands of AHR***

### **Endogenous ligands**

The AHR is known to be expressed in various mammalian tissues and to have a critical role in vasculature, embryonic development, liver development, and immune system.<sup>54</sup>

Phylogenetic analysis of the AHR sequences in vertebrates showed that N-terminal domains are highly conserved, suggesting that the AHR is an ancient protein evolved in structural diversity.<sup>13</sup> Orthologs of AHR in invertebrates are preserved and have physiological functions related to development and differentiations, but those do not bind to dioxin.<sup>13, 55</sup> Additionally, xenobiotic-independent AHR activation has been reported.<sup>56, 57</sup> These findings support a hypothesis of the existence of endogenous ligands for AHR (Figure 1-3). Naturally synthesized ligands from plants and mammals have been studied as putative endogenous agonists or antagonists for the AHR; however, a definitive endogenous ligand for AHR has still not been identified.<sup>13, 58</sup>

The strongest case for an endogenous ligand can be made for several tryptophan metabolites. These metabolites have varying functions in different cell types and tissues. For example, tryptamine is an AHR agonist in human colorectal adenocarcinoma CaCo2 cells but an AHR antagonist in young adult mouse colonic (YAMC) cells.<sup>28</sup> Also, tryptamine derivatives are selective AHR modulators. For instance, indole-3-acetate is an AHR agonist and indole-3-aldehyde is an AHR antagonist in YAMC cells.<sup>28</sup> In terms of putative endogenous AHR ligands, the most well-studied tryptophan metabolites are 6-formylindolo(3,2-b)carbazole (FICZ) and kynurenine. FICZ, a tryptophan photoproduct, is a potent AHR agonist having an EC<sub>50</sub> in the picomolar range in rat hepatoma cells, but FICZ-induced CYP1A1 quickly converts FICZ to a substrate of sulfotransferase.<sup>13</sup> FICZ also activates mitogen-activated protein kinase (MAPK) that mediates induction of cyclooxygenase-2 (COX-2) and both CYP1A1 and COX-2 contribute to development of skin carcinogenesis.<sup>14</sup> Also, FICZ stimulates T helper 17 (Th17) cell differentiation, which produces proinflammatory cytokines to promote immune responses.<sup>14</sup> Kynurenine is a metabolite from tryptophan breakdown by tryptophan-2, 3-dioxygenase. It has been hypothesized that the increased expression of tryptophan-2, 3-dioxygenase in various cancers would potentially drive higher endogenous kynurenine production, which would ultimately activate the AHR and promote tumor progression.<sup>59</sup> Unlike FICZ, kynurenine induces the production of FoxP3<sup>+</sup> regulatory T cells (Treg) in mice and suppresses anti-tumor immune

response in an AHR-dependent manner.<sup>55, 59</sup> These ligand-dependent AHR-mediated effects on different immune responses suggest that the AHR participates in regulating immune responses via adjusting the balance between Treg and Th17.<sup>14</sup>

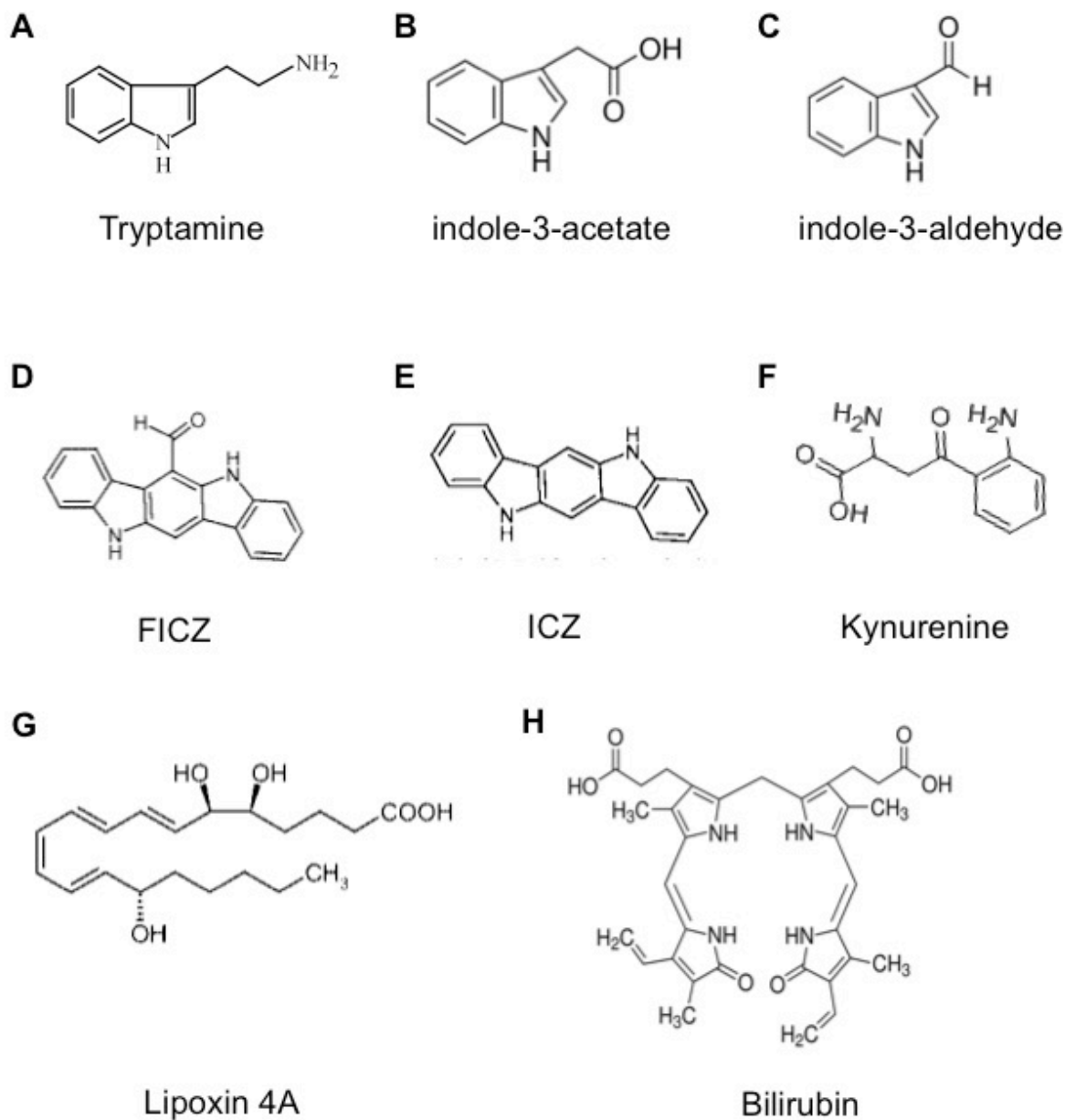


Figure 1-3. Endogenous ligands of AHR.

Arachidonic acid is a polyunsaturated fatty acid that is abundant in liver, brain, and muscle. Prostaglandin B<sub>2</sub>, D<sub>2</sub>, F<sub>3a</sub>, G<sub>2</sub>, H<sub>1</sub> and H<sub>2</sub>, and lipoxin 4A, metabolites of arachidonic acid, activate AHR and induce CYP1A enzymatic activity and inflammatory signals in a mouse hepatoma cell line.<sup>13, 60</sup> Lipoxin 4A has an EC<sub>50</sub> in the nanomolar range. In contrast, prostaglandins are weak ligands of AHR, having EC<sub>50</sub> in the micromolar range.<sup>13</sup> In addition, liver and lungs from C57BL/6 mice treated with TCDD had higher levels of epoxides of arachidonic acid, linolenic acid, eicosapentaenoic acid, and docosahexaenoic acid for anti-inflammatory response.<sup>60, 61</sup> Considering the above studies, therefore, arachidonic acid metabolism may be potentially linked to AHR signaling.<sup>13</sup>

Bilirubin, a breakdown product from the oxidation of heme, has also been suggested as a possible endogenous ligand of AHR.<sup>62</sup> The AHR has been shown to be involved in bilirubin-induced apoptosis. Given that apoptosis is a mitochondrial-dependent pathway, the involvement of the AHR in intrinsic (mitochondrial) apoptotic pathway may not be related to AHR transcriptional activity.<sup>62-64</sup> Biliverdin, a precursor of bilirubin and product of heme oxygenase, has also been suggested to be an AHR agonist, competing with TCDD *in vivo* and *in vitro*.<sup>13</sup>

A recent study suggested a new role of the AHR as a pattern recognition receptor that recognizes bacterial pigmented virulence factors.<sup>65</sup> This new type of AHR ligand, which is a structural analogue of the polycyclic aromatic hydrocarbon, activated the gene expression of AHR target genes and proinflammatory cytokine and chemokine genes.<sup>65</sup> Thus, another role of the AHR was explored, as a regulator of antibacterial defense.

## **Xenobiotics**

Known xenobiotic ligands of the AHR are divided into two structural groups, PAHs and HAHs (Figure 1-4).<sup>13</sup> PAHs are released from many different processes including the burning of coal, charbroiling food and smoking of cigarettes. The most studied PAHs, in terms of AHR

biology, are benzo[a]pyrene (BaP) and 3-methylcholanthrene.<sup>13</sup> BaP induces AHR signaling and is metabolized by Phase I and Phase II xenobiotic metabolizing enzymes.<sup>26</sup> Metabolized product epoxides are highly reactive with DNA and proteins.<sup>26</sup> BaP and 3-methylcholanthrene can also activate MAPK signaling, and this implies that AHR signaling may participate in crosstalk with many molecular pathways for physiological functions.<sup>15</sup>

HAHs include halogenated dibenzo-p-dioxin, dibenzofurans, polychlorinated biphenyls and naphthalenes. HAHs, like PAHs, are produced as byproducts of many industrial processes and are products of hydrocarbon incineration.<sup>14</sup> To be potent AHR agonists, these HAHs, must be planar in structure. HAHs with no halogen substitutions in the ortho-positions to the C-C bridge of inter-ring are potent compounds. Among HAHs, TCDD is the most potent AHR agonist. TCDD is a by-product of fungicides and herbicides synthesis, incineration, electronic recycling, and paper bleaching. TCDD is stable, poorly metabolized, and bioaccumulative. TCDD responses vary among tissue types, strains, and species.<sup>3</sup> Across species, AHR-mediated, TCDD-induced toxicity has a broad range of sensitivities and responses, including differences in median lethal dose (LD50), gene expression and metabolite profiles, related to multiple signaling pathways. These pathways include immune response pathways, sexual hormone regulation, cell cycle regulation, developmental signaling, mitochondrial functions, as well as xenobiotic metabolism.<sup>66-69</sup> Researchers have tried to understand TCDD-induced toxicity by studying transcriptomes, proteomics, metabolomes and pathological responses using TCDD-sensitive and TCDD-resistant animal models, such as C57BL/6J mouse (sensitive) vs. DBA/2J mouse (resistant), L-E rat (sensitive) vs. H/W rats (resistant) or mutant cell lines, such as hepa-1 cells vs. mutant hepa-1 derivatives.<sup>66, 69-72</sup>

Polychlorinated biphenyls (PCBs) are stable components of many commercial products such as polymeric implants, flame retardants, insulators, and adhesives.<sup>13</sup> The most potent PCB, in terms of AHR activation, is 3,3',4,4',5-pentachlorobiphenyl (PCB 126). Treatment of PCB126 to C57BL/6 mouse and mouse hepatoma cell line showed similar toxicity of TCDD.<sup>13, 27</sup>

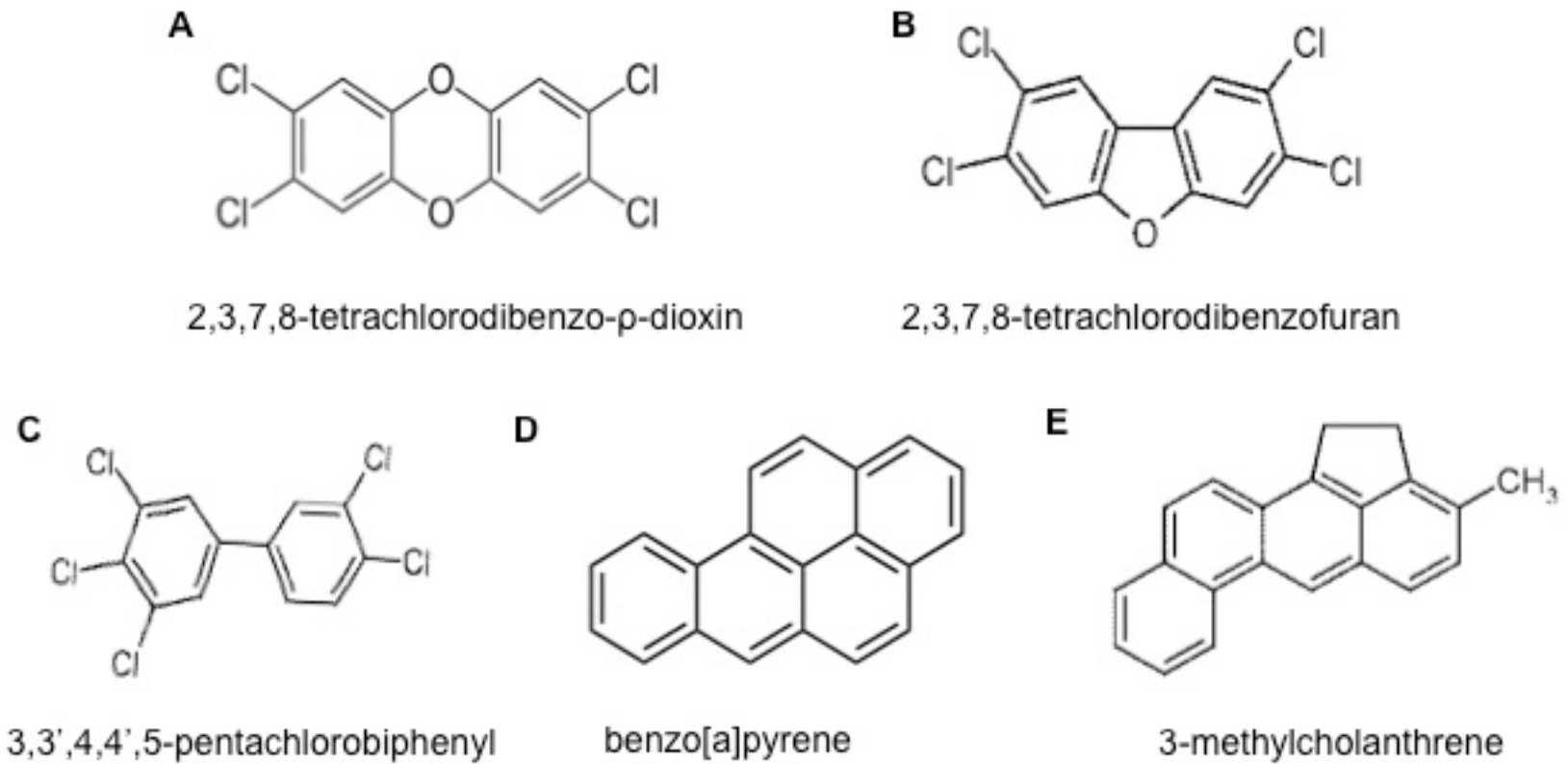


Figure 1-4. Xenobiotics of AHR.

For example, PCB126-mediated AHR activation caused suppressed phosphoenolpyruvate carboxykinase (PEPCK) induction and gluconeogenesis in mouse primary hepatocytes.<sup>73</sup> Female rats exposed to PCB126 via polymeric implants accumulated PCB126 in liver and mammary tissues resulting in induction of CYP1A enzymes, antioxidant enzyme transcripts and DNA adducts.<sup>74</sup>

### **AHR Target Genes**

PAH or HAH exposure induces a wide battery of detoxification genes involved in xenobiotic metabolism, such as cytochrome P450-dependent monooxygenases (CYPs), UDP-glucuronosyl transferase (UGTs), and glutathione S-transferase (GSTs).<sup>13, 75</sup> These drug detoxification genes encode proteins that can be categorized as either Phase I or Phase II enzymes.<sup>14, 26</sup> 13 genes (*Ahrr*, *Aldh3a1*, *Cyp1a1*, *Cyp1a2*, *Cyp1b1*, *Cyp2a1*, *Cyp2s1*, *Fmo1*, *Inmt*, *Nfe2l2*, *Nqo1*, *Tiparp* and *Ugt1a1*) have been explored as AHR-regulated genes for their potential role in causing AHR-mediated toxicity in many studies with TCDD sensitive and resistant rats.<sup>66</sup> Analysis of time- and dose-dependent gene expression identified that 7 of these genes (*Aldh3a1*, *Cyp1a2*, *Cyp1b1*, *Cyp2a1*, *Fmo1*, *Nfe2l2* and *Nqo1*) have inter-strain differences in expression and several of the genes (*Ahrr*, *Aldh3a1*, *Cyp1b1*, *Nfe2l2* and *Nqo1*) have biphasic responses. Among these genes, *Cyp1a1*, *Cyp1a2* and *Cyp1b1* are representative genes that have very low basal expression in rodent liver and are highly induced upon TCDD exposure in time-dependent manner.<sup>66</sup>

Phase I enzymes, such as CYPs, are expressed at the early stage of dioxin-toxicity. CYPs include, CYP1A1, CYP1A2, and CYP1B1, and each of these contain functional DREs in their enhancer region. CYP1A1 is the best-studied AHR target gene. The human CYP1A1 and CYP1A2 genes are on the chromosome 15 and their transcription start sites are separated from each other by 20 kb. This intergenic region has multiple DREs and acts bidirectionally for both

genes.<sup>26</sup> CYP1A1 is located in the endoplasmic reticulum (ER) and mitochondrial inner membrane and the amount of CYP1A1 in each organelle depends on species, tissues, age, and type of inducer.<sup>76, 77</sup> Using knock-in gene techniques, it has been shown that only CYP1A1 in the ER participated in detoxification of BaP and the absence of CYP1A1 localized in the ER induced the upregulation of the expression of both CYP1A2 and CYP1B1 to compensate for the loss of CYP enzymatic activity in ER.<sup>77</sup> However, the role of mitochondrial CYP1A1 induced by BaP is still not clear. CYP1B1, another AHR-regulated CYP1 enzyme, is highly expressed in hormone-mediated cancers.<sup>78</sup> PAHs challenged mice developed tumors slowly in *Cyp1b1* knockout mice compared to wild-type (WT) mice.<sup>79</sup> However, CYP1B1 induction is expressed approximately 100 fold less than *Cyp1A1* in the liver. In contrast, CYP1B1 is highly expressed in the lung and uterus, approximately 30 ~ 70 times more than that in liver.<sup>80</sup> PAH exposure to mammalian cells caused CYP1B1 targeting to both ER and mitochondria and lung mitochondrial CYP1B1 was more relative to PAH-mediated mitochondrial dysfunction than the microsomal enzyme.<sup>78</sup>

NAD(P)H:quinone oxidoreductase 1 (NQO1), UGTs, such as UGT1A1 and UGT1A6, aldehyde dehydrogenase (ALDH3A1), glutathione S-transferases (GSTs) and sulfotransferases (SULTs) belong to the Phase II class of enzymes. NQO1 is a flavoprotein that detoxifies quinones to quinols without generating reactive semiquinones.<sup>26</sup> Recent studies have shown that NQO1 is possibly localized in the mitochondria and ER, as well as the cytosol.<sup>80</sup> Quinols are conjugated by UGTs or SULTs and excreted via transporters such as multidrug resistance-associated proteins and breast cancer resistance protein.<sup>26</sup> The Human UGT1 gene encodes 9 UGT1 enzyme members, all of which are induced by AHR agonists. Among these, UGT1A1 and 1A6 are the most well-studied.<sup>14, 26</sup> UGT1A1 is mainly expressed in the liver and intestine. Functional DREs have also been identified in the human UGT1A1 gene, but not in murine gene. UGT1A1 catalyzes glucuronidation of bilirubin and  $\beta$ -estradiol. UGT1A6 conjugates a variety of planar phenols such as the neurotransmitter serotonin, 1-naphthol, acetaminophen and PAHs.<sup>26</sup>

ALDH3A1 oxidizes aldehydes, end products of lipid peroxidation, to ketones and carboxylic acids for detoxification. ALDH3A1 can block oxidative stress and affect the cell cycle.<sup>81</sup> Dysregulation of ALDH3A1, therefore, is associated with tumorigenesis.<sup>66</sup> The action of GST is coupled with glutathione synthesis. There are both cytosolic and mitochondrial GSTs. GSTs are multifunctional enzymes detoxifying many epoxide carcinogens.<sup>26</sup>

Phase II enzymes have antioxidant response elements (AREs), as well as DREs in their enhancer region.<sup>14, 26</sup> NF-E2 p45-related factor 2 (NRF2) is a basic leucine zipper domain (bZIP) nuclear transcription factor and main regulator of antioxidant defense. NRF2 binds to AREs as a complex with small MAFs.<sup>82</sup> This nuclear transcription factor is necessary for the expression of AHR-regulated drug metabolizing enzymes such as NQO1, UGTs, and GSTs.<sup>14, 26, 82</sup> AHR and NRF2 display crosstalk in multiple levels. Identification of DRE-like sequence upstream of *Nrf2* and AHR binding upstream of *Nrf2* in mouse liver cells suggests that TCDD-induced AHR activation increases *Nrf2* expression and consequently induces NRF2-target and Phase II enzymes.<sup>82</sup> NRF2 is considered to be a tightly regulated gene, being activated only in the presence of reactive oxygen species (ROS).<sup>26, 82</sup> The human *NQO1* gene contains a functional ARE but not a DRE-like element and the human *GSTA2* gene has no functional ARE or DRE. These results suggest that TCDD-induced CYP1 enzymes generate ROS, which directly or indirectly activates NRF2 target gene expression.<sup>26</sup> However, a recent study showed that the AHR- and NRF2-dependent expression of *Nqo1* could occur in the absence of oxidative stress in mouse hepatoma 1c1c7 cells.<sup>83</sup> The same study also suggested that TCDD-induced nuclear AHR physically interacted with NRF2 and KEAP1, a regulator of NRF2 degradation, with a sequentially delayed binding kinetics for target gene elements.<sup>83</sup> This suggested a crosstalk between AHR and NRF2 signaling via a direct formation of multi-protein complex.<sup>83</sup>

The role of NRF2 in TCDD-induced hepatic toxicity was revealed in the study using *Nrf2* knockout mice.<sup>84</sup> TCDD-exposed *Nrf2* null mice showed alterations in the expression of genes that encode proteins involved in inflammation, fibrogenesis, proliferation/apoptosis, lipid

metabolism, oxidative stress and DNA repair. TCDD-induced impaired adipogenesis was shown in *Nrf2* null mice and this was most likely caused by the downregulation of peroxisome proliferator-activated receptor (PPAR)- $\gamma$ . Thus, NRF2 has a protective role against TCDD-induced oxidative stress, DNA damage and impaired adipogenesis causing hepatic steatosis.<sup>84</sup>

### ***Physiological Roles of AHR***

Physiological stimuli can activate AHR in the absence of ligand. For example, cell density can regulate intracellular AHR localization and transactivation in human keratinocytes through post-translational modification in the form of phosphorylation on serine within the NES by p38-MAPK.<sup>57</sup> Sparse cell density resulting in loss of cell-to-cell contact induced nuclear AHR accumulation and transcription of AHR target genes. Human or rat blood vessel endothelial cells exposed to high glucose-containing media, caused AHR activation. Activated AHR did not bind to DREs but formed a complex with several other transcription factors at the thrombospondin-1 gene promoter.<sup>85</sup> Moreover, activation of AHR exposed to carotenoids and benzimidazole derivatives induced CYP1A1 as well as heavy metals did in human and mouse hepatocytes.<sup>4</sup> However, these compounds did not act as AHR ligands in terms of AHR:ARNT dimer formation.

AHR can also participate in crosstalk with other signaling pathways that might also play an important role in AHR-mediated physiological processes. These physiological effects include proliferation, endocrine disruption, differentiation, inflammation, apoptosis and proteolysis.<sup>14</sup> First, AHR can promote or inhibit cellular proliferation depending on types of cells and species. NF- $\kappa$ B is a pleiotropic transcription factor, consisting of a p65/RelA and a p50/NF- $\kappa$ B-1. In human breast cancer MCF7 cells, AHR interacted with p65/RelA, resulting in the transactivation of c-myc, a proto-oncogene.<sup>56</sup> Human lung A549 also increased proliferation rate via overexpression of AHR.

The AHR can also influence steroid signaling pathways within a cell at multiple levels. For example, the ligand-activated AHR:ARNT dimer associates with estrogen receptor- $\alpha$  and - $\beta$ , binds to estrogen responsive elements and recruits co-activator p300 to induce estrogen receptor target genes without a ligand of the estrogen receptor.<sup>86</sup> Induction of cathepsin D, a protease and breast cancer marker, by 17 $\beta$ -estradiol could be inhibited by TCDD-induced AHR activation in mammary tumor cells.<sup>14</sup> Estrone could be metabolized to estradiol by 17 $\beta$ -hydroxysteroid dehydrogenase.<sup>87</sup> Estradiol was further metabolized to genotoxic 4-hydroxylated estrogen by ICZ-activated AHR-induced CYP1B1, and 4-hydroxylated catecholesterogen induced estrogen-mediated carcinogenesis by being oxidized.<sup>87, 88</sup> Inversely, human *CYP1B1* gene was an estrogen receptor- $\alpha$  target gene expressed differently depending on a phase of menstrual cycle in endometrial glandular epithelial cells.<sup>89</sup> Finally, the ligand-activated AHR mediated ubiquitin-mediated degradation of the estrogen receptor- $\alpha$  (see below).<sup>90</sup> Thus, AHR signaling affects estrogen signaling by sharing its target gene and *vice versa*.

Next, hierarchical clustering of gene expression profiles in human hematopoietic cells suggests a possible role of AHR in differentiation of blood cells.<sup>91</sup> This suggested role of the AHR was demonstrated using a potent endogenous AHR ligand, FICZ. FICZ-induced AHR activation induced pluripotent stem cells to become hematopoietic progenitor cells and also contributed to further differentiation into erythroid-lineage cells. In contrast, the inhibition of the AHR by AHRR at the differentiation stage to erythroid-lineage cells stimulated megakaryocyte specification.<sup>91</sup> The expression of AHR and CYP1A1 increased in human keratinocyte under differentiation-promoting culture condition to induce gene expression involving in skin differentiation.<sup>92</sup> TCDD exposure in utero stimulated the formation of the fetal epidermal barrier. This suggests that endogenous ligands of the AHR may activate AHR signaling to support skin barrier formation.

In mouse adipocytes, somewhat differently, TCDD blocks adipocyte differentiation via inflammatory response.<sup>93</sup> TCDD induced the expression of COX-2 via induction of NF- $\kappa$ B, and

the subsequent increase in interleukin (IL)-8 and tumor necrosis factor- $\alpha$  (TNF- $\alpha$ ) secretion. This ultimately led to the reduction of lipid storage and lipoprotein lipase. In human primary hepatocytes, TNF- $\alpha$  and IL-1 $\beta$  induced NF- $\kappa$ B and suppressed CYP1A1 and 1A2. Similar results were observed in UVB-sensitive NF- $\kappa$ B in human hepatoma cells.<sup>14</sup> In mouse hepatoma 1c1c7 cells, TNF- $\alpha$ -induced NF- $\kappa$ B and ligand-activated AHR reciprocally suppressed each other's transcriptional activity through protein:protein interaction.<sup>94</sup> Ligand-activated AHR may enhance apoptotic stimuli, contributing to TCDD-induced immune suppression by NF- $\kappa$ B repression.<sup>94</sup> AHR-knockout mice also showed slow growth, a decrease in liver weight, abnormal vascular development in the liver and eyes, abnormal development and function in the prostate and ovaries, and reduced differentiation and immaturity in blood cells compared to WT.<sup>4, 95</sup> Finally, transforming growth factor- $\beta$  (TGF- $\beta$ ) was expressed in the liver of AHR-knockout mice, which would contribute to fibrosis and lower proliferation.<sup>4, 56</sup>

Activation of protein kinase signaling mediated AHR-dependent but ARNT-independent inflammatory responses. Human breast MCF10A cells exposed to TCDD caused AHR-dependent but ARNT-independent 1) increase in intracellular calcium concentration, 2) activation of cytosolic phospholipase A2 to release arachidonic acid and activation of COX-2 to synthesize prostaglandins, and 3) subsequent activation of protein kinases, such as calcium stimulated protein kinase C, arachidonic acid induced Src kinase and prostaglandin-dependent protein kinase A activation without induction of CYP1A1.<sup>93</sup>

Lastly, ligand-activated AHR is the adaptor component of E3-ubiquitin ligase for for estrogen receptor- $\alpha$ .<sup>90</sup> Steroid hormone receptors such as estrogen receptor- $\alpha$  and  $\beta$ , and androgen receptor are degraded by the ubiquitin-mediated proteasome system. Similarly,  $\beta$ -catenin is degraded by an E3 ubiquitin ligase complex, which has AHR as a component.<sup>96</sup> Wnt/ $\beta$ -catenin signaling induces the mitochondrial apoptotic pathway as well as proliferation depending on cell types.<sup>97</sup> These studies suggest that AHR is capable of functioning as a nongenomic mediator of cellular pathways, as well as a ligand-activated transcription.

## **MITOCHONDRIA**

Mitochondria are considered to have originated as endosymbionts from the engulfment of  $\alpha$ -proteobacterium by a primitive eukaryotic cell.<sup>98</sup> Mitochondria, therefore, have their own DNA, RNA and protein synthesis systems. Mitochondrial structure and function vary depending on cellular- and tissue-specific needs.<sup>99</sup> Mitochondria are double membrane bound organelles, which produce 90% of cellular energy by oxidation of chemical fuels coupled to the production of high energy intermediates (i.e., ATP). The carbon metabolic pathways of these chemical fuels, such as tricarboxylic acid (TCA) cycle and fatty acid oxidation, are at the junction of biomolecular metabolism, anabolism and catabolism. Mitochondria occupy a considerable volume of cytoplasm and have evolved to integrate multiple metabolic and signaling pathways.<sup>98</sup> Because of the central role of the mitochondria in metabolism, they are also linked to normal cellular processes, such as aging, differentiation and cell death. This also means that mitochondrial defects can result in diseases such as encephalopathy, neurodegenerative diseases, metabolic diseases and cancer.<sup>100</sup>

### ***Structure of Mitochondria***

The shape of mitochondria is flexible and can range from spherical to rod-like shape. Mitochondria have a double-layered membrane structure. The two membranes, the outer-membrane (OM) and inner-membrane (IM), separate the organelle into distinct compartments, including the matrix space and inter-membrane space (IMS). The OM is ion permeable membrane.<sup>101</sup> Like bacterial OM, the mitochondrial OM has a porin, an aqueous channel which is permeable to less than 5 kDa molecules. Because of this permeability, chemical composition of the IMS is similar to the cytosol regarding small molecules. The OM also has the mitochondrial transport machinery for delivery of proteins targeted to IMS, IM, and matrix space. On the other hand, the IM is a highly selective layer that is folded, forming cristae that serve to

further compartmentalize the organelle and increase the total amount of the IM. The IM contains the enzymes for the electron transport chain (ETC), ATP synthesis and specific transport systems for matrix proteins and metabolites.<sup>101</sup> Mitochondria cannot replicate on their own. Fusion and fission mechanisms and the import of synthesized macromolecules like proteins and lipids maintain orientation and distribution of mitochondria according to cell types and cellular status.<sup>102</sup>

### ***Mitochondrial DNA (mtDNA)***

A mitochondrion contains 2-10 copies of its DNA and there can be as many as 1000 mitochondria per cell. Many genes from the endosymbionts were transferred to nuclear chromosomes. It is estimated that approximately 1500 genes are scattered throughout the chromosomal DNA.<sup>98</sup> Human mtDNA is 16.6kb of a closed circular double strand molecule. mtDNA has no introns and little of no intergenic regions between genes.<sup>103</sup> The genes for 13 polypeptides, 22 tRNAs, and 2 small rRNAs are included in mtDNA. The 13 polypeptides are components of the ETC and ATP synthase complexes, including ND1, 2, 3, 4L, 4, 5, and 6 (subunits of complex I), cytochrome b (subunit of complex III), CO1, 2, and 3 (subunits of complex IV), and ATP6 and 8 (subunits of complex V).<sup>103</sup> mtDNA is maternally inherited and has regional genetic variances. Because mitochondria have multiple copies of their genome, an individual may be heteroplasmic (i.e., having more than one sequence of organellar genome within an individual).

In yeast, mtDNA nucleoids are associated with proteins in four functional groups: (I) mtDNA maintenance and gene expression; (II) protein import and mitochondrial biogenesis; (III) energy metabolism; and (IV) amino acid metabolism.<sup>104</sup> For example, aconitase, a TCA cycle enzyme, can replace ABF2, a mtDNA packaging protein.<sup>104</sup> LON protease is also identified as a component of the mitochondrial nucleoids, though LON protein level may not be essential for

mtDNA function.<sup>105</sup> The factors discussed in other sections, such as mitochondrial translation related factors, SLS1 and mitochondrial ribosomal protein L12 (MRPL12), or mitochondrial chaperones, mtHSP70, are also associated with mtDNA nucleoids.<sup>104</sup> Thus, mitochondria seem to utilize the pools of proteins diversely to maintain their own integrity.

### ***Synthesis of Mitochondrial Proteins***

Among identified ~1500 nuclear genes that encode mitochondrial proteins, a portion of these genes are thought to have been transferred from endosymbionts to the nucleus and the other part would have arisen during the evolutionary process.<sup>98</sup> To maintain mitochondrial function and morphology, mitochondria need nuclear-encoded proteins.<sup>100</sup> Analysis of *Saccharomyces cerevisiae* mitochondrial proteome assigned functional classification of the proteins; 12% of the proteins are involved directly in mitochondrial genome maintenance and mitochondrial gene expression, 15% in energy metabolism, such as respiratory chain complexes and TCA cycle, 25% in proteostasis, and 25% in other known functions such as lipid metabolism, iron metabolism, amino acids metabolism, redox regulation, signaling, and morphology. Still, the function of 20% of the proteins has not been assigned.<sup>98</sup>

### **Synthesis of mitochondrial gene encoded proteins**

Mitochondrial ribosomes are bound to the IM for co-translational protein assembly. Three yeast IM proteins, OXA1, MBA1 and Mdm38p, bind to large mitochondrial ribosome subunits and function to promote mitochondrial protein export via their translocase/insertase activity. Mitochondrial transcription occurs near the IM and mRNAs can be channeled to mitochondrial translation machinery. Rpo41p, yeast RNA polymerase, interacts with NAM1 through N-terminus and delivers mRNA to NAM1. NAM1 delivers mRNA to the activator, Pet309 or Pet111, in the IM surface, which binds mRNA 5'-UTR and mitochondrial ribosomes,

with membrane-associated proteins, SLS1 and Rmd9p.<sup>101</sup> Newly synthesized components of the respiratory chain form pre-assembly intermediates with a help of assembly factors in the IM.<sup>101, 106</sup>

### **Synthesis of nuclear gene encoded mitochondrial proteins**

There are two modes of nuclear gene encoded mitochondrial protein synthesis, protein synthesis machinery (polysomes) bound to the OM of the mitochondria and free polysomes in the cytosol.<sup>101</sup> In yeast, 3'-untranslated regions (3'-UTRs) of mRNA and N-terminal sequences of precursors act as signals for mitochondrial membrane binding of polysomes.<sup>107</sup> Puf3p, an RNA binding protein that induces deadenylation and degradation of mRNA, binds to the 3'-UTRs and guides the mRNA at the mitochondrial surface near sites associated with ER.<sup>101, 107</sup> The role of Puf3p and existence of other factors involved in mRNA stabilization or localization at the surface of mitochondria is not completely clear. It is expected, however, that a regulatory mechanism that maintains the ratio of protein synthesis at mitochondria bound polysome vs. free polysomes exists. The co-translational protein import into mitochondria does not seem to be the only purpose of translation at the mitochondrial surface because fully synthesized precursors were detected at the OM of the mitochondria. It is not clear whether attenuated import of precursors at the OM is destined to degradation or import.<sup>101</sup>

### ***Nuclear-encoded Mitochondrial Protein Translocation***

After being synthesized in the cytosol, nuclear-encoded mitochondrial protein precursors are imported via a mitochondrial targeting signal (MTS). These MTSs usually contain positively charged amphipathic helices. Mitochondrial protein import machinery has four major complexes; the translocase of the outer membrane (TOM), the translocase of the inner membrane (TIM), the presequence translocase-associated motor (PAM), and the outer

membrane sorting and assembly machinery (SAM). The translocases have multiple channels. Though a role of multiple channels is not clearly identified, it is suggested that they may increase transport efficiency or may recruit target proteins as well as regulatory factors.<sup>108</sup>

The translocation of proteins into the mitochondria begins with the interaction between a target protein and the TOM complex.<sup>46, 108</sup> TOM has two recognition receptors outside of the mitochondria, TOM20 and TOM70. TOM20 binds to the N-terminal MTS and TOM70 binds to hydrophobic internal sequences of transmembrane proteins. Mitochondrial precursors recognized by TOM20 or TOM70 are transferred to the common TOM22/TOM40 translocation pore. In mammals, cytosolic HSP90 and HSP70 interact to TOM70 in order to transfer mitochondrial preproteins to TOM70 core domain.<sup>46, 109</sup> Mitochondrial proteins targeting to TOM20 are also transferred by cytosolic chaperones such as HSP90 and AIP.<sup>45, 110, 111</sup> A recent model suggested another role of TOM20. In this model, TOM20 displaces HSP90/HSP70 bound to TOM70 when ATP hydrolysis by HSP90/HSP70 occurs and the displacement would facilitate a release of the target protein from TOM70 and a delivery to common translocation pore.<sup>112</sup>

According to the destination of target proteins, SAM sorts pore-forming  $\beta$ -barrel proteins to the OM. MIM1, interacting with SAM, identifies and inserts  $\alpha$ -helical proteins to the OM. TIM23 sorts matrix proteins by coordinating with PAM or IM proteins with the help of TIM21, and TIM22 sorts IMS proteins delivered from TOM.<sup>98, 108</sup> Mitochondrial membrane potential that is coupled with ATP production and mitochondrial matrix HSP70 (mtHSP70) drives further processing of protein import into matrix from TIM23.<sup>113</sup> mtHSP70 translocates matrix protein precursors from TIM23 to the matrix.<sup>108</sup> Matrix targeting signals are cleaved by mitochondrial-processing peptidase upon entering the matrix. TIM21, a subunit of TIM23 complex, facilitates protein localization into the IM.<sup>108, 113</sup> *In vitro* studies using yeast and *Escherichia coli* cells showed that TIM21 reduced the regional mitochondrial membrane potential by interacting with subunits of complex III and IV in the respiratory chain.<sup>113</sup> However, there is no clear mechanism

identified to explain a relationship between membrane potential and protein import to the inner membrane.<sup>108</sup>

Some precursors destined for the IMS have a “bipartite presequence consisting of a positively charged matrix targeting signal and a hydrophobic sorting signal”.<sup>98</sup> Mitochondrial-processing peptidase removes the matrix targeting signal and the inner membrane peptidase cleaves a hydrophobic sorting signal, subsequently the mature protein is released from the IM into the IMS.<sup>98</sup> Small TIM family members deliver precursors targeted to the IM from TOM complex to TIM22 across the IMS. One proposed transport mechanism for small proteins into the IMS is a folding mechanism involving disulfide-bond formation within a protein, maintaining a complex structure. Mia40 (TIM40) and Erv1 are known IM proteins that utilize disulfide-bond formation in their mitochondrial IMS import and assembly (MIA) pathway.<sup>108, 114</sup>

### ***Nuclear Transcription Factors for Mitochondrial Biogenesis***

Several transcription factors are important for the expression of nuclear genes that encode proteins destined for the mitochondria. For example, nuclear respiratory factor 1 (NRF1) regulates gene expressions of mtDNA replication and maintenance factors.<sup>115</sup> NRF1 is a transcription factor that binds to DNA as a homodimer, specifically at the promoter of cytochrome c, mitochondrial transcription factor A (TFAM), and mtTFB, as well as other genes involved in oxidative phosphorylation (OXPHOS), heme synthesis, ion channel synthesis, mitochondrial protein import, assembly, and shuttling.<sup>103</sup> NRF1 target genes are not only involved in mitochondrial function but also related to metabolic enzymes and growth regulatory E2F target genes.<sup>103</sup> Nuclear respiratory factor 2 (GABP), binding to DNA as a heterotetramer, activates transcription of subunits of cytochrome c oxidase.<sup>116</sup> Both NRF1 and GABP regulate gene expression of all 4 subunits of succinate dehydrogenase.<sup>103, 117</sup> PPAR- $\gamma$  coactivator-1 $\alpha$  (PGC-1 $\alpha$ ) is a coactivator and binds several nuclear hormone receptors, NRF1, GABP, and

PPAR- $\alpha$  and - $\gamma$ . NRF1 and GABP genes have hormone responsive elements and are also target genes of PGC-1 $\alpha$ .<sup>103, 118</sup> PGC-1 $\alpha$  is well studied with regard to mitochondrial biogenesis and function.<sup>119-122</sup> PGC-1 $\alpha$  associates with various nuclear transcription factors, as well as induces expression of nuclear transcription factors in response to extracellular signals.<sup>103, 119, 122</sup> Steroid/thyroid hormone receptors, such as glucocorticoid, estrogen, androgen and thyroid receptors are localized in both nucleus and mitochondrial matrix and induce transcription of OXPHOS genes and mitochondrial transcription factors in liver, heart, skeletal muscle, kidney, and brain.<sup>118</sup> Estrogen-related receptor, an orphan receptor, and PPAR- $\alpha$  and - $\gamma$ , regulate fatty acid oxidation.<sup>103</sup> Also, mitochondrial glucocorticoid receptor induces apoptotic pathways in immune cells. In contrast, mitochondrial estrogen receptor induces anti-apoptotic effects in breast cancer cells. Finally, Sp1, CREB, p53, NF- $\kappa$ B, AP-1, and c-MYC have also been investigated as regulators of mitochondrial function.<sup>103, 118</sup>

### ***Mitochondrial Respiration and Reactive Oxygen Species***

Aerobic respiration is the main process by which the mitochondria produce energy. Aerobic respiration involves three distinct phases: oxidation of substrates (e.g., glucose, fatty acid), electron transport, and ATP synthesis. In this process, reducing equivalents, primarily derived from the TCA cycle, are transferred to the ETC and ultimately to O<sub>2</sub>. The energetically favorable movement of electrons within the ETC is coupled to the production of an electrochemical gradient across the IM of the mitochondria, which is used to drive ATP synthesis (Figure 1-5). The respiratory chain in the IM contains four enzyme complexes (I, II, III and IV) through which electrons pass on their way to reducing O<sub>2</sub> to water. Complex I is referred to as NADH dehydrogenase consisting of 46 polypeptides and reduces ubiquinone at the expense of NADH, resulting in the net transfer of four protons across the IM. Complex II, also known as succinate dehydrogenase, consists of only four peptides and is thus the simplest

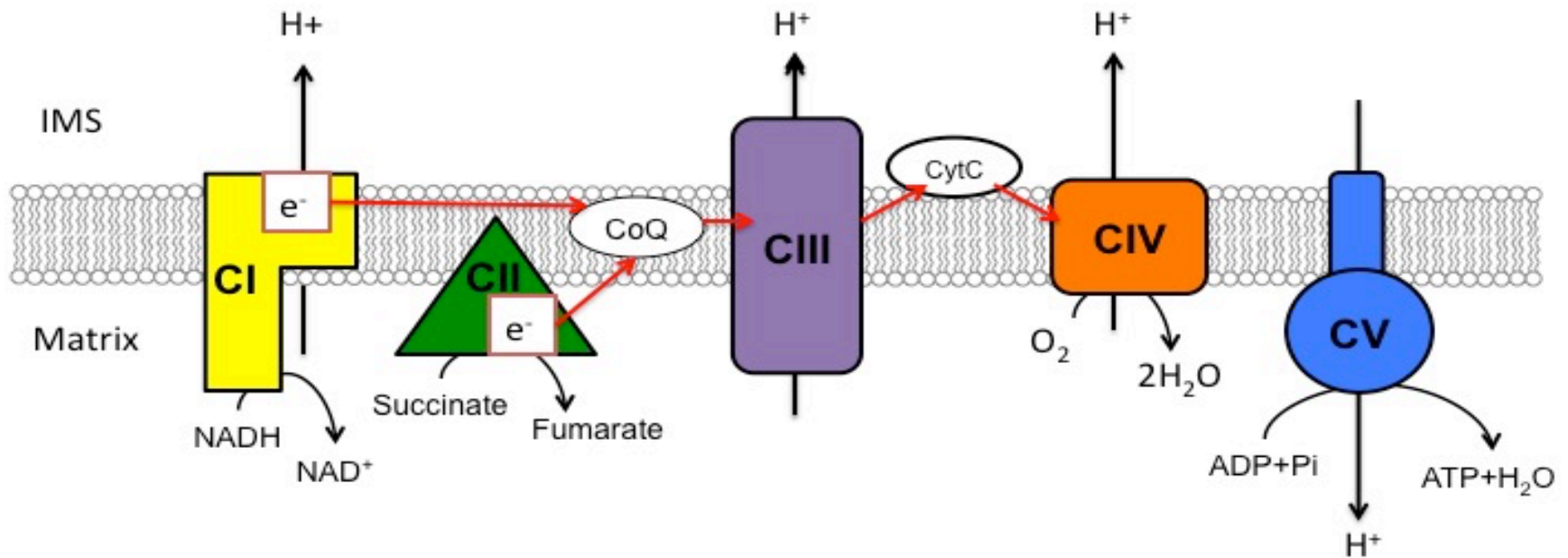
of all the complexes of the ETC. Complex II is also a TCA cycle enzyme and directly links the oxidation of succinate to fumarate with the reduction of ubiquinone to ubiquinol but does not translocate protons across the IM. Complex III (aka  $bc_1$  complex, or ubiquinol-cytochrome-*c* oxidoreductase) consists of 11 polypeptides and enzymatically couples proton transfer to the oxidization of ubiquinol and the reduction of cytochrome *c*. Finally, Complex IV, cytochrome *c* oxidase consisting of 13 polypeptides, completes the ETC by transferring the electrons from cytochrome *c* to  $O_2$  and utilizing the exergonic oxygen reduction reaction to pump protons. Complex V, ATP synthase also known as  $F_1F_0$ -ATPase, couples the generated proton motive force through ETC to ATP synthesis. Complex V, consisting of 16 polypeptides, transports protons back to the matrix through the  $F_0$  channel and synthesizes ATP at the  $F_1$  catalytic site.

The production of mitochondrial ROS is affected by the redox state of the ETC and the proton motive force.<sup>120</sup> Inhibition of the ETC results in more reduced electron carriers, which have more tendency to generate ROS. The proton pump driven by the ETC contributes to the proton motive force, and increased proton motive force induces more mitochondrial ROS accumulation. ROS generated in the mitochondria are mainly produced by complex I and III.<sup>123</sup>  
<sup>124</sup> The flavin site (IF) of complex I, consisting of flavin mononucleotide and 8 Fe-S clusters, produces ROS when the site IF is fully reduced. When pyruvate and malate drive the forward electron transport of complex I and downstream of electron transport is blocked, the site IF significantly generates ROS. Succinate or glycerol-3-phosphate converts ubiquinone to ubiquinol of the Q-binding site (IQ) of complex I, which delivers electrons to  $NAD^+$  through complex II to complex I by a high membrane potential. During this reverse electron transfer, superoxide is generated at the site IQ, which is a bridge point between flavin, 8 iron-sulfur clusters, and ubiquinone of complex I. However, there is a controversy if both two sites of complex I rather than one generate ROS under physiological condition. Superoxide generation from complex I is the highest portion of mitochondrial ROS. The ubiquinone-oxidation site of the Q-cycle in complex III is also a superoxide production site (IIIQo). When electron transfer from

cytochrome b to the ubiquinone is inhibited, semiubiquinone is accumulated and reduces oxygen to superoxide.

Superoxide produced by complex I is distributed to the matrix and that produced by complex III is distributed mainly to IMS. ROS generated by complex I damages macromolecules irreversibly. In contrast, ROS generated by complex III has selectivity in their targets for redox signaling.<sup>124</sup> For instance, thiol oxidation of mitochondrial proteins occurred differentially depending on the source of ROS generation. ROS production by complex III is required for cardioprotection under ischemic preconditioning and for stabilization of HIF1 $\alpha$  under hypoxia.<sup>120</sup> Moreover, there is a suggestion that assembly subunit of complex III may control ROS production at the site IIIQo.<sup>125</sup> Other IM proteins, electron transferring flavin protein Q oxidoreductase, pyruvate dehydrogenase,  $\alpha$ -ketoglutarate dehydrogenase, glycerol 3-phosphate dehydrogenase and complex II and IV, are considered ROS producing sites in mitochondria.<sup>123</sup> However, the production rates of these are negligible compared to complex I and III and very little information on characteristics of those is established.<sup>120</sup>

ROS oxidizes macromolecules and this damage causes impaired cellular functions or aging related diseases.<sup>123</sup> Biological system developed a defense system having a broad range of scavengers for oxidizing radicals. One of those, superoxide dismutase (SOD) converts superoxide to hydrogen peroxide, which can diffuse out of the membrane.<sup>123</sup> SOD1 (Cu/Zn-SOD) is in the mitochondrial IMS and SOD2 (Mn-SOD) is found in mitochondrial matrix.<sup>120</sup> Peroxiredoxin, glutathione peroxidase, and catalase convert hydrogen peroxide to water. Mitochondria have isoforms of peroxiredoxin and glutathione peroxidase.<sup>120</sup> Cytosolic or nonmitochondrial enzymes can catalyze a conversion of mitochondrially generated ROS that diffuse out of the organelle. Glutathione peroxidase 1 utilizes GSH to convert hydrogen peroxide to water and glutathione reductase converts an oxidized glutathione to a reduced form, GSH. Even though antioxidant defense systems exist, mitochondria have a limited ability to protect a



	CI NADH dehydrogenase	CII Succinate dehydrogenase	CIII bc1 complex	CIV Cytochrome c oxidase	CV ATP synthase
mtDNA encoded subunits	7	0	1	3	2
nuDNA encoded subunits	39	4	10	10	14

**Figure 1-5. Schematic of Electron transport chain complexes and ATP synthase.**

Complex I (CI), III (CIII), IV (CIV), and V (CV) are composed of mitochondrial DNA (mtDNA) encoded subunits and nuclear DNA (nuDNA) encoded subunits. Complex II (CII) is composed of nuDNA encoded subunits. Another name for each complex is described below the scheme. Red arrows indicate electron flow from CI or CII to CIV.

cell from oxidative damage. Recent research has reported that low levels of ROS, which might be residual after detoxification by ROS scavengers, might function as a signaling molecule to adapt to stress by crosstalk with other cellular pathways such as autophagy, hypoxia, differentiation and immune response.<sup>120</sup> Therefore, both defense system against oxidative stress and regulations of cellular processes by ROS are important to maintain mitochondrial integrity and function.<sup>121</sup>

### **TCA Cycle**

The tricarboxylic acid (TCA) cycle (also known as Krebs cycle or citric acid cycle) in the mitochondria is the major site that provides biomolecular precursors and reducing equivalents that can be used by the ETC to conserve energy for ATP generation (Figure1-6).<sup>126</sup> The TCA cycle oxidizes acetyl-CoA to two CO<sub>2</sub> through the reactions of 8 enzymes and generates 3 moles of NADH, 1 mole of FADH<sub>2</sub>, 1 GTP molecule and intermediates for other metabolic pathways. Liver cells, for example, utilize the electron carriers, NADH and FADH<sub>2</sub> in the ETC and intermediates of the TCA cycle in the part of synthesis of glucose, fatty acids, cholesterol, amino acids and porphyrins. The cytosolic isoforms of some enzymes in the TCA cycle and active carriers for metabolites in mitochondrial IM create an interconnection between the TCA cycle and other metabolic pathways. Oxaloacetate, the substrate of citrate synthase, can be converted to phosphoenolpyruvate for gluconeogenesis. Acetyl-CoA, another substrate of citrate synthase, can be utilized for fatty acid and cholesterol synthesis.  $\alpha$ -ketoglutarate, succinyl-CoA, fumarate and oxaloacetate are converted from amino acids and  $\alpha$ -ketoglutarate and oxaloacetate can also be converted to amino acids. Because of these amphibolic characteristics, the TCA cycle is an important metabolic hub.

The flux of the TCA cycle is modulated by cellular metabolic demand. The TCA cycle is regulated by availability of substrates and enzymatic activities and this is related to hormone

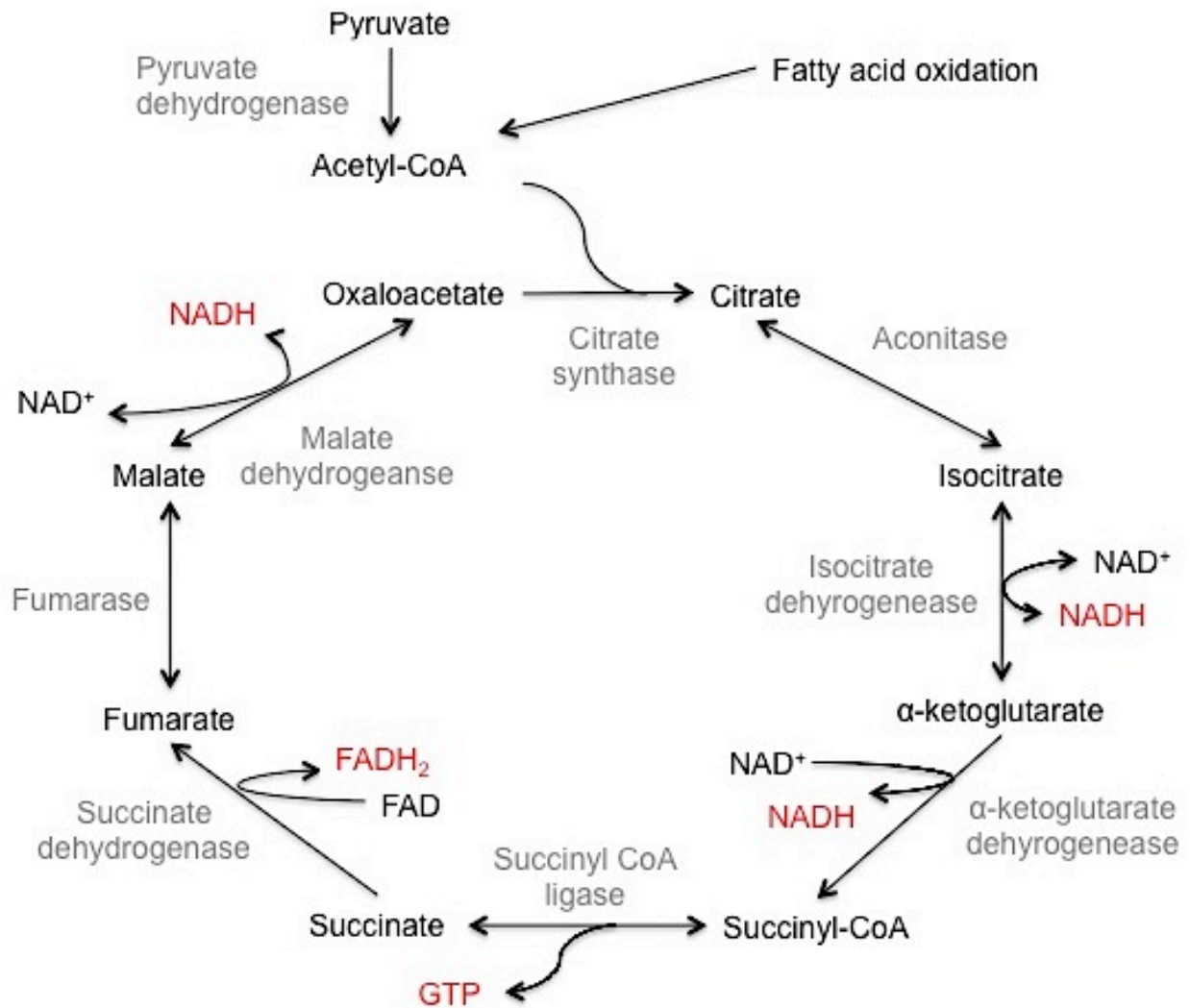


**Figure 1-6. TCA cycle.**

signaling, calcium as a secondary signaling molecule, phosphorylation modification on enzymes, and energy status. The ratios of  $[\text{CoA}]/[\text{Acetyl-CoA}]$ ,  $[\text{ADP}]/[\text{ATP}]$  and  $[\text{NAD}^+]/[\text{NADH}]$  regulate the flow of the TCA cycle via their role as substrates/products for various reactions and as allosteric effectors. Acetyl-CoA is provided from fatty acid oxidation or oxidative decarboxylation of pyruvate via pyruvate dehydrogenase complex (PDH), whose activity is regulated by PDH kinase (PDK). PDK, a HIF1 target gene, phosphorylates E1 subunit of PDH for inactivation. Inactivation of PDH by PDK reduces influx of acetyl-CoA into TCA cycle and stimulates

glycolysis under specific circumstances such as hypoxic stress or in cancer.<sup>127</sup> On the other hand, high glucose concentration in blood stimulates insulin secretion and calcium release, and activates PDH phosphatase to activate PDH.

*Caenorhabditis elegans* exposed to  $\alpha$ -ketoglutarate displays an extended life span.<sup>128</sup> This was thought to be caused by ATP synthase inhibition upon  $\alpha$ -ketoglutarate binding of ATP synthase  $\beta$  subunit, resulting in decreased respiration and activity of the target of rapamycin (TOR) and inducing autophagy.<sup>128</sup> Endogenous levels of  $\alpha$ -ketoglutarate under dietary restriction can be increased through activation of gluconeogenesis. This suggests that  $\alpha$ -ketoglutarate may be a key metabolite that can be a target for aging or therapeutics for aging-related disease. Mutant isocitrate dehydrogenase catalyzes the conversion of  $\alpha$ -ketoglutarate to 2-hydroxyglutarate, a competitive inhibitor of  $\alpha$ -ketoglutarate utilizing enzymes such as  $\alpha$ -ketoglutarate dehydrogenase and  $\alpha$ -ketoglutarate-dependent dioxygenase.<sup>129, 130</sup> The enzymes inhibited by accumulated 2-hydroxyglutarate are related to regulation of histone and DNA methylation and HIF1 $\alpha$  stabilization, which may promote tumorigenesis.<sup>130</sup> Structural analogs of  $\alpha$ -ketoglutarate in the TCA cycle, such as fumarate, succinate and citrate, are competitive inhibitors of prolyl hydroxylase domain proteins.<sup>131</sup> Treatment of cell lines with derivatives of fumarate and succinate induced HIF1 $\alpha$  stabilization and expressions of HIF1 target genes. Fumarase and succinate dehydrogenase are considered to be tumor suppressors.<sup>132</sup> Mutations in subunits of succinate dehydrogenase (B, C, and D) developed paraganglioma or pheochromocytoma and mutations in fumarase developed leiomyoma, leiomyosarcoma or renal cell carcinoma.<sup>132</sup> Mutation or deficiency of fumarase and succinate dehydrogenase cause accumulation of fumarate and succinate in mitochondria, and consequently these metabolites are leaked into cytosol and react with other enzymes.

A new role of metabolites of the TCA cycle has been discovered as substrates of post-translational modification.<sup>133</sup> Proteomic analysis with human liver tissues showed that all of the enzymes participating in the TCA cycle and fatty acid oxidation are targets for acetyl

modification.<sup>134</sup> Sirtuin (SIRT), an NAD-dependent protein deacetylase, is involved in many cellular metabolic processes. Deacetylation on lysine residues by SIRT3-5 is a representative example for post-translational modification of mitochondrial proteins.<sup>133</sup> Human SIRT3 deacetylates and activates glutamate dehydrogenase and isocitrate dehydrogenase. Mouse SIRT5 localized in the IMS deacetylates cytochrome c, which regulates respiration and apoptosis.<sup>135</sup> Succinylation on lysine residues or succination on cysteine residues is also related to tumor formation.<sup>133</sup> Succinylation on lysine residue of SOD1 in the IMS has a positive relationship with tumor cell growth.<sup>136</sup> Renal cell cancer syndrome associated with germ line mutations in the fumarase gene is associated with aberrant succinated cysteine-containing proteins.<sup>133</sup> Post-translational modification by metabolites of the TCA cycle also occurs in nonmitochondrial sites. Succination on KEAP1, a regulator of NRF2 stabilization, induce NRF2 signaling against stress.<sup>133</sup> Hydroxylation on proline residues of HIF $\alpha$  by  $\alpha$ -ketoglutarate-dependent dioxygenase induced degradation of HIF $\alpha$  subunits.<sup>137</sup>

### ***Fatty Acid $\beta$ -oxidation and Ketogenesis***

Fatty acid  $\beta$ -oxidation is another metabolic pathway that occurs within the mitochondrial matrix and generates acetyl-CoA, NADH and FADH<sub>2</sub>.<sup>138</sup> Fatty acid in cytosol must be primed with CoA by thiokinase in an energy dependent process. The acyl-CoA is then transferred to mitochondria by forming acyl-carnitine and being transported by the carnitine carrier protein. In the oxidation process, thiolysis at the  $\beta$ -carbon of acyl group releases the 2 units of carbon component as an acetyl-CoA. Propionyl-CoA is the end product of odd-chain fatty acid oxidation. Propionyl-CoA can be carboxylated to succinyl-CoA, which can be further metabolized for other metabolic pathways. Acetyl-CoA can be utilized in TCA cycle or ketone body formation and electron carriers can be utilized in ETC and ATP synthase. Skeletal muscle and heart utilize fatty acids as their primary energy source. The liver utilizes fatty acids for

energy production when there are low levels of blood glucose, such as during starvation.

Accumulated acetyl-CoA in liver mitochondria is converted to ketone bodies, acetoacetate and  $\beta$ -hydroxybutyrate, important fuels for extrahepatic organs under starvation or glucose depletion. It is important to note that acidosis can occur if the blood levels of ketone bodies get higher than the demand of peripheral tissue. Hormonal regulation stimulated by nutrient state activates transcriptional regulators such as sterol regulatory element-binding protein 1c and carbohydrate responsive element-binding protein (i.e., by insulin), and PPAR- $\alpha$  (i.e., by glucagon) to regulate *de novo* lipogenesis, fatty acid oxidation and ketogenesis. Insulin resistance in white adipose tissue and muscle causes lysis of triacylglycerol and increases translocation of nonesterified fatty acid into the liver.<sup>139</sup> Insulin resistance also activates sterol regulatory element-binding protein 1c. Hyperglycemia during type 2-diabetes activates carbohydrate responsive element-binding protein and contributes to fatty liver. Hyperglycemia and ketoacidosis that can also occur during type-2 diabetes increases CYP2E1 expression and promotes ROS production within the liver causing lipotoxicity.<sup>139</sup> Deletion of SIRT1 in liver impairs PPAR- $\alpha$  signaling, which results in decrease in fatty acid  $\beta$ -oxidation and ketogenesis.<sup>138</sup> Deacetylation of PGC-1 $\alpha$ , another co-activator for transcription, by SIRT1 and phosphorylation by p38MAPK activates PGC-1 $\alpha$ .<sup>138</sup> Liver-specific deletion of PGC-1 $\alpha$  in mice causes hepatic steatosis and overexpression of PGC-1 $\alpha$  in liver induces increase in fatty acid  $\beta$ -oxidation through regulation of mitochondrial contents and function.<sup>138</sup> Mitochondrial SIRT3 also regulates fatty acid  $\beta$ -oxidation as well as SOD2 activation.<sup>138</sup>

## **TCDD-INDUCED TOXICITIES AND METABOLIC DYSFUNCTION**

The various deleterious physiological effects by TCDD exposure are tumor promotion, chloracne, wasting syndrome, and hepatic steatosis.<sup>140</sup> In 1997, the International Agency for Research on Cancer (IARC) defined TCDD as a human carcinogen.<sup>141</sup> The studies about the

cohort in Soveso, Italy related to the accident in 1976, dioxin exposure from a chemical production plant operated by Roche group, revealed high mortality in lung cancer, lymphopoietic neoplasms and rectal cancer in men, and increased incidence of breast cancer and liver cancer in women.<sup>141</sup> Dioxin influences the thyroid hormone metabolism as an endocrine disruptor.<sup>140</sup> Thyroid hormone is essential for brain development and a low level of thyroid hormone in early pregnancy is related to low children's intellectual ability.<sup>140</sup> Chloracne, a noninflammatory skin disorder characterized by metaplasia and hyperkeratosis, is a representative human dioxin-induced toxicity.<sup>140</sup> Women exposed to high doses of TCDD in their workplace in Vienna in 1997 suffered from severe chloracne.<sup>4</sup> In 2004, Ukrainian presidential candidate, Viktor Yushchenko, was poisoned with TCDD and suffered from severe chloracne.<sup>4</sup> The mechanism of developing chloracne is not clear. The suggested mechanism is that keratinocyte terminal differentiation is accelerated via expression of filaggrin, a differentiation-specific protein produced in keratinocytes by AHR activation.<sup>60</sup>

Interestingly, overexpression of constitutively active AHR in keratinocytes leads to dermatitis, skin inflammation that is phenotypically different from dioxin-induced chloracne.<sup>60</sup> Moreover, AHR-null mice showed hyperkeratosis and dermal fibrosis. Why hyperkeratosis happens in both sustained AHR activation and lack of AHR is not understood. AHR-null mice also display accelerated skin-wound healing than WT mice potentially caused by increased epithelial cell migration rate. Interestingly, migration rate of endothelial cells and fibroblasts were decreased.<sup>92</sup> This is considered to be due to reduced inflammation. This suggests that AHR has an important role in tightly controlling cytokine secretion from skin immune cells, which protects the organism against extracellular invade.<sup>60</sup>

The severe loss of body weight, wasting syndrome, accompanies hyperlipidemia in serum, accumulation of fat in the liver, decrease in the adipose tissue weight, downregulation of PEPCK in liver and loss of appetite.<sup>93, 142, 143</sup> Epidermal growth factor receptor (EGFR) signaling is related to TCDD-induced symptoms. EGFR signaling can be activated by protein kinases,

including Src. Src-null mice are less susceptible to TCDD-induced wasting syndrome than WT mice. In addition, AHR target genes that regulate metabolism can also be mediators of wasting syndrome.<sup>68, 142, 144-146</sup>

TCDD-induced hepatotoxicity related to metabolic pathways is mediated by the direct regulation of gene expression of key enzymes or secondary signaling by metabolites.<sup>143</sup> TCDD exposure to C57BL/6 mice downregulates gene expressions of enzymes involved in cholesterol biosynthesis, fatty acid synthesis and glucose metabolism in liver depending on AHR expression.<sup>147</sup> The study using human hepatoma cells suggested that this AHR-dependent repression of cholesterol biosynthesis might be a result from nongenomic AHR activation.<sup>148</sup> TCDD also induces increased levels of unsaturated fatty acid in liver and decreased levels of serum cholesterol and lipoproteins, and this suggests that dietary lipids cause the AHR-mediated hepatic steatosis rather than lipid *de novo* synthesis.<sup>149</sup> Steatosis is defined as an abnormal accumulation of lipids within a cell. During TCDD-elicited steatosis, hepatocytes display increased triglycerides, free fatty acids, alterations in fatty acid composition, lipid metabolizing enzymes and transporters, vacuolization and inflammation.<sup>143, 146, 149</sup> Many of these changes are dependent upon Stearoyl-CoA desaturase 1 (*Scd1*) gene expression, which is the rate-limiting step in monounsaturated fatty acid biosynthesis.<sup>146</sup> TiPARP, another AHR target gene, suppresses gluconeogenesis by regulation of posttranslational modification of PGC-1 $\alpha$  and PEPCK.<sup>142, 145</sup> Decreased gluconeogenesis is a dioxin-induced response, which can lead to hypoglycemia.<sup>81</sup> TiPARP induction depletes NAD<sup>+</sup>, deactivates SIRT3, decreases SOD2 activity, and, consequently, induces oxidative stress that triggers liver injury with lipid accumulation.<sup>150</sup> Another TCDD-induced metabolic dysfunction is disruption in tryptophan homeostasis.<sup>151</sup> TCDD causes inhibition of liver tryptophan pyrrolase and, conversely, increase of free tryptophan levels in blood plasma in TCDD-susceptible Long-Evans rat strain. It should also be noted that tryptophan metabolites have been proposed to be endogenous ligands for the AHR (see Ligands of AHR).

Many studies have been reported that oxidative stress is a main dioxin-induced response.<sup>84, 152-154</sup> CYP1A1 and CYP1B1 produce reactive oxygenate metabolites and this can cause oxidative stress, which consequently would elevate protein amounts and enzymatic activities of SOD and GSH and NADPH producing enzymes.<sup>61, 81</sup> Upregulation of Phase II detoxification enzyme by the AHR and NRF2 is also a response of oxidative stress.<sup>84</sup> UGT1-knockout rats have elevated CYP1A1 and CYP1A2 and GSTM1-knockout also caused increases in *Cyp1a1* transcript.<sup>81</sup> Antioxidant treatment attenuates NF- $\kappa$ B activation, which may induce TCDD toxicity.<sup>154</sup> The relationship between oxidative stress and cytokine production has been studied in several metabolic dysfunctions and metal toxic responses.<sup>155-157</sup> Reactive oxidative metabolites can activate transcription factors, such as NF- $\kappa$ B and AP-1, which induce gene expression of cytokines, such as ILs, TNF- $\alpha$  and TGF- $\beta$ . As mentioned previously, gene expression of CYP1A1 and 1A2 are also regulated by cytokines, which induce NF- $\kappa$ B in human and mouse primary hepatocytes.<sup>14, 94</sup> Recent studies using human dendritic cells and mouse thymus revealed that RelA, a subunit of NF- $\kappa$ B, is critical to regulate TCDD-induced AHR signaling or to enhance AHR induction when stimulated with both TCDD and inflammatory stimuli like LPS.<sup>158</sup>

Mitochondria are also considerable sites for oxidative stress induced by TCDD. Livers from C57BL/6 mice exposed to dioxin produced succinate-dependent mitochondrial ROS at complex II and III in a mitochondrial respiration-dependent manner, by decreasing complex IV activity and ATP production.<sup>159</sup> Mitochondrial antioxidant protein, SOD2 does not change in protein levels or enzymatic activities in C57BL/6 mice liver exposed to TCDD.<sup>160</sup> Rather, enzyme activities of mitochondrial glutathione reductase and glutathione peroxidase and the ratio of mitochondrial GSH/GSSG were increased upon TCDD exposure. Interestingly, TCDD caused an AHR-mediated increase in the ratio of mitochondrial GSH/GSSG and a decrease in cytosolic GSH/GSSG ratio due to increased ROS in C57BL6J.<sup>152</sup> Thus, TCDD-induced mitochondrial ROS production and glutathione redox state were AHR-dependent.<sup>152, 159, 160</sup>

Additionally, the study using knockout mice revealed that TCDD-induced mitochondrial oxidative stress in liver is AHR-dependent, but does not require CYP1A1 or CYP1A2.<sup>160</sup> These previous researches led researchers to propose the “TCDD-induced mitochondrial thiol oxidative stress” to explain TCDD-mediated pathologies.<sup>152</sup> This model considers the mitochondrial reduction potential by glutathione as a primary driving force for ROS production. The ratio of GSH/GSSG acts as a switch to open/close the mitochondrial permeability transition pore (MPTP) through glutathione reduction potential. More negative reduction potential (i.e., high GSH/GSSG ratio) closes MPTP and causes mitochondrial hyperpolarization resulting in more electron flow in Q cycle in complex III and reverse electron flow in complex I, which generates more superoxides.

Activities of antioxidative enzymes, SOD, catalase, glutathione peroxidase and glutathione reductase, were decreased in a time-dependent and TCDD dose-dependent manner in rat hepatocytes.<sup>161</sup> Corresponding to the enzyme activities, superoxide production and lipid peroxidation were increased with decreased enzyme activities of complex II and IV of ETC and mitochondrial membrane potential.<sup>161</sup> The recent study with C57BL/6 mice lung showed that induction of CYP1B1 by TCDD exposure increased mitochondrial ROS production and suppressed complex I and IV activities and these changes were accompanied by mitochondrial DNA loss.<sup>78</sup> In addition, cigarette smoke extract exposure for 6 h to lung fibroblast and epithelial cells showed that AHR protected cells from apoptotic cell death by regulating the expression of SOD rather than other antioxidant proteins such as GSH, heme oxygenase 1 and NRF2.<sup>162</sup> As shown in these several studies, AHR-mediated oxidative stress upon TCDD exposure can be mediated by different molecular mechanisms depending on tissue types.

TCDD is considered to be a nongenotoxic carcinogen, but loss of functional NRF2 causes severe oxidative stress resulting in DNA damage in C57BL/6 mice liver.<sup>84</sup> In addition, previous reports have shown that TCDD-induced oxidative stress can also cause both nuclear and mitochondrial DNA damage in C57BL/6 mouse liver.<sup>152</sup> In fact, a higher degree of mitochondrial DNA damage was observed compared to that of nuclear DNA damage following

TCDD exposure and this occurred together with increased GSH/GSSG ratio and mitochondrial membrane hyperpolarization.<sup>152</sup>

It should also be noted that some of the TCDD-induced mitochondrial toxicities might be independent of AHR-mediated transcription. ARNT knockdown in mouse skeletal myoblast C2C12 cells, which causes a lack TCDD-induced AHR-mediated transcription, showed TCDD-induced disruption of mitochondrial membrane potential, reduction in mtDNA gene expression, induction in nuclear *Cox4i1* gene expression, stimulation of calcium-dependent phosphatase-mediated NF- $\kappa$ B pathway and increase of invasiveness.<sup>163</sup> These responses were related to mitochondrial stress signals and inhibition of mitochondrial transcription. Therefore, TCDD may cause tumor progression through blocking mitochondrial transcription and inducing mitochondrial stress signals.

## **CHAPTER 2. HYPOTHESIS AND SPECIFIC AIMS**

TCDD-induced metabolic disorders such as hepatic steatosis and wasting syndrome suggest that AHR-mediated pathology involves mitochondrial dysfunction. To support this hypothesis, recent studies using high-throughput quantitative real-time PCR have shown that TCDD induces changes in the expression of nuclear genes that encode subunits of the ETC and ATP synthase complexes.<sup>164</sup> Another study demonstrated that the AHR can induce changes in metabolic flux independent of transcription.<sup>165</sup> TCDD exposure for 6 hrs caused AHR-dependent, but transcription-independent, hyperpolarization of the inner membrane of the mitochondria without a change in ATP production. This suggests the possibility that the ATP synthase becomes less efficient following TCDD exposure and requires a higher membrane polarization to maintain ATP levels. In addition, the high-throughput proteomic analysis showed an interaction between the AHR and ATP5 $\alpha$ 1, an ATP synthase subunit, and between the AHR and MRPL40, a mitochondrial ribosomal protein. Interestingly, these interactions were lost upon exposure to TCDD.<sup>165, 166</sup> The cytosolic binding partners of the AHR (i.e., AIP and HSP90) can bind the mitochondrial translocase complex, TOM, and facilitate mitochondrial import of proteins lacking classic MTS, such as the AHR. Moreover, AIP can also interact with other mitochondrial-targeted proteins such as survivin, preornithine transcarbamylase, preaspartate aminotransferase, preserine:pyruvate aminotransferase, and enoyl-CoA hydratase 1.<sup>111, 167</sup> Given this preliminary data and literature documenting a link between TCDD exposure and metabolic dysfunction, this study has focused on elucidating a mechanism of AHR import into mitochondria and evaluation of TCDD-induced AHR-dependent effects on mitochondrial dysfunction.

## **HYPOTHESIS**

The AHR can impact mitochondrial function via direct interaction with the mitochondrial respiratory system and transcriptional regulation of genes that involves in key metabolic pathways. To test this hypothesis, three specific aims have been proposed:

## **SPECIFIC AIMS**

Specific Aim 1. Characterize the mechanism by which the AHR translocates into the mitochondria and determine its localization within the organelle.

Specific Aim 2. Determine AHR-mediated TCDD-induced changes in respiratory efficiency.

Specific Aim 3. Determine the role of AHR in TCDD-induced mitochondrial dysfunction through quantitative analysis of mitochondrial proteomics.

## **CHAPTER 3. MATERIALS AND METHODS**

## **CELL CULTURE**

Mouse hepatoma cell line, hepa1c1c7, were grown in Dulbecco's modified Eagle's Medium (DMEM) (#11965, Gibco, Life Technologies, Grand Island, NY) supplemented with 10% cosmic calf serum (Hyclones, GE, Logan, UT), 1 mM sodium pyruvate (#11360, Gibco), 100 U/mL penicillin and 100  $\mu$ g/mL streptomycin (#15140, Gibco). Mouse hepatoma cell line, C12, were grown in DMEM (#11965, Gibco) supplemented with 10% cosmic calf serum (Hyclones) and 1 mM sodium pyruvate (#11360, Gibco). All cell culture work was performed under standard cell culture conditions (5% CO<sub>2</sub>, 35% humidity and 37 °C) in a NAPCO 7000 incubator (NAPCO, Winchester, VA) unless specified.

## **PREPERATION OF INTRACELLULAR FRACTIONS**

Nuclear, cytosolic, and mitochondrial fractions were isolated using protocols adapted from previous reports.<sup>168-170</sup> Cells were washed with cold PBS (4 °C) and removed from the plate surface by being scraped in mitochondrial buffer A (250 mM sucrose, 20 mM HEPES, 1 mM EDTA, 1 mM EGTA, 1 mM dithiothreitol, and 0.1 mM PMSF). Each sample was then homogenized with 100 strokes in a dounce homogenizer on ice. A 50  $\mu$ L aliquot was saved and represents a whole cell lysate. Insoluble material was removed by centrifugation (400 x g for 10 min at 4 °C), and the pellet was collected for further preparation of a nuclear fraction (see below). The supernatant was cleared by centrifugation (10000g for 10 min at 4 °C). The subsequent supernatant was collected as a cytosolic fraction, and the pellet was resuspended in mitochondrial buffer A. The remaining insoluble material was removed by centrifugation (400 x g for 10 min at 4 °C). The supernatant was further cleared by centrifugation (10000g for 10 min at 4 °C) and aspirated, and the mitochondrial pellet was obtained for further analysis. The nuclear pellet was suspended with nuclear extraction buffer [10 mM Tris (pH 7.5), 1.5 mM

MgCl<sub>2</sub>, 10 mM KCl, 2 mM dithiothreitol, 1 mM sodium orthovanadate, and 0.4 mM PMSF and Complete-mini EDTA-free protease inhibitor (Roche Applied Science, Indianapolis, IN)], incubated for 30 min at 4 °C, and, then, cleared by centrifugation (17000g for 30 min at 4 °C). The supernatant was collected for nuclear fraction. Each intracellular fraction was stored at -80°C until appropriate assays were performed.

### **TRYPSIN TREATMENT OF DIGITONIN EXTRACTED MITOCHONDRIA**

Protease protection in combination with digitonin extraction of mitochondria was adapted from the previous report.<sup>171</sup> Briefly, purified mitochondria, which were washed with mitochondrial buffer A without dithiothreitol and PMSF and diluted to 1 µg/µL, were treated with different concentrations of digitonin (final concentration = 0, 0.2, 0.4, 0.6, 1.0, 1.5, 2.0 mg digitonin/mg protein) and 100 µg trypsin/mL. Samples were rotated in a cold room for 30 min and digestion was stopped with the addition of 266 µL of cold 20% trichloroacetic acid for 400µg of mitochondria. After vortexing immediately, samples were incubated at 65 °C for 5 min, and then on ice for 1 h. Samples were pelleted by centrifugation (17000g for 10 min) and washed with 1 mL of cold acetone. After centrifugation at 17000g for 5 min, pellets were dried on ice for 10 min and dissolved in 80 µL of 1X Laemmli sample buffer. 1 µL of 1 M Tris was added to adjust sample pH and 35 µL of each sample was loaded on 4~12% NuPAGE gel (Invitrogen, Life Technologies) for Western blot analysis.

### **siRNA KNOCKDOWN OF AIP OR TOM20**

Hepa1c1c7 cells were grown in 15 cm plates. When cells were 50% confluent, the siRNAs specific for AIP (Ambion s62179 (siAIP1) and s62181 (siAIP2), Life Technologies) and the Silencer® Select Negative Control no. 1 siRNA (Ambion) were transfected into hepa1c1c7

cells using Lipofectamine 2000 (Invitrogen) following the manufacturer's protocol. For TOM20 knockdown, the siRNA for TOM20 proteins (Tom20 ON-TARGET plus, SMARTpool L-006487-01-0005, Dharmacon, GE) and the nontargeting siRNA (Dharmacon, GE) were transfected into hepa1c1c7 cells. After a 72 h incubation, cells were harvested with 1 mL of mitochondrial buffer A per 15 cm plate after being washed with cold PBS (4 °C) three times. Cells were stored at -80 °C until purification of nuclear, cytosolic, and mitochondrial fractions was performed.

### **HSP90 INHIBITION BY GELDANAMYCIN**

Hepa1c1c7 cells were grown in 15 cm plates. When cells were 50% confluent, they were treated with geldanamycin (GA, 32 nM or 100 nM) or DMSO. After incubation (72 h), cells were harvested with 1 mL of mitochondrial buffer A per 15 cm plate after being washed with cold PBS (4 °C) three times. Cells were stored at -80 °C until purification of nuclear, cytosolic, and mitochondrial fractions was performed.

### **WESTERN BLOTTING**

The same amount of protein from each sample was separated by sodium dodecyl sulfate-polyacrylamide gel electrophoresis (SDS-PAGE) and transferred to a nitrocellulose membrane. The nitrocellulose membrane was probed with one of the following antibodies: rabbit polyclonal anti-AHR BEAR3 (generous gift from Dr. Christopher Bradfield, University of Wisconsin-Madison) for the samples from AIP and TOM20 knockdown, HSP90 inhibition and digitonin/trypsin treatment to hepa1c1c7 cells, rabbit anti-AHR (BML-SA210, Enzo Life Sciences Inc., Farmingdale, NY) for digitonin/trypsin treatment to hepa1c1c7 cells exposed to TCDD, goat polyclonal anti-AIP (#115588, Abcam, Cambridge, MA), rabbit polyclonal anti-LDH (a generous gift from Dr. John Wang, Michigan State University), rabbit anti-histone H3 (ab1791, Abcam),

mouse monoclonal anti-ATP5 $\alpha$  (ab14748, Abcam), rabbit polyclonal anti-HSP90 (ab19021, Abcam), mouse monoclonal anti-COX4 (A21348, Invitrogen), mouse monoclonal  $\alpha$ -tubulin (ab28439, Abcam), rabbit polyclonal anti-TOM20 (sc-11415, Santa Cruz Biotechnology, Dallas, TX), mouse monoclonal anti-SMAC (NB500-213, Novus Biologicals, Inc., Littleton, CO), rabbit polyclonal anti-ENTPD2 (ABIN1385820, Antibodies-online, Inc., Atlanta, GA), rabbit polyclonal anti-ACOT2 (ABIN405459, Antibodies-online Inc.), rabbit polyclonal anti-H6PD (ab170895, Abcam), rabbit polyclonal anti-CPOX (ab102938, Abcam), rabbit polyclonal anti-COX4I1 (ABIN310391, Antibodies-online Inc.), rabbit polyclonal anti-CYB5A (ABIN1529444, Antibodies-online Inc.), horseradish peroxidase-conjugated donkey anti-goat IgG (sc-2033, Santa Cruz Biotechnology), goat anti-rabbit IgG (sc-2004, Santa Cruz Biotechnology), or goat anti-mouse IgG (sc-2005, Santa Cruz Biotechnology). The western blot was visualized with an ECL Western blot system (Pierce).

## **OXYGEN CONSUMPTION RATE (OCR) MEASUREMENT**

OCR was measured using an XF24 Extracellular Flux Analyzer (Seahorse Bioscience, Billerica, MA) as described in the manufacturer's instruction. Briefly, hepa1c1c7 cells were plated in growth medium at 20000 cells/well and c12 cells at 40000 cells/well. After 24 h, the culture medium was then replaced with specific XF24 assay medium containing TCDD (10 nM or 30 nM) or 0.03% DMSO (vehicle control). XF24 assay medium consisted of DMEM base (#D5030, Sigma-Aldrich, St. Louis, MO) supplemented with 25 mM glucose, 31 mM NaCl, 1 mM sodium pyruvate (#11360, Gibco), 2 mM GlutaMAX (#35050, Gibco), and 15 mg/L phenol red (#P3532, Sigma-Aldrich). Measurement of OCR was started 90 min after switching to XF24 assay medium containing TCDD or DMSO and the inhibitors of ETC and OXPHOS system were injected in the following order: oligomycin A (0.5  $\mu$ M), FCCP (1.0  $\mu$ M for 1c1c7 and 0.5  $\mu$ M for c12 cells), and antimycin A (0.5  $\mu$ M). The concentrations of inhibitors for each cell line were

optimized by measuring OCR in XF24 assay medium. The OCR (picomoles per minute) was divided by the number of cells plated for each well and parameters related to mitochondrial function were calculated by the manufacturer's software, XF Mito Stress Test Report Generator, and the equation in the previous study.<sup>172</sup>

## **STATISTICAL ANALYSIS**

The result of respiratory parameters was analyzed for significant differences by analysis of variance (ANOVA) followed by Tukey's post hoc test.

## **ENZYMATIC ASSAY OF OXPHOS SYSTEM**

The activities of the individual ETC complexes, ATP synthase and citrate synthase were determined as previously described with slight modifications.<sup>173, 174</sup> Hepa1c1c7 and c12 cells were exposed to 30 nM TCDD or 0.01% DMSO as a vehicle control for 6 or 24 h when cells had reached 70% confluency. Cells were washed with cold PBS (4 °C) and removed from the plate surface by being scraped in mitochondrial buffer A. Mitochondria were prepared from each treated cells as described above. Each enzyme solution was prepared by suspension of mitochondrial pellets either in a hypotonic buffer [25 mM KPO<sub>4</sub> (pH 7.4) and 5 mM MgCl<sub>2</sub>] for citrate synthase, complex I, complex II, complex IV, and complex V or in mitochondrial buffer A for complex II+III and complex III. After three cycles of freezing/thawing, protein concentrations were determined. The enzyme activities were determined at 37 °C for complex I and V and at 30 °C for the other ETC complexes and citrate synthase. The enzyme activity was calculated by

$$(\Delta\text{Abs}/\text{min}) \times (\text{total assay volume}) / [\epsilon \times (\text{mitochondrial volume}) \times (\text{mitochondrial concentration})]$$

with units of micromoles per min per milligram ( $\epsilon$ : extinction coefficient). The enzymatic activity was calculated as a ratio, dividing each activity in micromoles per min per milligram protein by the citrate synthase activity. The absorbance for each enzymatic activity was measured using a SpectraMax M2 spectrophotometer (Molecular Devices, Sunnyvale, CA). Cytochrome c was bovine heart cytochrome c.

### ***Citrate Synthase Assay***

5  $\mu\text{g}$  of each enzyme solution was incubated with citrate synthase buffer [50 mM  $\text{KPO}_4$  (pH 7.4), and 0.1 mM DTNB] containing 100  $\mu\text{M}$  acetyl CoA, in a cuvette for 5 min. The change of absorbance was measured at 412 nm for 2 min for reference. After addition of 100  $\mu\text{M}$  oxaloacetate, the change in absorbance at 412 nm was recorded for 3 min. Enzyme activity was calculated with  $\epsilon$  for the thionitrobenzoate anion ( $13.6 \text{ mM}^{-1}\text{cm}^{-1}$ ).

### ***Complex I Assay***

50  $\mu\text{g}$  of each enzyme solution was mixed with complex I buffer [50 mM  $\text{KPO}_4$  (pH 7.4), 140  $\mu\text{M}$  NADH, 1 mM KCN, 10  $\mu\text{M}$  antimycin A, 0.1% BSA, and 50  $\mu\text{M}$  DCPIP] with 1% ethanol and 50  $\mu\text{M}$  Coenzyme  $\text{Q}_1$  ( $\text{CoQ}_1$ ) in a cuvette. The change in absorbance at 340 nm was recorded for 3 min. Reference was measured in the presence of 2.5  $\mu\text{M}$  rotenone (dissolved in ethanol). Enzyme activity was calculated with  $\epsilon$  for the NADH ( $6.22 \text{ mM}^{-1}\text{cm}^{-1}$ ).

### ***Complex II assay***

10  $\mu\text{g}$  of each enzyme solution was incubated with complex II buffer [50 mM  $\text{KPO}_4$  (pH 7.4), 10 mM succinate, 1 mM KCN, 2.5  $\mu\text{M}$  rotenone, and 10  $\mu\text{M}$  antimycin A] for 10 min in a cuvette. After addition of 50  $\mu\text{M}$  DCPIP, the change in absorbance at 600 nm was recorded for 2

min for reference. The change in absorbance at 600 nm was then recorded for 3min in the presence of 50  $\mu\text{M}$  CoQ<sub>1</sub>. Enzyme activity was calculated with  $\epsilon$  for the DCPIP ( $19.1 \text{ mM}^{-1}\text{cm}^{-1}$ ).

### ***Complex II+III assay***

10  $\mu\text{g}$  of each enzyme solution was incubated with complex II+III buffer [50 mM KPO<sub>4</sub> (pH 7.4), 10 mM succinate, 1 mM KCN, 2.5  $\mu\text{M}$  rotenone, 0.1% BSA, 0.075% EDTA, and 1 mM ATP] in a cuvette for 5 min. Upon addition of 32  $\mu\text{M}$  cytochrome c, absorbance at 550 nm was recorded for 5 min. The reference was measured in the absence of cytochrome c. Enzyme activity was calculated with  $\epsilon$  for the reduced cytochrome c ( $19.6 \text{ mM}^{-1}\text{cm}^{-1}$ ).

### ***Complex III assay***

5  $\mu\text{g}$  of each enzyme solution was mixed with complex III buffer [50 mM KPO<sub>4</sub> (pH 7.4), 1 mM n-dodecyl maltoside, 1 mM KCN, 2.5  $\mu\text{M}$  rotenone, and 0.1% BSA] with 100  $\mu\text{M}$  decylbenzolquinol and 30  $\mu\text{M}$  cytochrome c in a cuvette. The change in absorbance at 550 nm was recorded for 3 min. Cytochrome c was fully reduced at the end of the measurement with dithionite. The reference was measured without enzyme solution. Enzyme activity was calculated with  $\epsilon$  for the reduced cytochrome c ( $19.6 \text{ mM}^{-1}\text{cm}^{-1}$ ).

### ***Complex IV Assay***

Reduced cytochrome c was prepared using sodium dithionite. 10  $\mu\text{g}$  of each enzyme solution was mixed with complex IV buffer [40 mM KPO<sub>4</sub> buffer (pH 6.8), 0.5% Tween 80, and 0.4 mg/mL reduced cytochrome c] in a cuvette. The change in absorbance at 550 nm was recorded for 2 min. 5 mM potassium ferricyanide was added to fully oxidized cytochrome c at the end of the measurement. The reference was measured without enzyme solution. Enzyme activity was calculated with  $\epsilon$  for the reduced cytochrome c ( $19.6 \text{ mM}^{-1}\text{cm}^{-1}$ ).

### ***Complex V Assay***

Complex V buffer [40 mM Tris-HCO<sub>3</sub> (pH 8.0), 1 mM EGTA, 5 mM MgCl<sub>2</sub>, 0.2 mM NADH, 2.5 mM phosphoenolpyruvate, 0.5 μM antimycin A, 15 μM CCCP, 50 μg/mL lactate dehydrogenase, and 50 μg/mL pyruvate kinase] was incubated with 2.5 mM ATP for 2 min in a cuvette. After 10 μg of each enzyme solution was added to the above mixture, the change in absorbance at 340 nm was recorded for 5 min. The reference was measured in the presence of 2 μM oligomycin for 5 min. Enzyme activity was calculated with ε for the NADH (6.22 mM<sup>-1</sup>cm<sup>-1</sup>).

## **STABLE ISOTOPIC LABELING BY AMINO ACIDS IN CELL CULTURE (SILAC) AND QUANTITATIVE PROTEOMIC ANALYSIS**

### ***Preparation of Mitochondrial Proteins***

Cells were grown in SILAC<sup>TM</sup>-DMEM supplemented with 10% dialyzed fetal bovine serum, 1 mM sodium pyruvate, 2 mM L-glutamine, 100 μg/mL L-arginine, and 100 μg/mL L-lysine (light L-lysine HCl/L-arginine, medium <sup>13</sup>C<sub>6</sub>-L-lysine HCl/<sup>15</sup>N<sub>4</sub>-L-arginin, or heavy <sup>13</sup>C<sub>6</sub><sup>15</sup>N<sub>2</sub>-L-lysine HCl/<sup>13</sup>C<sub>6</sub><sup>15</sup>N<sub>4</sub>-L-arginine (SILAC<sup>TM</sup> media kit, Invitrogen and Cambridge Isotope Laboratories)) for 5 cell doublings to insure full incorporation of labeled amino acids into cellular proteins. Cells were then treated with 10 nM TCDD or 0.01% DMSO (vehicle control) for 72 h as described in Figure 3. Each treated cells were harvested and mitochondrial fractions were isolated as described above. After protein quantification, equal amount of proteins (35μg) labeled with light, medium, or heavy amino acids within one experimental set were combined. When samples from the four independent experimental were collected, proteins were separated by SDS-PAGE.

### **Mass Spectrometry (MS)**

SDS-PAGE gels were divided into 10 equal slices, and each slice was digested with trypsin by in-gel digestion according to Shevchenko, *et al.* with modifications.<sup>175</sup> Peptides were extracted from the gel and dissolved in 2% acetonitrile/0.1% trifluoroacetic acid. Peptides were automatically injected by a Thermo EASYnLC 1000 onto a Thermo Acclaim PepMap RSLC 0.075mm x 250mm C18 column (Buffer A = 99.9% Water/0.1% Formic Acid, Buffer B = 99.9% Acetonitrile/0.1% Formic Acid) and eluted over 90 min with a gradient of 2%B to 30%B in 79 min, ramping to 100%B at 80 min and held at 100%B for the duration of the run. Eluted peptides were sprayed into a ThermoFisher Q-Exactive mass spectrometer using a FlexSpray spray ion source. Survey scans were taken in the Orbi trap (70000 resolution, determined at m/z 200) and the top ten ions in each survey scan were then subjected to automatic higher energy collision induced dissociation (HCD) with fragment spectra acquired at 17500 resolution.

### **Data Analysis**

The resulting MS/MS spectra were converted to peak lists using MaxQuant, v1.4.1.2 ([www.maxquant.org](http://www.maxquant.org)), and searched against a database containing Uniprot Mouse protein sequences ([www.uniprot.org](http://www.uniprot.org)) and appended with common laboratory contaminants using the Andromeda search algorithm, a part of the MaxQuant environment.<sup>176, 177</sup> Assignments validated using the MaxQuant maximum 1% false discovery rate (FDR) confidence filter are considered true. Andromeda parameters for all databases were as follows: quantification triple SILAC labeling: light (Arg0, Lys0), medium (Arg4, Lys6), heavy (Arg10, Lys8); allowing maximum 2 missed trypsin sites, fixed modification of carbamidomethyl cysteine, variable modification of oxidation of methionine; peptide tolerance of +/- 5ppm, fragment ion tolerance of 0.3 Da and FDR calculated using randomized database search. From each quantified SILAC labeling, three isotope ratios were calculated in each independent experiment. To ensure that

each independent set provided similar results, ratios from identical treatments and the same cell lines between each independent set were compared with a Pearson's Correlation Coefficient (r). Briefly, the ratios of an identical protein were matched from two independent sets for the same cell type, 1c1c7 or c12, exposed to the same treatment and undetected proteins in both independent sets were removed prior to correlation analysis. Data from the matched independent sets were log-transformed and checked with a histogram and QQ plot prior to correlation to ensure comparison of normal distributions. Pearson's Correlation Coefficients were  $\geq 0.5$  in comparing each identical treatment between the 4 independent samples sets. Subsequently, data were combined and averaged across all independent sets to obtain triplicate for each treatment and each cell type. The triplicate ratios were averaged to obtain mean fold changes for all detected proteins and mean |fold changes|  $\geq 2$  were considered significant. Significant mean fold changes of identical proteins from differing treatments were matched and, subsequently, compared with a Student's t-test with the Benjamini-Hochberg multiple comparison correction to assess type I error. Adjusted p-values  $\leq 0.05$  were considered significant. Python version 2.7.6 was used for all data processing and R version 3.1.2 was used for all statistical analyses.

## **PROTEIN CONCENTRATION DETERMINATION**

Protein concentrations for samples used for the SILAC experiments were determined using Pierce<sup>TM</sup> BCA protein assay kit (Thermo Scientific, Waltham, MA). Protein concentrations for samples used for all other experiments were determined using Bio-Rad (Hercules, CA) Bradford assay kit and BSA standards.<sup>178</sup>



## **CHAPTER 4. RESULTS**

## CHARACTERIZATION OF MITOCHONDRIAL AHR IMPORT

### *Identification of a Mitochondrial Compartment of AHR Location*

To examine the sub-compartmental localization of AHR within the mitochondria, protease protection and digitonin extraction assays were performed. Mitochondria from hepa1c1c7 cells were treated with trypsin in the absence and presence of increasing concentrations of digitonin, and Western blot analysis was performed to detect proteins that remained in mitochondrial pellets (Figure 4-1). In the presence of trypsin alone, the OM protein TOM20 was lost from the mitochondrial pellet, while AHR remained, suggesting that the AHR is not bound to the mitochondria nonspecifically. Upon the addition of increasing amounts of digitonin, the AHR was lost from the pellet in a similar pattern as the IMS marker, SMAC, suggesting that most of the AHR is found within this compartment.

To further explore the mitochondrial localization of the AHR, hepa1c1c7 cells were treated with DMSO (vehicle control) or TCDD (10 nM). In the presence of DMSO, the AHR was localized to the IMS, confirming the results from naïve cells (Figure 4-2). TCDD exposure for 6 h decreased the level of AHR within the IMS compared to the DMSO-treated controls, suggesting that AHR ligands can impact the mitochondrial localization of the receptor. Similar results were observed following 24 h of TCDD exposure (Figure 4-2). In addition, the overall level of AHR within the mitochondria was also decreased by TCDD exposure (compare lane 1 and 4, Figure 4-2). This corresponded to the decreased level of cellular AHR isolated from the same cells exposed to TCDD (compare lane 7 and 8, Figure 4-2)). Thus, TCDD exposure induced both cytosolic and mitochondrial proteolysis of the AHR.

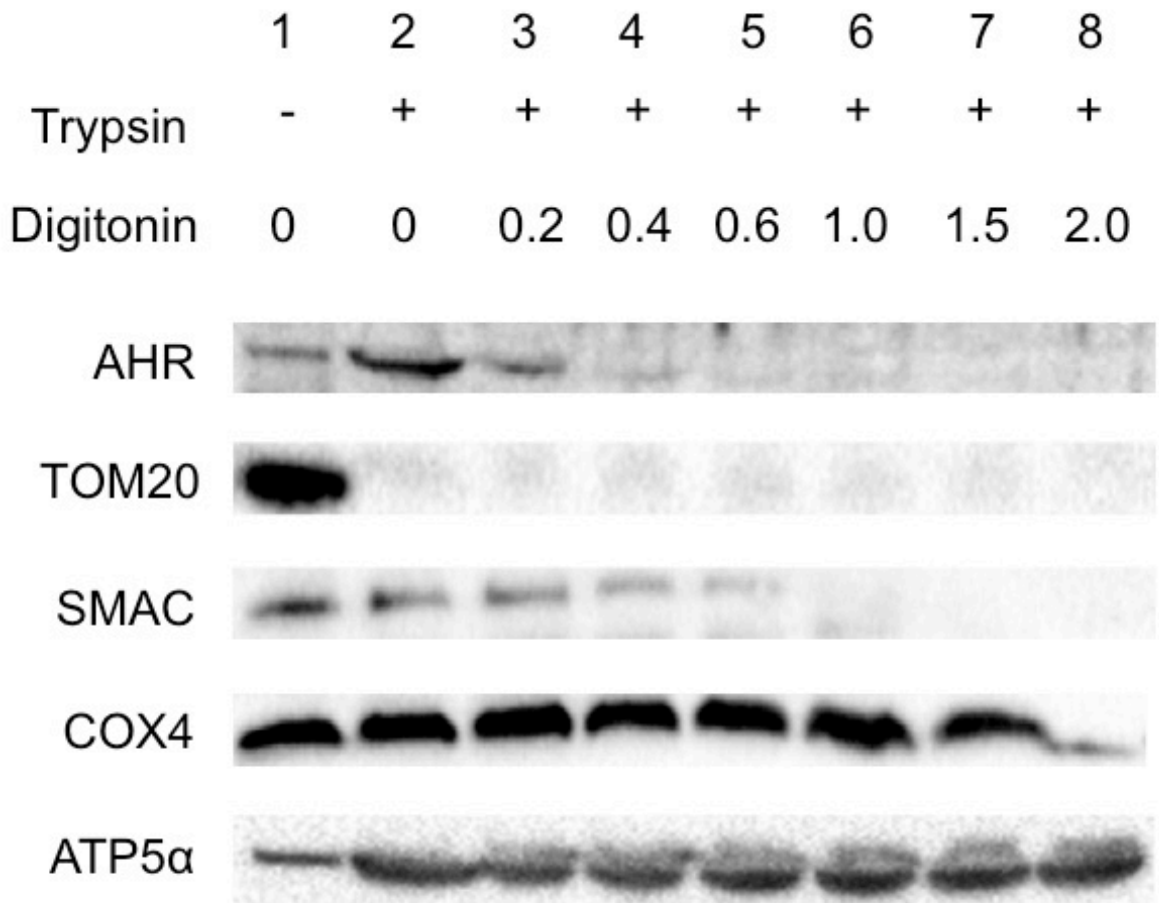


**Figure 4-1. Mitochondrial sub-compartment analysis.**

Accessibility of trypsin to proteins within isolated mitochondria of hepa1c1c7 cells following exposure to increasing concentration of digitonin (mg of digitonin/mg of protein) was evaluated. Proteins that remained in mitochondrial pellets were analyzed by Western blotting. TOM20 was used as an outer-membrane (OM) marker. SMAC was an inter-membrane space (IMS)-localized protein. COX4 was a mitochondrial inner-membrane (IM) protein and ATP5 $\alpha$  was a mitochondrial matrix protein. Results shown are representative of 3 independent experiments.

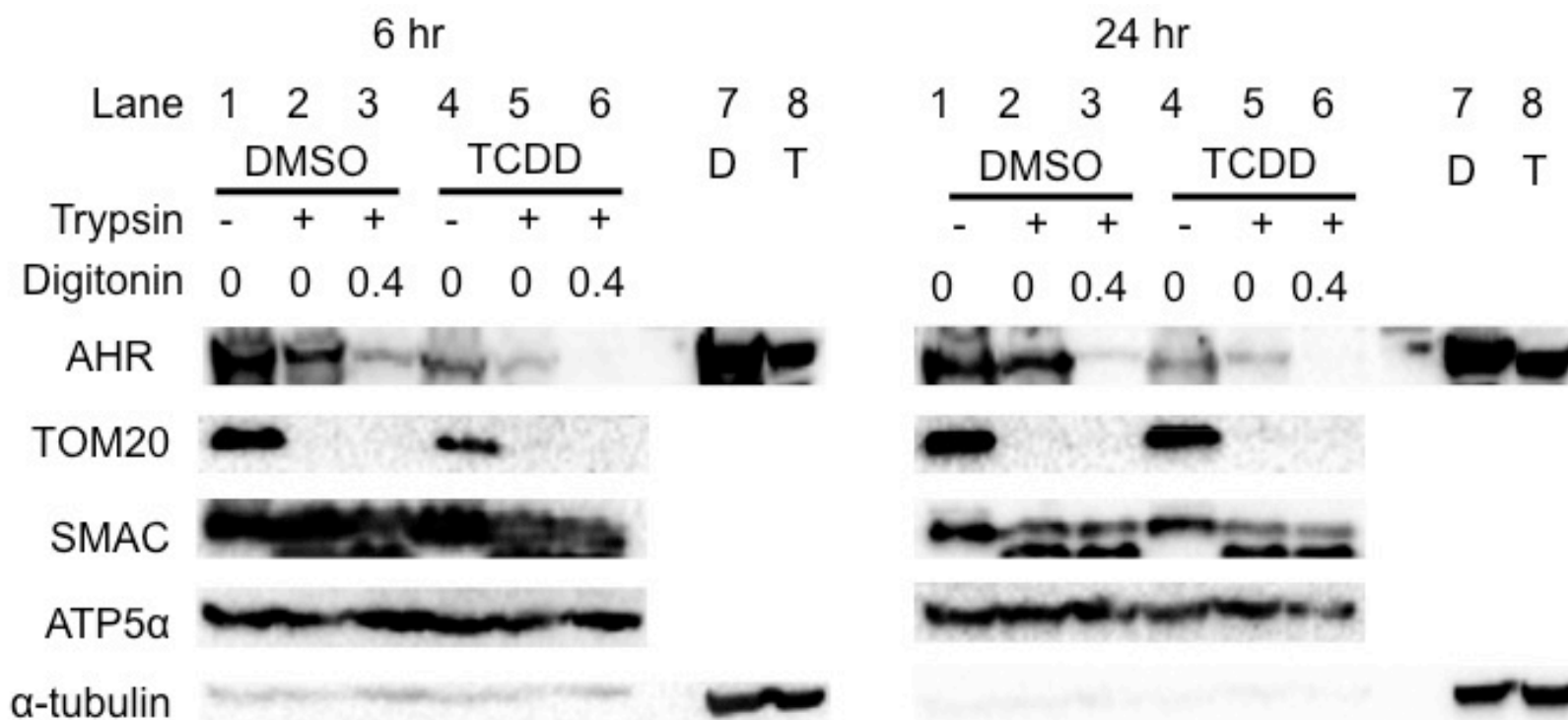


**Figure 4-2. The effects of ligand exposure on protease accessibility to digitonin extracted mitochondria.**

Hepa1c1c7 were exposed to 0.01% DMSO or 10 nM TCDD for 6 or 24 h. Isolated mitochondria were trypsinized (lane 2, 3, 5 and 6) in the absence (Lane 1, 2, 4, and 5) or presence of digitonin (0.4 mg of digitonin/mg of protein, lane 3 and 6). Proteins that remained in mitochondrial pellets were analyzed by Western blotting. TOM20 was used as an OM marker. SMAC was an IMS-localized protein. ATP5α was a mitochondrial matrix protein. α-tubulin was a cytosolic marker. Cytosolic proteins (lane 7 and 8) were included to assess level of TCDD-induced AHR degradation. D: DMSO, T: 10 nM TCDD. Results shown are representative of 3 independent experiments.

### ***Prediction of MTS of AHR***

To predict a MTS in AHR, the MitoProtII, a web-system for prediction of N-terminal MTS was used (<http://ihg.gsf.de/ihg/mitoprot.html>).<sup>179</sup> The MitoProtII predicted 17 amino acids N-terminal targeting of the mouse AHR (NP\_038492.1) with a probability of 0.74 and 18 amino acids of the human AHR (NP\_001612.1) with a probability of 0.81. The predicted cleavage sequence for the mouse AHR was “MSSGANITYASRKRRK” and for human was “MNSSSANITYASRKRRK.” Both sequences partly overlapped with the sequence for a nuclear localization signal. Another web-system for prediction of N-terminal MTS and cleavage site, MitoFates predicted TOM20 recognition motif at 46-50 amino acids and a cleavage site of mitochondrial-processing peptidase at 38 histidine in mouse AHR.<sup>180</sup>

### ***Change in AHR Expression by AIP Knockdown***

The AIP is known to interact with TOM20. To test whether it is involved in mitochondrial AHR import, AIP was knocked down in hepa1c1c7 cells using siRNA. AHR expression in each subcellular fraction was analyzed by Western blotting (Figure 4-3). The level of AIP expression was decreased approximately 80 and 65% by siAip1 and siAip2, respectively, when compared to a lipomock control (transfectant control) in whole cell lysate. The AIP knockdown by siAip2 was less efficient than siAip1, which, subsequently, caused different degrees in AHR destabilization in cellular fractions. The level of AHR expression in whole cell lysate was decreased by 80% by siAIP1 and 40% by siAip2, respectively. The levels of cytosolic and nuclear AHR were also decreased by 40-60% upon transfection of siAip1 and siAip2. The level of mitochondrial AHR was decreased to approximately 20% expression by siAip1 and 60% expression by siAip2. These results suggest that the AHR in all cellular fractions was destabilized by knockdown of the AIP.

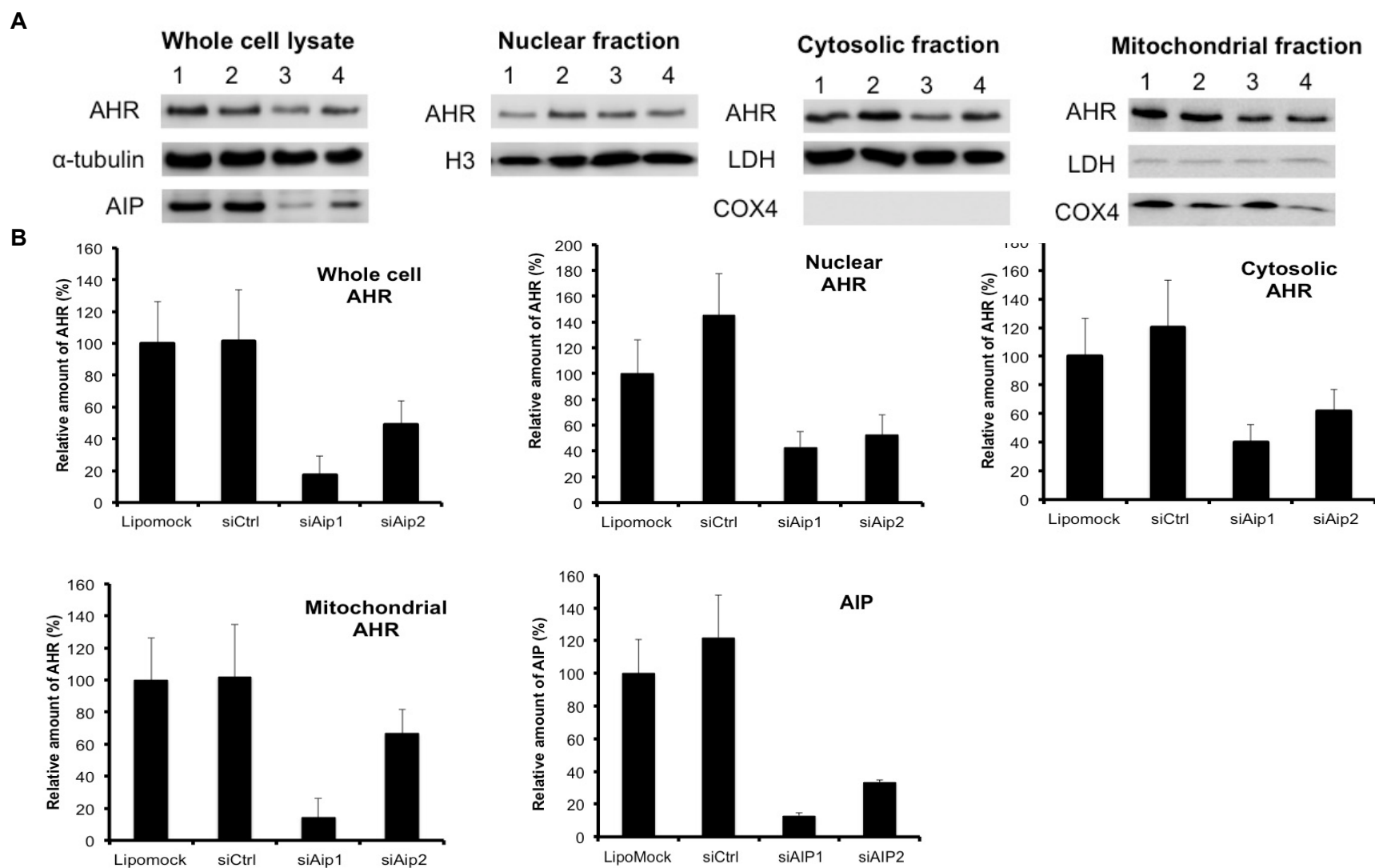
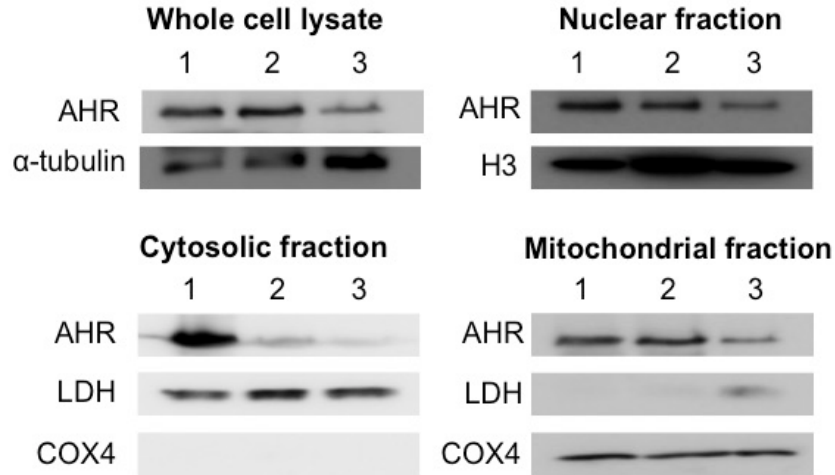
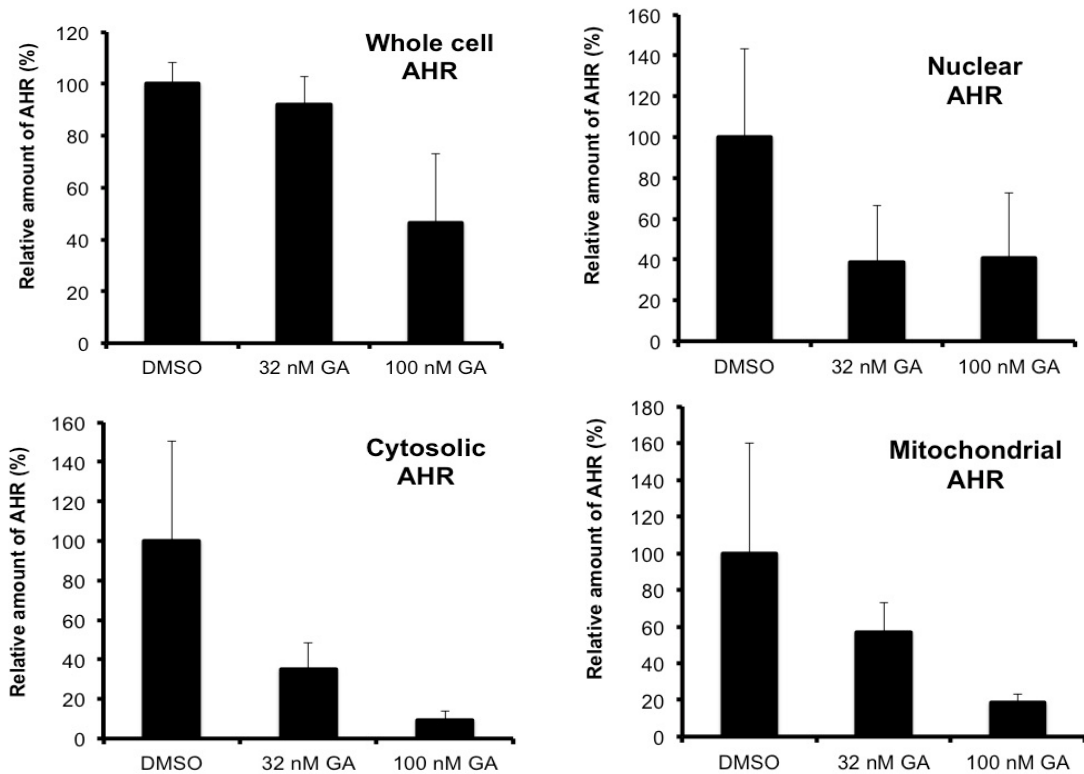


Figure 4-3. The effect of AIP knockdown on the levels of the AHR in cellular fractions of hepa1c1c7 cells.

**Figure 4-3. (cont'd)** siRNA was used to knockdown AIP in Hepa1c1c7 cells. Western blot analysis for AIP and AHR expression was performed from whole cell lysate, and nuclear, cytosolic, and mitochondrial fractions.  $\alpha$ -tubulin was used as a loading control for the whole cell lysate, histone H3 (H3) was a loading control for the nuclear fraction, lactate dehydrogenase (LDH) was a loading control for the cytosolic fraction, and cytochrome c oxidase subunit IV (COX4) was a loading control for the mitochondrial fraction. **(A)** Results shown are representative of 3 independent experiments. Lane 1: lipofectamine treatment (Lipomock), lane 2: 10 nM Silencer® Select Negative Control #1 siRNA (siCtrl), lane 3: 10 nM siRNA1 for AIP (siAIP1), lane4: 10 nM siRNA2 for AIP (siAIP2). **(B)** Densitometry was determined with a Fuji Image analyzer. The levels of expressions of AIP and AHR protein were normalized to each loading control. The normalized protein expression levels were compared with each other by re-normalization with the protein expression from which cells were affected by lipofectamine only (Lipomock). The bars represent mean  $\pm$  the standard errors (n=3).

**A****B**

**Figure 4-4. The effect of geldanamycin (GA)-induced HSP90 inhibition on the level of AHR protein within cellular fraction of hepa1c1c7.**

GA treatment to hepa1c1c7 cells was performed for 72 h. Western blot analysis for AHR expression was performed from whole cell lysate, and nuclear, cytosolic and mitochondrial fraction.  $\alpha$ -tubulin was used as a loading control for the whole cell lysate, histone H3 (H3) was a loading control for the nuclear fraction, lactate dehydrogenase (LDH) was a loading control for the cytosolic fraction, and cytochrome c oxidase subunit IV (COX4) was a loading control for the

**Figure 4-4. (cont'd)** mitochondrial fractions. **(A)** Results shown are representative of 3 independent experiments. Lane 1: DMSO treated (DMSO), lane 2: 32 nM GA treated, lane 3: 100 nM GA treated. **(B)** Densitometry was determined with a Fuji Image analyzer. AIP and AHR protein expression was normalized to each loading control. The normalized protein expression levels were compared each other by re-normalization with the protein expression from which cells were affected by DMSO. The bars represent mean  $\pm$  the standard errors (n=3).

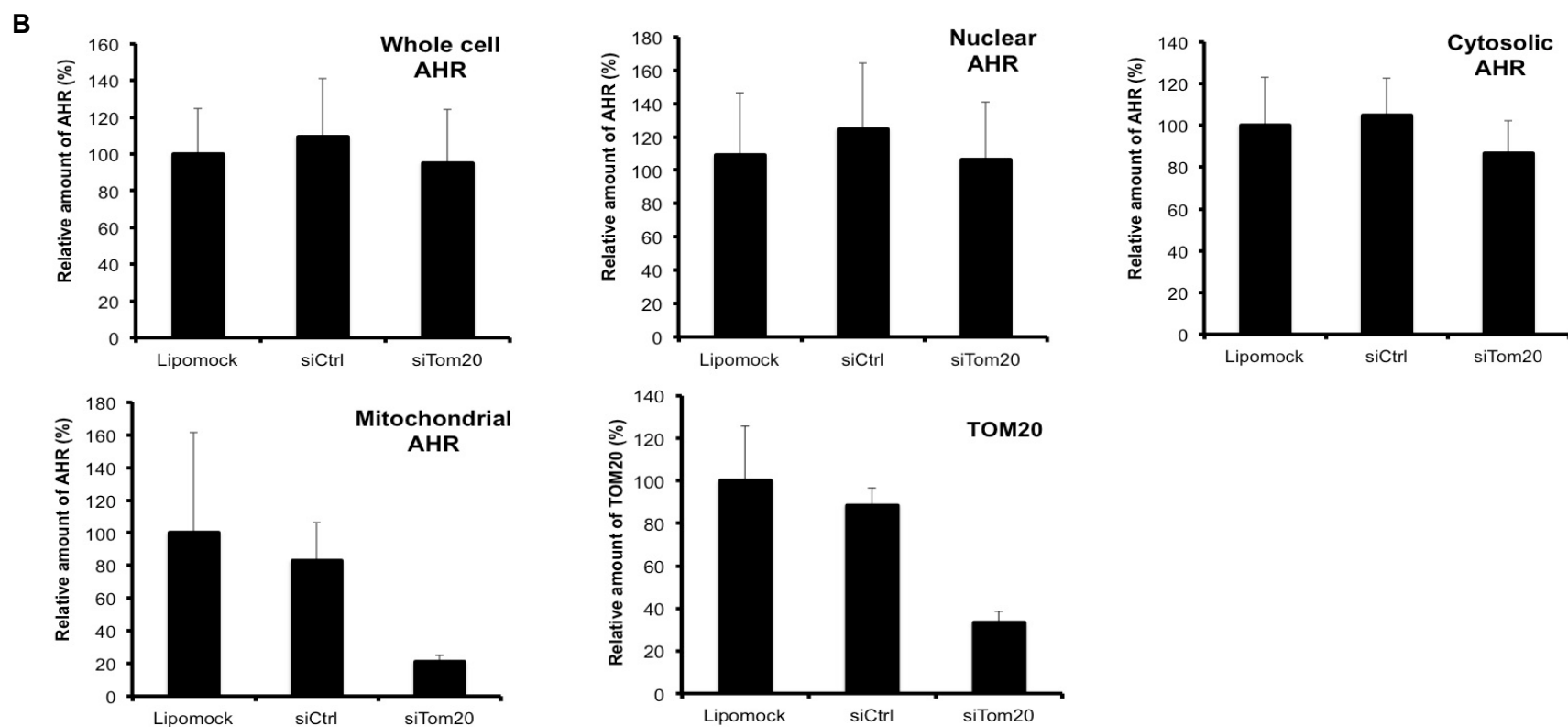
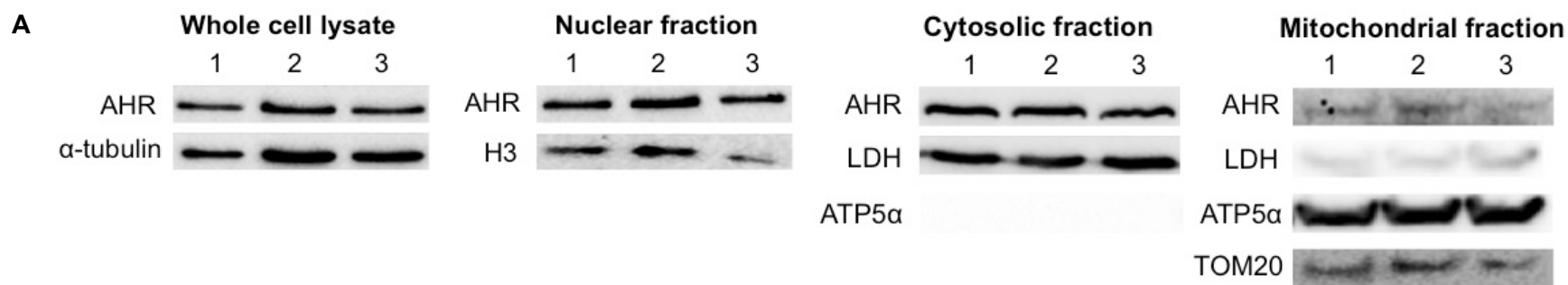


**Figure 4-5.** The effect of TOM20 knockdown on the level of AHR protein in cellular fractions of hepa1c1c7 cells.

**Figure 4-5. (cont'd)** siRNA was used to knockdown TOM20 in Hepa1c1c7 cells. Western blot analysis for TOM20 and AHR expression was performed from whole cell lysate, and nuclear, cytosolic and mitochondrial fractions.  $\alpha$ -tubulin was used as a loading control for the whole cell lysate, histone H3 (H3) was a loading control for the nuclear fraction, lactate dehydrogenase (LDH) was a loading control for the cytosolic fraction and ATP5 $\alpha$  was a loading control for the mitochondrial fraction. **(A)** Results shown are representative of 3 independent experiments. Lane 1: lipofectamine treatment (Lipomock), lane 2: 10 nM nontargeting siRNA (siCtrl), lane 3: 10 nM siRNA for TOM20 (siTOM20). **(B)** Densitometry was determined with a Fuji Image analyzer. The expressions of TOM20 and AHR protein were normalized to each loading control. The normalized protein expression levels were compared each other by re-normalization with the protein expression from which cells were affected by lipofectamine only (Lipomock). The bars represent mean  $\pm$  the standard errors (n=3).

### ***Change in AHR Expression by HSP90 Activity Inhibition***

HSP90 is involved in the trafficking of proteins into the mitochondria, especially those that lack a classic MTS. To test whether HSP90, one of the cytosolic co-chaperone of AHR, is involved in AHR translocation into the mitochondria, the ATPase activity of HSP90 in hepa1c1c7 cells was inhibited by geldanamycin. The level of AHR expression in each cellular fraction except the whole cell lysate was decreased with 40~60% expression by 32 nM geldanamycin treatment compared to that of DMSO control. 90% of AHR expression was observed in a whole cell lysate treated with 32 nM geldanamycin compared to that in cells treated with DMSO. However, inhibition of HSP90 ATPase by 100 nM geldanamycin decreased the level of AHR expression by 50% in whole cell lysate compared to that of DMSO control. The levels of cytosolic and mitochondrial AHR protein were also decreased by 100 nM geldanamycin, showing 9% AHR expression in cytosol and 18% in mitochondria compared to that of DMSO control. However, the nuclear AHR expression of cells treated with 100 nM geldanamycin (41%) was the same as that of 30 nM geldanamycin (38%) (Figure 4-4).

### ***Change in AHR Expression by TOM20 Knockdown***

To test whether TOM20 is involved in import of the AHR into the mitochondria, it was knocked down in hepa1c1c7 cells using siRNA. Following knockdown, the level of expression of AHR in each subcellular fraction was examined by Western blot analysis. The level of TOM20 expression in the mitochondria was decreased by approximately 70% in the siTom20-transfected cells compared to a lipomock control (transfectant control) (Figure 4-5). The amount of AHR found within the mitochondria was also decreased by approximately 70% following siTOM20 transfection compared to a lipomock control (Figure 4-5B). In contrast, there was no change in the level of AHR in the cytosol or nuclear fractions or whole cell lysate, following

knockdown of TOM20. These results suggest that TOM20 is involved in mitochondrial AHR localization.

## **AHR-MEDIATED TCDD-INDUCED MITOCHONDRIAL DYSFUNCTION**

### ***Cellular Respiration in Mouse Hepatoma Cells under TCDD Exposure***

The results presented suggest that a fraction of intracellular AHR can be found within the mitochondria and probably within the IMS. Previous published research has demonstrated that AHR ligands can impact mitochondrial function. To further explore the role of the AHR and AHR ligands in mitochondrial homeostasis, the oxygen consumption rates (OCRs) of two mouse hepatoma cell lines, 1c1c7 (AHR-expressing) and c12 (AHR-deficient), under TCDD exposure were measured. The two cell lines were treated with TCDD (10 or 30 nM) or DMSO (0.01%, vehicle control), and OCR was monitored in the presence of ATP synthase inhibitor, oligomycin A (A), and ETC inhibitors, FCCP (B) and antimycin A (C) (Figure 4-6A and 7A). The key parameters of mitochondrial function, basal respiration, maximal respiration, spare respiratory capacity, and respiratory control ratio were calculated as described in table 4-1. Hepa1c1c7 displayed a TCDD-dose-dependent decrease in basal and maximal respiration that reached significance at 30 nM (Figure 4-6). The hepac12 cells displayed no difference in basal respiration rates following TCDD exposure (Figure 4-7). The hepac12 cells exposed to 10 nM or 30 nM TCDD showed a slight increase in maximal respiration rates following TCDD exposure, but these were not significant when compared to that of the DMSO-treated cells. This induced a significant increase in respiratory control ratio at 30 nM TCDD exposure to hepac12 cells (Figure 4-7). There was no significant difference in spare respiratory capacity in either cell line exposed to TCDD (data not shown).

**Table 4-1. The equations for mitochondrial stress parameters by XF mito stress test reporter generator.**

Parameters	Definition
Basal Respiration	(Last rate measurement before first injection) – (Minimum rate measurement after antimycin-A injection)
Maximal Respiration	(Maximum rate measurement after FCCP injection) – (Minimum rate measurement after antimycin-A injection)
Spare Respiratory Capacity	(Maximal Respiration) – (Basal Respiration)
Respiratory Control Ratio (state3u/state4o)	(Maximal Respiration)/(Proton Leak)

Note: table was adapted from the company's manual and published article.<sup>172</sup>

State3u: state 3 achieved by adding FCCP

State4o: state 4 achieved by adding oligomycin

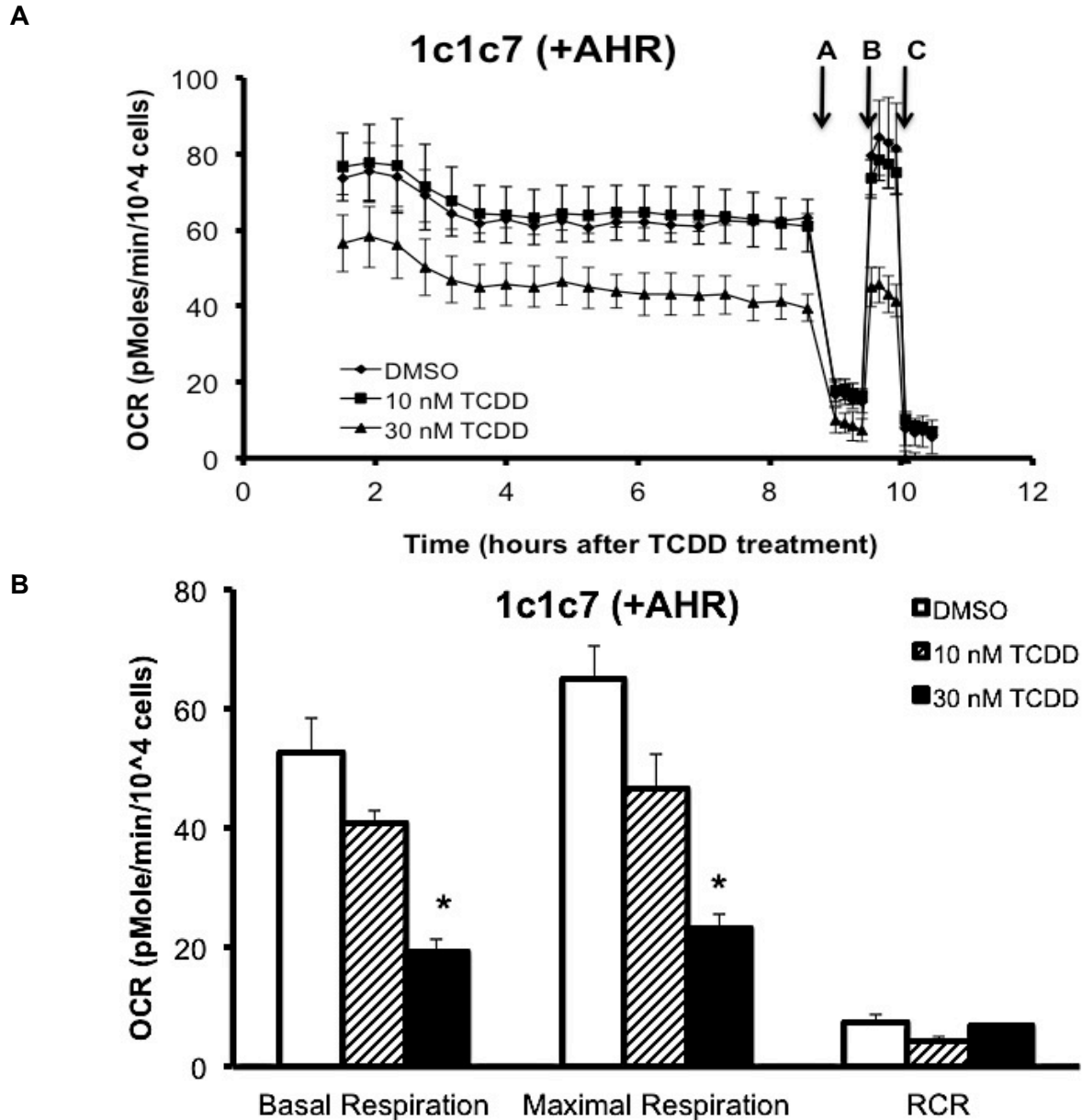


**Figure 4-6. Measurement of oxygen consumption rate (OCR) from hepa1c1c7 cells.**

**(A)** OCR, calculated as (pmole/min/10<sup>4</sup> cells) in hepa1c1c7 cells exposed to 10 nM or 30 nM TCDD or vehicle control (DMSO 0.01%) was measured basally or following addition of (a) oligomycin (0.5  $\mu$ M), (b) FCCP (1  $\mu$ M), and (c) antimycin A (0.5  $\mu$ M). Lines indicate average values  $\pm$  the standard errors (n=3). **(B)** Basal respiration and maximal respiration were calculated by manufacturer's software, the XF Mito Stress Test Report Generator. RCR was calculated by the equation mentioned in the table 4-1. Data were analyzed for significant differences by ANOVA followed by Tukey's post hoc test. A star indicates significant differences at  $p < 0.05$  when compared to vehicle control.

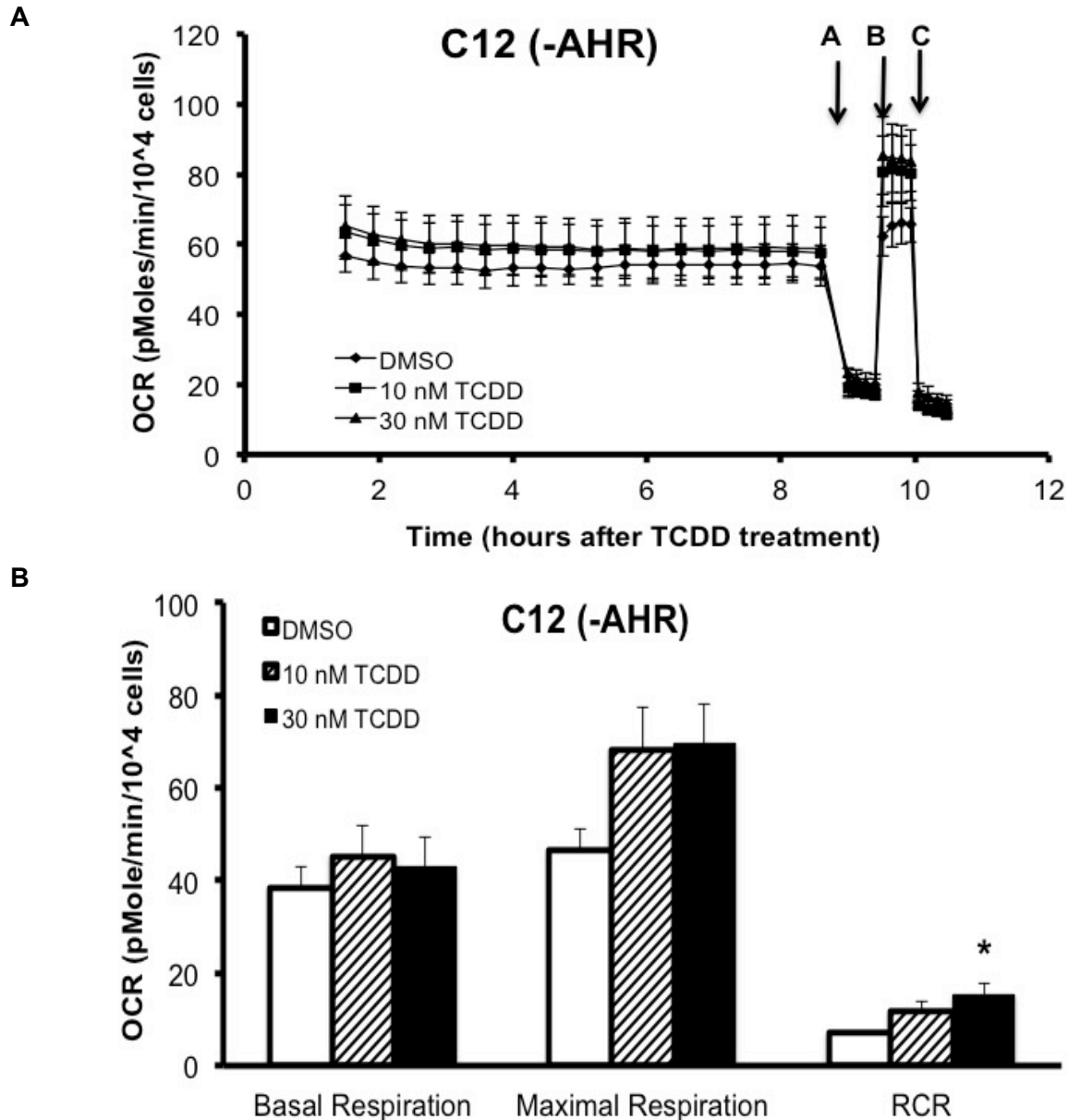


**Figure 4-7. Measurement of oxygen consumption rate (OCR) from hepac12 cells.**

(A) OCR, calculated as (pmole/min/10<sup>4</sup> cells) in hepac12 cells exposed to 10 nM or 30 nM TCDD or vehicle control (DMSO 0.01%) was measured basally or following addition of (a) oligomycin (0.5  $\mu$ M), (b) FCCP (0.5  $\mu$ M), and (c) antimycin A (0.5  $\mu$ M). Lines indicate average values  $\pm$  the standard errors (n=3). (B) Basal respiration and maximal respiration were calculated by manufacturer's software, the XF Mito Stress Test Report Generator. RCR was calculated by the equation mentioned in the table 4-1. Data were analyzed for significant differences by ANOVA followed by Tukey's post hoc test. A star indicates significant differences at  $p < 0.05$  when compared to vehicle control.

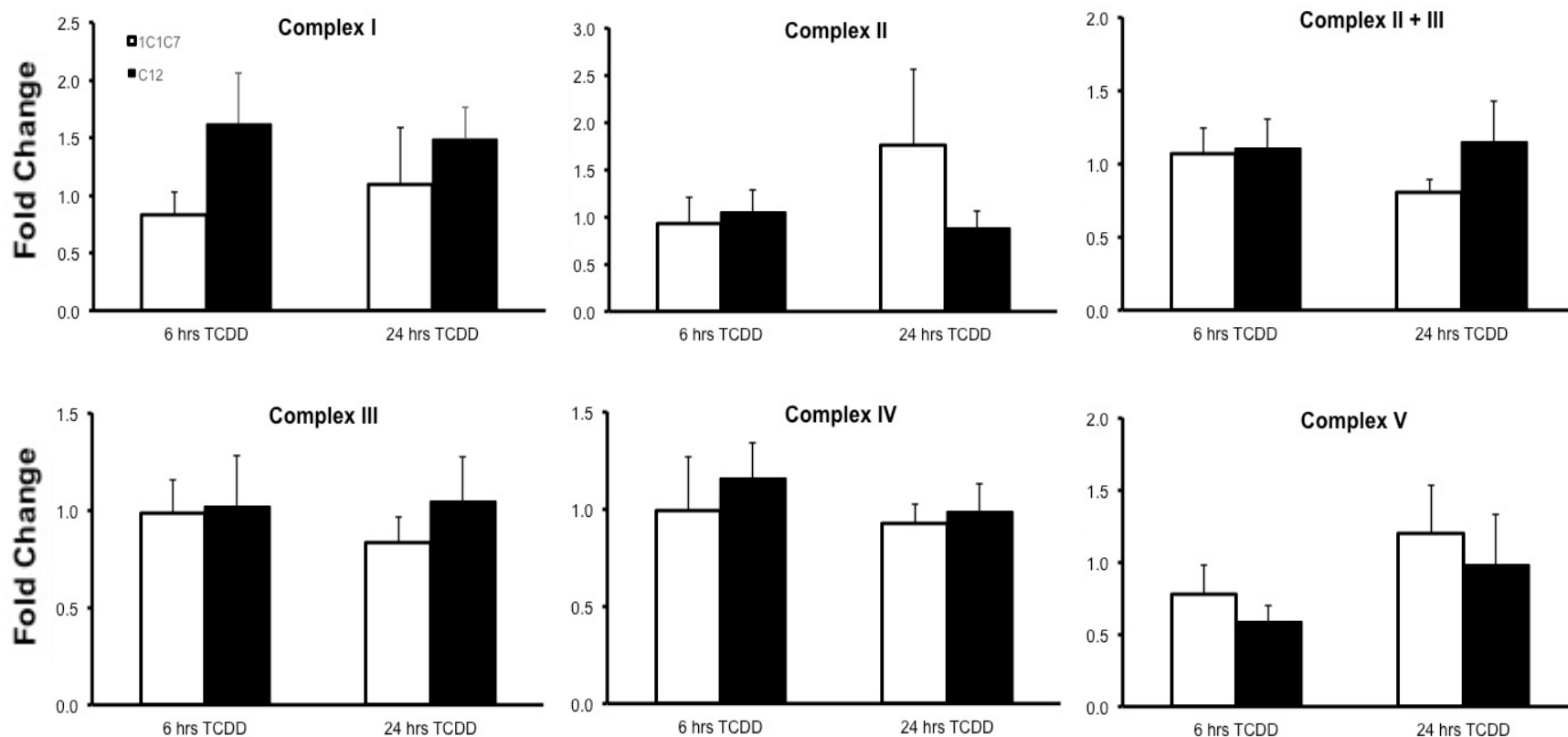


**Figure 4-8. Activities of ETC complexes and ATP synthase.**

The activities of the ETC complexes and ATP synthase were measured with isolated mitochondria from hepa1c1c7 and c12 cells exposed to 30 nM TCDD or vehicle control (DMSO 0.01%) for 6 and 24 h. The activity of each complex was normalized with the activity of citrate synthase (CS). The fold change was calculated by re-normalization of enzyme activity from cells exposed to TCDD with the activity relative to time-matched vehicle control. The bars represent mean  $\pm$  the standard errors (n=4).

### ***Change of OXPHOS Activity in Mouse Hepa Cells upon TCDD Exposure***

Change in TCDD-induced enzyme activity was calculated as a fold change via comparison to the activity relative to time-matched vehicle control (Figure 4-8). The enzyme activity of each ETC complex and ATP synthase was normalized with citrate synthase activity, which represents an assessment of mitochondrial amount and integrity of each sample. TCDD exposure did not change in the activity of complex I from hepa1c1c7 cells, but caused a change in the activity of complex I from hepac12 cells showing over 1.5 fold changes for both 6 h (fold change=1.6) and 24 h (fold change=1.5) though these values were not significant. TCDD exposure for 24 h to hepa1c1c7 cells caused an approximate 2-fold increase in complex II activity. TCDD exposure for 6 h caused a slight decrease in complex V activity in both cells and this decrease was recovered at 24 h exposures. However, the changes in TCDD-induced enzyme activity mentioned above were not significant. TCDD did not cause any changes in activities of the complex III, (II + III), and IV.

### ***Identification of Proteins Differently Expressed upon TCDD Exposure***

Previous reports and the OCR and ETC complex results presented above suggest that the AHR can impact mitochondrial function directly. To determine the role of the AHR in modulating mitochondrial function, a stable isotope labeling by amino acids in cell culture (SILAC) experiment was performed. SILAC-labeled hepa1c1c7 cells and c12 cells that had been exposed to DMSO (0.01%, vehicle control) or TCDD (10 nM) for 72 h were fractionated to isolate mitochondria. Proteins from these purified mitochondria were resolved by 4-12% gradient SDS-PAGE and MS analysis was performed on gel slices as described in the Materials and methods. MaxQuant analysis identified approximately 2,500 proteins. Comparison between hepa1c1c7 TCDD/1c1c7 DMSO (C7T/C7D) and C12 TCDD/C12 DMSO (C12T/C12D) identified about 1,200 proteins. Of these, 164 proteins were differentially regulated (Benjamini-

Hochberg corrected  $p \leq 0.05$ ). 95 were established mitochondrial proteins, 69 were previously assigned to different organelles (Figure 4-9 and table A-1 and A-2). This ratio of mitochondrial proteins versus other organelles' is similar to previous published reports looking at the yeast mitochondrial proteome.<sup>181</sup> The identification of these proteins from other cellular compartments was attributed to various reasons, including misrepresentation due to overexpression, homologous proteins from different organelles, dual localization, and contamination of the mitochondrial preparation. To further prioritize the data, proteins with a mean fold change equal to or above 2 in hepa1c1c7 cells were considered ( $|\text{fold change}| \geq 2$ ). 17 proteins met this criterion for the comparison between 1c1c7TCDD/1c1c7DMSO (C7T/C7D) and c12TCDD/c12DMSO (C12T/C12D) (Table 4-2). Of these differentially expressed proteins, 9 proteins were upregulated and 8 proteins in hepa1c1c7 were downregulated. The upregulated proteins included those involved in metabolic pathways (e.g., H6PD, CPOX and CYB5) and the downregulated proteins included those involved in mitochondrial biogenesis (e.g., WARS2 and MRPS28).

### ***Validation of Proteomic Results***

To verify the SILAC-based proteomic quantification, 6 proteins were measured by Western blot analysis (Figure 4-10). Four upregulated proteins (i.e., H6PD, CPOX and CYB5, ENTPD2), which were identified by ( $|\text{fold change}| \geq 2$ ) cut-offs, were tested (Table 4-2). In addition, two other proteins were assessed (ACOT2 and COX4I1). These proteins were chosen because of their identification in mRNA expression studies and for their potential role in TCDD-induced changes in mitochondrial function (COX4I1) and dyslipidemia (ACOT2).<sup>164</sup>

Density of each western signal was measured and normalized to the density of the control, VDAC1. Western blot analysis was performed three times independently. The density measured for H6PD, CPOX, CYB5, COX4I1 and ACOT2 expression corresponded to the

quantification of MS (Table 4-2 and Figure 4-10). The Western blot analysis of ENTPD2 expression did not agree to the MS data (Figure 4-10). The relationship between three independent Western blot analysis and MS data was summarized in table 4-3.

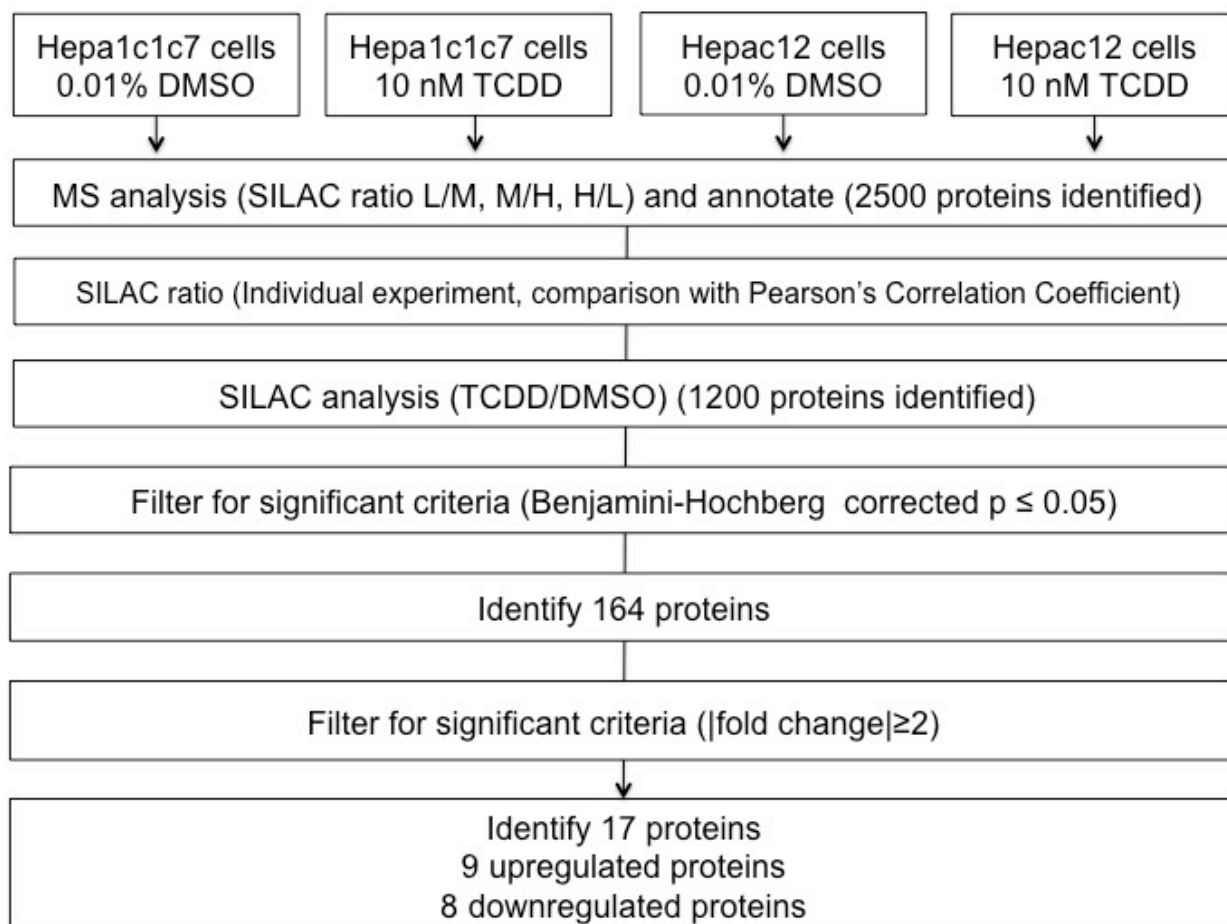


**Figure 4-9. SILAC analysis of differentially expressed proteins by TCDD.**

The data were filtered for differentially expressed by mean  $|\text{fold changes}| \geq 2$  and Benjamini-Hochberg multiple comparison corrected  $p \leq 0.05$ . Datasets were compared to identify AHR-dependently expressed proteins by TCDD exposure.

**Table 4-2. Identified proteins differentially regulated by 10 nM TCDD exposure for 72 h in an AHR-dependent manner.**

Protein Name	Gene Name	Entrez number	C7T/C7D VS C12T/C12D		
			C7T/C7D Mean Ratio	C12T/C12D Mean Ratio	Adjusted P-value
* Ectonucleoside triphosphate diphosphohydrolase 2	<i>Entpd2</i>	12496	7.413	1.196	0.029
Tyrosine-protein kinase receptor UFO	<i>Axl</i>	26362	4.569	0.772	0.106
Tenascin XB	<i>Tnxb</i>	81877	3.416	1.273	0.034
Retinol-binding protein 4	<i>Rbp4</i>	19662	2.859	0.926	0.004
* Coproporphyrinogen-III oxidase, mitochondrial	<i>Cpox</i>	12892	2.433	1.229	0.017
* Cytochrome b5	<i>Cyb5; Cyb5a</i>	109672	2.289	0.997	0.003
V-type proton ATPase subunit D	<i>Atp6v1d</i>	73834	2.139	1.669	0.661
Dehydrogenase/reductase SDR family member 1	<i>Dhrs1</i>	52585	2.051	1.117	0.141
* GDH/6PGL endoplasmic bifunctionalprotein;Glucose 1-dehydrogenase;6-phosphogluconolactonase	<i>H6pd</i>	100198	2.025	1.252	0.051
Collagen alpha-1(XII) chain	<i>Col12a1</i>	12816	0.448	0.989	0.039
Tryptophan--tRNA ligase, mitochondrial	<i>Wars2</i>	70560	0.440	1.056	0.141
Thioredoxin reductase 1, cytoplasmic	<i>Txnrd1</i>	50493	0.401	0.704	0.051
Serine (or cysteine) peptidase inhibitor, clade B, member 9b	<i>Serpinb9b</i>	20706	0.396	1.274	0.088
28S ribosomal protein S28, mitochondrial	<i>Mrps28</i>	66230	0.384	0.969	0.385
Leukocyte surface antigen CD47	<i>Cd47</i>	16423	0.334	1.042	0.017
Myosin-14	<i>Myh14</i>	71960	0.262	1.007	0.033
FYVE, RhoGEF and PH domain-containing protein 5	<i>Fgd5</i>	232237	0.016	0.387	0.385

Note: Proteins included meet fold change (|fold change|≥2) cut-offs.

\*. validated by Western blot analysis.

**Table 4-3. Relationship between MS quantification and Western blot quantification.**

<b>Protein</b>	<b>Western #1</b>	<b>Western #2</b>	<b>Western #3</b>
H6PD	+	+	+
CPOX	+	+	+
CYB5	+	+	+
ACOT2	+	+	NA
COX411	+	-	+
ENTPD2	-	-	-

Note: +. positive relationship

- . negative relationship

NA. not applicable due to failure in detection of western signals.

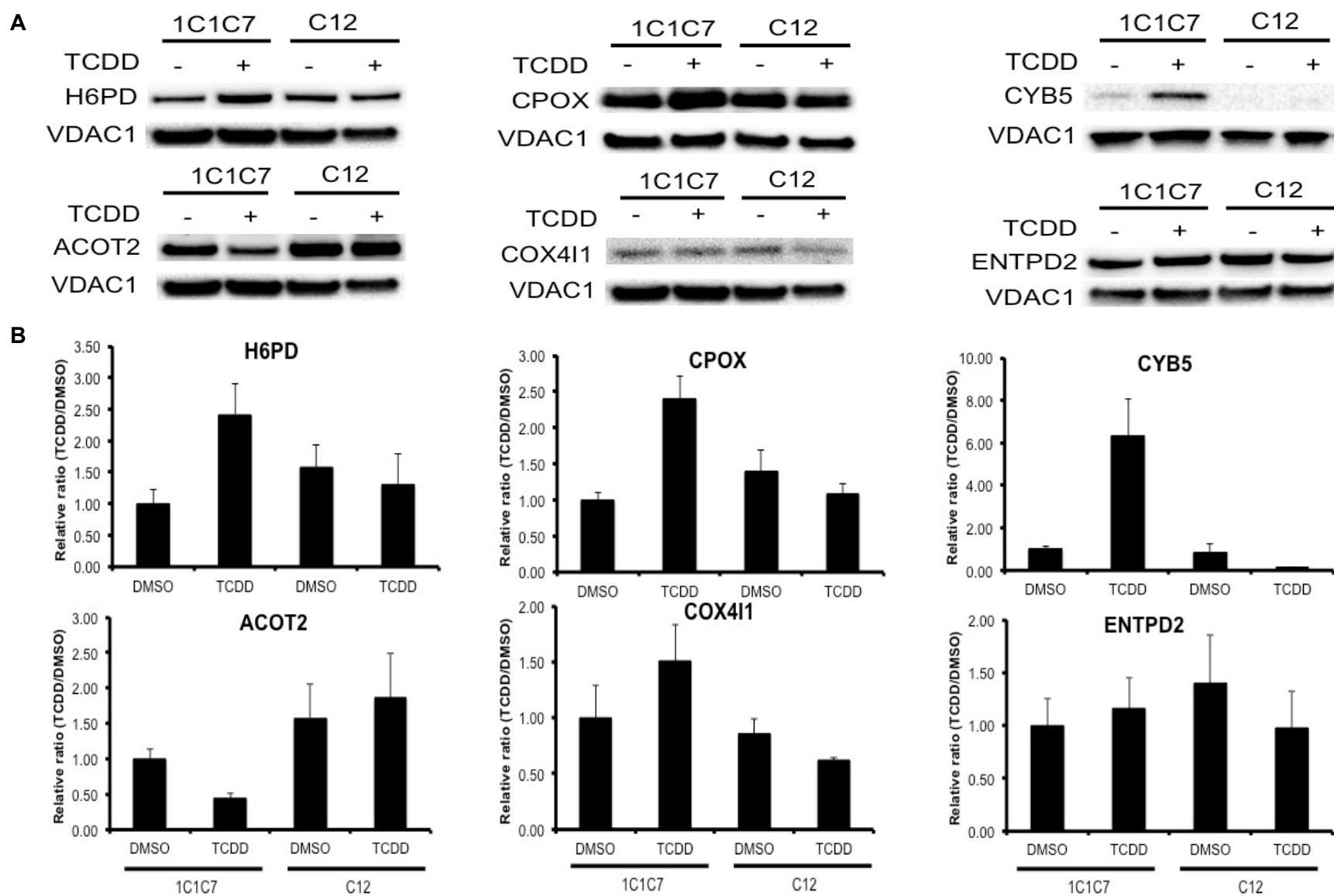


Figure 4-10. Western blot analysis of differentially expressed proteins identified by SILAC in hepatoma 1c1c7 and c12 cells

**Figure 4-10 (cont'd) exposed to DMSO or TCDD.**

Western blot was performed on mitochondrial fractions prepared from the two cell lines following exposure to DMSO (0.01%) or TCDD (10 nM). VDAC1 was used as a loading control. **(A)** Results shown are representative of 3 independent experiments. **(B)** Densitometry was determined with a Bio-Rad ChemiDoc MP SystemImage analyzer. Each protein expression was normalized to the loading control. The normalized protein expression levels were compared with each other by re-normalization with the protein expression from hepa1c1c7 cells exposed to DMSO. The bars represent mean  $\pm$  the standard errors (n=3).

## **CHAPTER 5. DISCUSSION**

## CHARACTERIZATION OF MITOCHONDRIAL AHR IMPORT

AHR is a transcription factor, which resides as a complex with molecular chaperones in the cytosol in the absence of ligand. In the presence of ligand, AHR is translocated into the nucleus and activates its target gene expressions including CYPs and TiPARP. Because CYPs stimulate ROS production during their xenobiotic metabolizing reactions and TiPARP does through downstream targets, TCDD-induced oxidative stress such as lipid peroxidation, regulation of antioxidant enzymes, DNA damage, and control of glutathione levels has been investigated as a potential mechanism for TCDD-induced toxicity.<sup>145, 152</sup> Accumulated research data have suggested that AHR-dependent oxidative stress would be from not only transcription activation but also nontranscriptional responses and TCDD-induced oxidative stress happened through not only microsomal superoxide molecules or nuclear damage but also mitochondrial superoxide or mitochondrial DNA damages.<sup>152, 153</sup> In addition, because mitochondria are the amphibolic sites having the TCA cycle and main sites for energy production, researches have targeted TCDD-induced mitochondrial dysfunction as a potential player in TCDD-induced toxic symptoms.<sup>77, 80, 161</sup> Thus, herein it was investigated how the AHR impacts mitochondrial function and AHR-mediated mitochondrial changes affect TCDD-toxicity.

Previous studies from our lab identified that the AHR could be localized in mitochondria, as well as interacting with mitochondrial matrix proteins, ATP5 $\alpha$ 1 and MRPL40.<sup>165, 166</sup> The probability of mitochondrial localization of the AHR was further supported by MTS prediction programs such as MitoProtII and MitoFates.<sup>179, 180</sup> Finally, and most convincingly, the mitochondrial localization of the AHR was supported by protease protection assay for mitochondrial compartments. These experiments clearly demonstrate that the AHR is localized in the IMS of the mitochondria (Figure 4-1). A combination of protease treatment and digitonin extraction of mitochondrial protein provided a more clear view for a location of mitochondrial AHR.

The previous study utilized confocal microscopy and co-immunoprecipitation to detect mitochondrial AHR.<sup>165</sup> Considering the size of mitochondria (0.5 - 1  $\mu\text{m}$ ), the structure of mitochondrial IM, which is baffled, therefore, not easily separating the IMS from the matrix, and the resolution of the confocal microscopy (400 nm), distinguishing the mitochondrial compartments would be ambiguous. Also, considering the experimental condition for the co-immunoprecipitation, such as utilizing the whole cell lysate rather than the mitochondrial fraction for protein solution and utilizing the mitochondrial buffer without detergent dissolving membrane components, the interaction between AHR and matrix proteins might not occur under a physiological environment. Another possibility is that the AHR interacts indirectly with matrix proteins *in vivo*. In this case, the AHR would be bound to proteins within the IM that are directly bound to ATP5 $\alpha$ 1 or MRPL40. Finally, it is possible that, like the AHR, a pool of these proteins can be found within the IM.

Cytochrome c heme lyase is known as an IMS protein, where it is bound to the outer surface of the IM.<sup>182</sup> The translocation of heme lyase into mitochondria is a distinct feature compared to other internal proteins because it is independent of TIM complex, mitochondrial membrane potential and ATP availability. In addition, this protein has no N-terminal MTS but 60 amino acids length of MTS in third quarter of the sequence, which is amphiphilic and conserved through species. When AHR sequence is compared to the MTS of heme lyase using the SIM, a protein sequence alignment tool, a possibility was suggested that AHR might have the internal sequence for mitochondrial localization (data not shown).<sup>183</sup>

Protease protection assay also confirmed that mitochondrial AHR is also a target for the AHR degradation pathway activated by TCDD, which means that mitochondrial AHR may also be involved in TCDD-induced toxicity signaling. The AHR localized in the IMS was decreased by TCDD, similar to the TCDD-induced cytosolic AHR decrease (Figure 4-2). One of the negative feedbacks that regulate AHR signaling is dioxin-induced receptor proteolysis. Thus, TCDD exposure may induce a proteolysis mechanism for both cytosolic and mitochondrial AHR

or trigger mitochondrial AHR export to the cytosol for proteolysis. The half-life of the unliganded and cytoplasmic AHR in hepa1c1c7 cells is 28 h, but that of TCDD-activated AHR is 3 h.<sup>31</sup> TCDD-induced AHR degradation by ubiquitin-mediated proteasome system is a fast reaction. The study using hepa1c1c7 cells showed that a majority of cytosolic AHR was transferred to the nucleus within 1 h after ligand exposure and over 80% of intracellular AHR was degraded within 4 h. It should be noted that the 20% of remaining AHR resided in cells even more than 24 h after ligand exposure.<sup>184</sup> Another study also showed that a small portion of AHR was resistant to ligand-activated degradation.<sup>23</sup> Our measurement of AHR amount in a cell after TCDD exposure to compare to that in the mitochondrial fraction was performed only in the cytosolic fraction, which neglected a comparison of nuclear AHR amount between the treatments, TCDD and vehicle control, DMSO. In these experiments, the intracellular AHR distribution under normal condition was cytosolic, 94%, nuclear, 5%, and mitochondrial, 1% (data not shown). Because of the abundance of AHR in the cytosol of hepa1c1c7 cells in our system, a change in the level of AHR expression in cytosol would reflect a representative amount for remained AHR after proteolysis in cells.

Because the AIP contributes to mitochondrial protein localization via interacting with TOM20 and TOM20 is known to recognize N-terminal target sequences of mitochondrial proteins,<sup>111, 167</sup> the probability of an N-terminal MTS and TOM20 recognition site in the AHR based on computer prediction suggested that the AIP might have a role in mitochondrial AHR import. In addition, Hsp90 has a documented role in assisting the translocations of proteins into the mitochondria. The decreased expression of mitochondrial AHR by AIP knockdown and inhibition of HSP90 activity suggest that stability of the AHR, both cytosolic and mitochondrial, depends on the amount and activity of both cytosolic chaperones. As previously mentioned, AIP status in cells is critical for stabilization of cytosolic AHR in mice.<sup>23, 185</sup> HSP90 is one of major cellular chaperones involved in protein folding, degradation, transport into organelles and cell signaling.<sup>21, 47, 109</sup> Considering together other studies and our data here, AIP and HSP90 are

important for mitochondrial AHR import as well as maintenance of cellular level of AHR. *In vitro* studies suggest a model that AIP plays a role of chaperone to maintain stability of unfolded mitochondrial preprotein and to transfer mitochondrial target protein to TOM20.<sup>111, 167</sup> In addition, TOM20 mediates a delivery of mitochondrial-targeted protein by HSP90/HSP70 to TOM70.<sup>112</sup> The decreased expression of mitochondrial AHR by TOM20 knockdown but no changes in expression of nuclear and cytosolic AHR corresponds to the prediction of existence of MTS in AHR and suggests that TOM20 may be the recognition protein for mitochondrial AHR import.

One possible function for mitochondrial AHR is as a recognition component for ubiquitin-mediated degradation of mitochondrial proteins to regulate mitochondrial respiratory efficiency. One possible model of ubiquitin-mediated degradation of mitochondrial proteins has been suggested as a model of UCP2.<sup>186</sup> In fact, the mouse *Ucp2* gene contains DREs and is induced by TCDD temporal and dose dependently.<sup>143, 164</sup> UCP2 expression and activity is up-regulated in metabolic diseases such as obesity and diabetes. UCP2 is a metabolic switch regulated by fatty acid and purine metabolism and a ROS production attenuator, regulated by superoxide and lipid peroxide to dissipate mitochondrial proton motive force.<sup>187</sup> In addition, ATP production and proton motive force is important in UCP2 degradation.<sup>186</sup> Thus, UCP2 might be a new candidate of AHR-mediated ubiquitin degradation. As suggested in the model for UCP2 degradation and the model for cytosolic steroid hormone receptor degradation by AHR,<sup>90, 186</sup> mitochondrial steroid/thyroid hormone receptors may be targeted by AHR component of E3 ubiquitin ligase to regulate mitochondrial respiration and lipid oxidation.

The other possible role of mitochondrial AHR is a controller of respiratory efficiency as an early responder to TCDD toxicity but not as a transcription factor. ATP5 $\alpha$ 1 is a component of ATP synthase and MRPL40 acts as a supporter in assembling the supercomplex. TCDD exposure caused a decrease in the interaction between AHR and ATP5 $\alpha$ 1.<sup>165</sup> The interaction between AHR and MRPL40 was identified under both vehicle control and TCDD exposure, but decreased levels of mitochondrial MRPL40 by TCDD exposure for 6 h was observed.<sup>166</sup> These

observations suggest that AHR can affect stability or structure of the supercomplex via direct protein:protein interaction with critical subunits at the surface of the IM. TCDD-induced loss of mitochondrial AHR from this site may cause alteration in chemical gradients or respiratory efficiency. Moreover, the loss of mitochondrial AHR from the IM site may cause TCDD-induced oxidative stress, resulting in turning on nongenomic AHR-mediated TCDD toxicity.

AHR is not only a ligand-activated transcription factor, but might also be a ligand-activated mitochondrial regulator. The evidence supporting the exact role of mitochondrial AHR is limited, however, the results do suggest ability to directly impact mitochondrial function. Simply, two possible roles are suggested here. One is an E3 ubiquitin ligase component in ubiquitin-mediated proteolysis for detecting and exporting a target mitochondrial protein. The other is a regulator of respiratory machinery to maintain efficiency by interacting with the supercomplex or to stimulate xenobiotic signaling by losing an interaction with the supercomplex. The previous study confirmed that TCDD-induced AHR mediated mitochondrial hyperpolarization is independent of AHR transcriptional activity.<sup>165</sup> In addition, here, AHR is found to localize in the IMS not in the matrix. Therefore, the role of mitochondrial AHR must be considered as nontranscriptional factor (Figure 5-1).

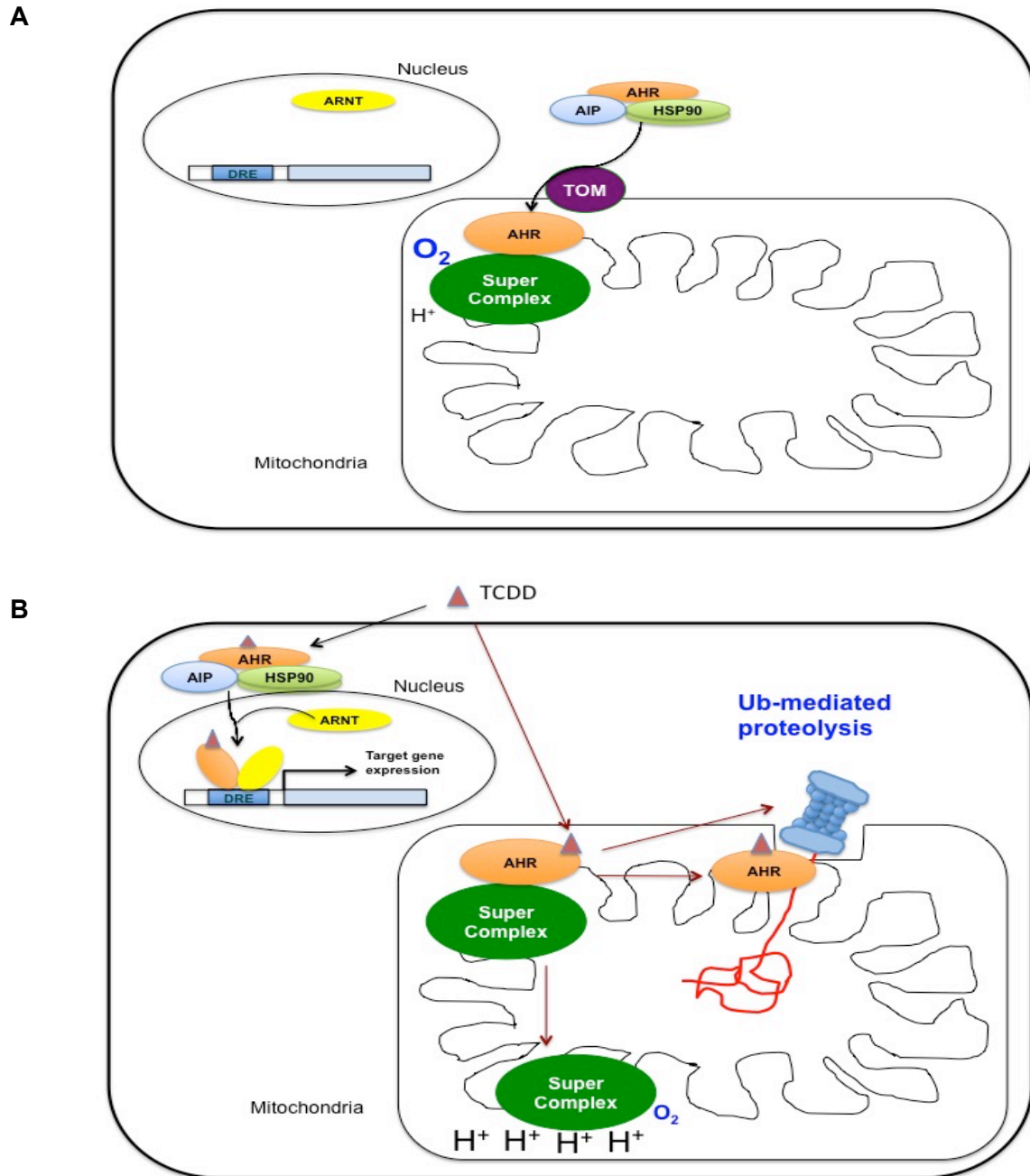


**Figure 5-1. Suggested role of mitochondrial AHR.**

**(A)** Mitochondrial AHR resides in the IMS and is bound to the component interacting with ATP5a1 or MRPL40 in the IM. **(B)** TCDD-activated mitochondrial AHR is dissociated from the interacting protein in the IM. The possible role of the dissociated TCDD-bound AHR is 1) recognizing the target proteins that are destined for the ubiquitin-mediated degradation and 2) dissociating from the supercomplex that subsequently would have the altered efficiency in proton pumping and respiration.

## AHR-MEDIATED TCDD-INDUCED MITOCHONDRIAL DYSFUNCTION

TCDD-induced oxidative stress has been extensively studied.<sup>81, 84, 146, 150, 152, 159, 160, 163</sup> Considering that mitochondria are the organelles that utilize most of the cellular oxygen and main source of ROS, it is tempting to hypothesize that AHR-mediated TCDD-induced toxicity involves mitochondrial dysfunction. TCDD-induced mitochondrial hyperpolarization and changes in enzyme activity of ETC complexes were observed in several studies, but those studies did not investigate whether the TCDD-induced mitochondrial respiratory change were AHR-dependent.<sup>152, 161, 188</sup> The previous study from our lab showed that the TCDD-induced hyperpolarization across the mitochondrial IM and caused no corresponding change in cellular ATP levels in murine hepatoma and B cell lines expressing AHR.<sup>165</sup> Also, TCDD caused differential expression of nuclear-encoded ETC genes in C57BL/6 mice.<sup>164</sup> In addition, TCDD-induced changes in OCR and activities of ETC and ATP synthase complexes were determined. 30 nM TCDD exposure to hepa1c1c7 cells caused a significant decrease in basal respiration and maximal respiration whereas no change in hepac12 cells was observed (Figure 4-6B and 4-7B). This led us to speculate that cytochrome c oxidase, CIV, may have a decreased efficiency under TCDD exposure and this might be caused by AHR-mediated TCDD-induced oxidative stress. Interestingly, 30 nM TCDD exposure to hepa1c1c7 cells did not significantly alter the activities of ETC complexes or ATP synthase though several trended towards modulation (Figure 4-8). This suggests that decreased cellular OCR in hepa1c1c7 cells by TCDD may not be caused by lack of efficiency in complex IV or other individual component of the ETC and ATP synthase.

*In vitro* assays of ETC complex and ATP synthase were performed under sufficient amount of substrates and cofactors for each enzyme complex to evaluate an individual enzyme activity. However, a real-time measurement of cellular OCR was performed under nutrients similar to cell culture, which would have more complicated supply and demand requirements for

the reactions that compromise the ETC and ATP synthase. In addition, the interaction of these components and the cytosol would remain intact. Discrepancies between the individual complex data and the OCR might be caused by changes in the regulation in supply of electron carriers in cells or a disruption of the normal cellular signaling between these two cellular compartments. The main source of electron carriers for the ETC is fatty acid oxidation and TCA cycle. As discussed earlier, TCDD upregulated lipid biosynthesis and fatty acid  $\beta$ -oxidation in liver and skeletal muscle in both AHR responsive and nonresponsive mice, and irregular lipid and fatty acid uptake are signs of TCDD-induced metabolic perturbation in skeletal muscle in C57BL/6 mice.<sup>71</sup> TCDD also led to an increase in fatty acid uptake and downregulated *de novo* lipogenesis and gluconeogenesis in C57BL/6 mice liver.<sup>68, 143, 146</sup> Analysis of AHR-mediated TCDD-induced gene expressions changes indicated alterations in the expression of genes that encode mitochondrial metabolic enzymes involved in the generation of electron carriers including the TCA cycle.<sup>27, 143, 146, 189</sup> Considering that TCA cycle is stimulated by acetyl-CoA from fatty acid  $\beta$ -oxidation and TCDD decreases TCA cycle activity, mitochondrial fatty acid oxidation might not be completed or not efficient enough to provide the necessary acetyl CoA for TCA cycle and subsequently reducing equivalents for OXPHOS. Drug metabolizing enzymes, CYPs, are highly expressed in both mitochondria and ER by TCDD-activated AHR, and produce oxidative stress, which affects cellular redox potential. These may cause AHR-mediated TCDD-induced lack of reducing equivalents in mitochondria, which can be one of contributors for the changes observed in OCR, OXPHOS activity and mitochondrial membrane potential.

Studies analyzing succinate-stimulated mitochondrial hyperpolarization showed AHR-dependent increased mitochondrial thiol redox potential. This increased thiol redox potential can cause mitochondrial hyperpolarization by closing MPTP and generate more superoxides through Q cycle in complex III and reverse electron flow in complex I.<sup>152</sup> TCDD treated C57BL/6J mice had enhanced succinate level in the liver.<sup>71</sup> Similar to this, glutamine in

hepatoma cell culture media might also elevate succinate levels via the reactions of the TCA cycle and this could accelerate the electron flow through complex II, succinate dehydrogenase, and create mitochondrial hyperpolarization and ROS that can ultimately inhibit respiration efficiency.

Spare respiratory capacity was not affected by TCDD exposure in either hepa1c1c7 or hepaC12. However, respiratory control ratio achieved by addition of uncoupler and complex V inhibitor, oligomycin was increased in the hepaC12 cells following 30 nM TCDD exposure. Interestingly, respiratory control ratio was not changed by TCDD in either WT and AHR knockout mice in a previous study.<sup>160</sup> Considering that cellular ATP levels was not changed in AHR expressing cells in the previous study and that respiratory control ratio was not changed by TCDD exposure to hepa1c1c7, a cell line that expresses AHR, the efficiency of mitochondrial ETC complex and ATP production may be maintained by AHR for a certain amount of time until TCDD-induced oxidative stress is accumulated enough to damage cellular context.

On the other hand, TCDD exposure to hepac12 cells caused no changes in activities of ETC and ATP synthase except in complex I and V though these changes were not significant (Figure 4-8). This AHR-independent enzyme activity changes and increased respiratory control ratio by 30 nM TCDD in hepac12 cells may support the above idea that the decreased OCR and mitochondrial hyperpolarization in hepa1c1c7 may have a link to AHR-dependent homeostasis in the regulation of respiratory control ratio, (e.g., mitochondrial coupling efficiency). This means that AHR might have a role in cellular ability to cope with TCDD-induced lack of electron carriers via regulation of ETC. Because ETC complexes consist of multiple nuclear- and mitochondrial-encoded subunits, it is hard to define whether the regulation of ETC is AHR-mediated TCDD-induced regulation of gene expression or indirect regulation via allosteric regulation of enzymes. However, considering that the pools of electron carriers are generated in the metabolic pathways regulated by AHR and cellular redox potential homeostasis was dependent on AHR expression,<sup>152</sup> it cannot be ruled out that AHR may be a regulator of the

influx of electrons into ETC to maintain cellular respiration capacity.

Given the observed AHR-dependent TCDD-induced changes in mitochondrial respiration, the role of the AHR in modulating mitochondrial function was investigated further using the proteomic analysis. Proteomic analysis with adult zebrafish heart exposed to TCDD revealed that TCDD caused significantly different protein expression related to calcium handling, energy metabolism and the cellular redox state.<sup>190</sup> Proteomic analysis with 5L hepatoma rat cells exposed to TCDD revealed that TCDD upregulated voltage-dependent anion channel-selective protein 2 (VDAC2) as an adaptive response to TCDD-induced oxidative stress to inhibit the mitochondrial apoptotic pathway.<sup>191</sup> Phosphoprotein quantification using SILAC with 5L rat hepatoma cells identified TCDD-induced alteration in phosphorylation modification in the ARNT, transcriptional coregulators, small GTPase regulators and oncoproteins.<sup>192</sup> The above studies utilized short (1 to 8 h) TCDD exposure. Considering the effect of retrograde signaling (mitochondria-to-nuclear stress signaling), the SILAC-based proteomic analysis was performed with TCDD exposure for 72 h to identify novel TCDD-induced changes in the mitochondrial proteome and to develop our understanding of AHR signaling for toxic effects. We identified 17 proteins with a mean  $|\text{fold change}| \geq 2$  (Table 2), and proteins involved in metabolic pathways were further investigated (Figure 4-10).

H6PD, CPOX, and CYB5 were induced with 2.0-2.5 fold by TCDD exposure in hepa1c1c7 cells but not in hepac12 cells. All these proteins are involved in anabolic pathways and H6PD and CYB5 are involved in the regulation of reducing equivalents. H6PD is a bifunctional enzyme, which has glucose 1-dehydrogenase and 6-phosphogluconolactonase activity. H6PD isoforms reside in different intracellular and extracellular locations. H6PD in the ER performs the first reaction, a rate-limiting step in the pentose phosphate pathway. H6PD produces NADPH as a by-product that can be utilized to maintain cellular redox state via glutathione levels under oxidative stress. Because the pentose phosphate pathway is a main source of NADPH in cells, cellular oxidative stress may affect H6PD enzymatic activity and

protein expression.<sup>193</sup> It was observed in mouse embryo fibroblast derived from extrahepatic tissue that TCDD induced cytosolic H6PD and glycerol-3-phosphate dehydrogenase, and also induced Acyl-CoA oxidase that performs the first step of the peroxisomal  $\beta$ -oxidation.<sup>144</sup> Because NADH produced from the proxisomal  $\beta$ -oxidation is usually utilized in lipids oxidation and fatty acid synthesis, not in mitochondrial ATP production, it is suggested that TCDD-induced proxisomal  $\beta$ -oxidation might contribute to the wasting syndrome.<sup>144</sup> Recently, H6PD was found to localize in mitochondrial matrix and its suggested role is to produce NADPH pool for antioxidant defense or for a possible conversion between NADH/NADPH.<sup>194</sup> Another suggested role of H6PD in the mitochondria is interaction with hexokinase at the mitochondrial OM to manage glucose-6 phosphate, which can increase ROS level and apoptosis. This suggestion is supported by the observation that the level of mitochondrial H6PD was regulated by nutrient status.<sup>194</sup> TCDD-induced restricted mitochondrial respiration may affect upregulation of both cytosolic and mitochondrial H6PD to produce reducing power against oxidative stress and corresponding to demand for lipid metabolism.

Coproporphyrinogen-III oxidase (CPOX) found in the IMS of mitochondria is the key enzyme in heme biosynthesis. It catalyzes oxidative decarboxylation of coproporphyrinogen III to protoporphyrinogen IX, a precursor of heme.<sup>195</sup> Heme is essential for many biological reactions such as oxygen transport, energy metabolism, and drug metabolism. CYP families and cytochromes have a heme group as a cofactor. When xenobiotics induce CYP1 family members, heme biosynthesis would also be accelerated to generate functional CYPs. The rate-limiting steps of heme biosynthesis are a reaction of 5-aminolevulinic acid (ALA) synthase, which catalyzes condensation of glycine and succinyl-CoA to produce ALA and a transport of CPOX substrate from cytosol to mitochondria.<sup>196</sup> The substrate of CPOX, coproporphyrinogen III, is synthesized in the cytosol and transported into the mitochondria by the mitochondrial ATP binding cassette transporter, ABCB6, which is also an AHR target gene.<sup>196</sup> In addition to that AHR Global Chip-Chip analysis identified AHR enrichment region in the *Cpox* gene,<sup>197</sup>

increased protein expression of CPOX and ABCB6 would be required by CYP1 family induction and other electron transfer reactions that utilize cytochromes. TCDD-elicited CPOX induction might also contribute to hepatocarcinoma development in a similar manner of that of ABCB6.<sup>196</sup> TCDD-inducible CYPs accumulates porphyrins, which may cause hepatic fibrosis resulting in malignant tumor.<sup>198</sup> High dose of TCDD exposure to mice is known to cause porphyria, inducing CYP1A enzymes oxidizing porphyrinogens and aberrant iron metabolism.<sup>199</sup> Heme oxidase, another heme metabolizing enzyme, which is up-regulated by other transcription factors, such as NRF2, AP-1, and NFκB, is generally induced by TCDD, converts heme to bilirubin and induces mitochondrial-dependent apoptosis although HO-1 regulation by TCDD was not clearly observed here.<sup>62, 200</sup>

Cytochrome b5 (CYB5) is an ER membrane bound heme protein, which functions as an electron carrier for several membrane bound oxygenases, such as NADH-cytochrome b5 reductase (CYB5R). CYB5R reduces methemoglobin to normal hemoglobin. During the reaction, electrons are transferred from electron carriers to CYB5, and these electrons are utilized in desaturation of fatty acids by SCD1. TCDD-elicited steatosis depends on AHR-mediated *Scd1* and *Tiparp* induction, which result in the accumulation of lipids, and increases in oxidative stress, fibrosis and inflammation in liver.<sup>146, 150</sup>

Acyl-CoA thioesterase 2 (ACOT2) catalyzes the hydrolysis of long-chain acyl-CoA to the free fatty acid and coenzyme A to facilitate fatty acid β-oxidation.<sup>201</sup> This protein did not meet the cut-off for the 2-fold change in the MS data, but its expression was reduced by 1.7-fold by TCDD exposure in hepa1c1c7 cells but not in hepac12 cells (data not shown), and this was confirmed by Western blot analysis (Figure 4-10). Accelerated ACOT2 activity accumulates and release free fatty acid from mitochondria. Returning free fatty acid to the mitochondria to utilize for fatty acid oxidation promotes proton back and subsequent proton leak occurs.<sup>201</sup> This phenomenon uncouples respiration and may drive lipid consumption for energy compensation.<sup>201</sup> TCDD suppressed ACOT2 expression in an AHR-dependent manner. Lower

activity of fatty acid  $\beta$ -oxidation would result in decreased supply of reducing equivalents for ETC complex and ATP synthase, and this may result in reduced respiration and ATP production.

ENTPD2, ecto-nucleoside triphosphate diphosphohydrolase, is a plasma membrane protein and hydrolyzes nucleoside triphosphates and nucleoside diphosphates in the presence of divalent cofactors,  $Mg^{2+}$  or  $Ca^{2+}$ . ENTPD2 is involved in physiological pathways that use ATP as an intracellular signal, such as eye and brain development, taste bud function.<sup>202, 203</sup> ENTPD2 is also involved in the inflammatory response and IL-6, a marker of biliary cirrhosis, downregulated *Entpd2* gene expression.<sup>204, 205</sup> TCDD activated ENTPD2 expression in mouse hepa1c1c7 cells.<sup>206, 207</sup> SILAC analysis showed 7.4-fold induction of ENTPD2, but this induction was not detected by Western blot analysis, which might be due to a lack of proper antibodies detecting a molecule residing in intracellular organelles (Table 2 and Figure 4-10). So far, ENTPD2 localized in intracellular organelles was confirmed in only human species.<sup>205</sup> While human ENTPD2 alpha is an active enzyme and found in plasma membranes, ENTPD2 beta and gamma have no catalytic activity and are found in the ER membrane. The beta and gamma isoforms are alternative splicing variants having partial loss of exon 8, which has a critical Cys residue for disulfide bond, and are not being fully glycosylated. The study of human ENTPD2 cloning suggested that loss of disulfide bond sites and lacking full glycosylation in the alternative splice variants might inhibit correct folding and oligomerization that are critical for enzyme function.<sup>205</sup> The authors also suggested that ENTPD2 beta/gamma would have a role in purinergic signaling termination by formation of hetero-oligomer with the alpha form.<sup>205</sup> On the other hand, rat ENTPD2 also has alternative splice variants, but both are active enzymes and the subcellular localization of these isoforms, except for the plasma membrane, has not been confirmed.<sup>208</sup> The isoforms of ENTPD2 in human and rat and unknown functions of these isoforms raises a question about the intracellular localization and the role of ENTPD2 induced by TCDD. Because ENTPD2 regulates liver cell growth and IL-6, which is important in liver

fibrosis, downregulates ENTPD2 expression, TCDD-induced ENTPD2 expression might be a response against liver fibrosis.<sup>204</sup>

*Cox4i1* was induced by TCDD-exposure in C57BL/6 mice liver.<sup>164</sup> However, other studies analyzing gene expression using microarray did not show upregulated *Cox4i1*.<sup>27, 206</sup> Here, MS data did not show any changes in COX411 proteins expression by TCDD exposure. Two Western blot analysis agreed to MS data while one Western blot analysis showed the increased level of COX411 in hepa1c1c7 cells exposed to TCDD. Considering that *Cox4i1* is regulated by hypoxia, TCDD-induced COX411 expression might be temporal and dose-dependent, ultimately relying on oxidative stress signaling.<sup>209, 210</sup>

WARS2 is the mitochondrial tryptophan-tRNA ligase, which was decreased 2-fold by TCDD exposure in hepa1c1c7 cells (Table 2). TCDD caused the downregulation in the expression of genes that encode proteins related to amino acid metabolism and purine metabolism was observed.<sup>27, 143</sup> Metabolomic analysis using C57BL/6J, AHR-responsive and DBA/2J, AHR-nonresponsive mice exposed to TCDD showed decreased levels of amino acids including tryptophan and purines, as well as decreased TCA cycle activities.<sup>71</sup> MRPS28, which was decreased more than 2-fold in the expression by TCDD exposure in hepa1c1c7 cells, was previously named as MRPS35. MRP consists of MRPS28 and MRPL39. Given the published metabolomic data, the decreased WARS2 and MRPS28 protein levels observed in the MS of our study suggest a TCDD-mediated suppression of mitochondrial biogenesis.

Collectively, the mitochondrial proteins identified with significant AHR-mediated changes in expression following TCDD challenge are related to redox potential regulation (H6PD), redox related enzyme reaction (CYB5), heme metabolism (CPOX), lipid metabolism (ACOT2), and mitochondrial biogenesis (WARS2 and MRPS28) (Figure 5-2). Our results support previous suggestions of AHR-mediated energy metabolic alterations and hepatosteatosis and consequently TCDD-induced toxicity. Though the experimental conditions for the TCDD-induced effects on mitochondrial respiration and mitochondrial protein expression were not identical, it is

certain that the main factors in mitochondria affected by TCDD exposure are related to redox potential and lipid metabolism, which also affect energy maintenance. The ability of the AHR to crosstalk with other signaling pathways and mitochondrial retrograde signaling may orchestrate temporally different cellular responses upon TCDD exposure. The effort to find a connection between early and later mitochondrial responses against TCDD needs to be considered in any future study of AHR-mediated TCDD-induced liver diseases.

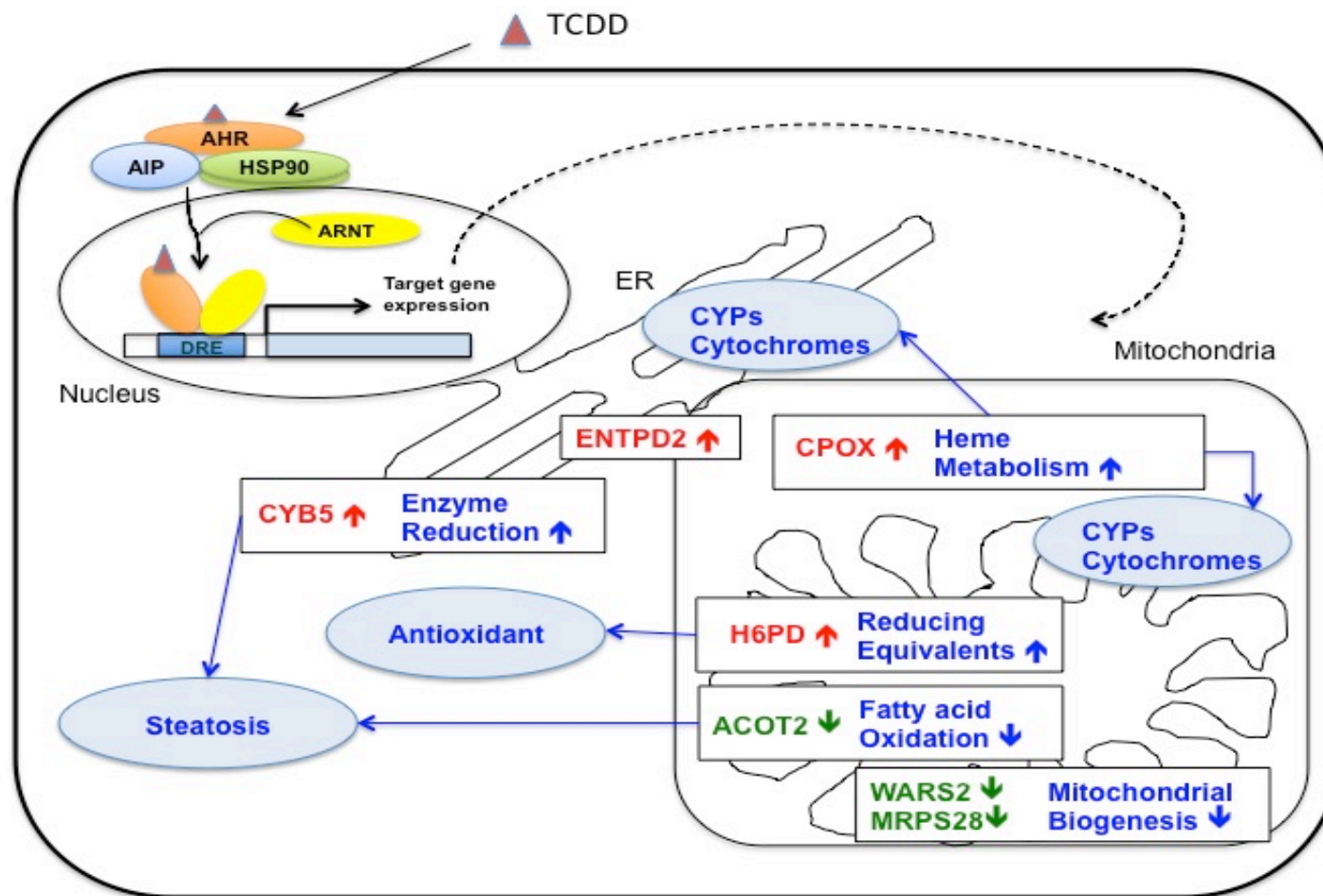


**Figure 5-2. AHR-mediated TCDD-induced regulation of protein expression in metabolic pathways.**

TCDD-activated AHR upregulates or downregulates its target protein expressions. TCDD-induced AHR target proteins are related to heme metabolism, lipid metabolism, redox potential regulation, mitochondrial biogenesis, and unknown functions. Red indicates upregulated proteins, green indicates downregulated proteins, and blue indicates metabolic pathways and its targets.

## **CHAPTER 6. CONCLUSIONS AND FUTURE STUDIES**

The AHR is a well-studied ligand-activated transcription factor. TCDD is the most potent agonist of the AHR and the physiological effects by TCDD have been researched focusing on metabolic syndromes. For example, major AHR target genes include the cytochrome P450 enzymes that are capable of producing TCDD-induced oxidative stress, which causes detrimental effects on mitochondria. To further explore the role of the mitochondria in TCDD-induced AHR-mediated toxicity, the research within this dissertation explores the possibility that a pool of cellular AHR can be found within the mitochondria. In addition, it characterizes the impact of TCDD-induced changes to mitochondrial function and proteome. The research shows that the AHR localizes in the IMS of the mitochondria and describes AHR-mediated changes to oxygen consumption and regulation in protein expression.

First, mitochondrial AHR is localized in the IMS by recognition of TOM20 in concert with the cytosolic chaperones, AIP and HSP90. The possible MTSs were predicted in the N-terminus and internal sequences of the AHR. The level of mitochondrial AHR is also regulated by TCDD-induced proteolysis and this suggests that mitochondrial AHR may participate in TCDD-induced toxic responses. Two possible roles of mitochondrial AHR were suggested; 1) AHR acts as E3 ubiquitin ligase for mitochondrial steroid hormones or other possible factors related to regulation in respiratory machinery, and 2) AHR acts as a regulator for respiratory machinery via interacting with a factor that might be localized in the IM. The role of mitochondrial AHR would be independent of transcription activation.

Next, mitochondrial AHR contributes to make a balance between mitochondrial hyperpolarization and reduced respiration. This was reflected in constant respiratory control ratio and efficiency of enzymatic activities of the individual ETC complex and ATP synthase following TCDD exposure in AHR-expressing cells. Moreover, this observation supports the suggested roles of mitochondrial AHR mentioned above, as a controller for respiratory

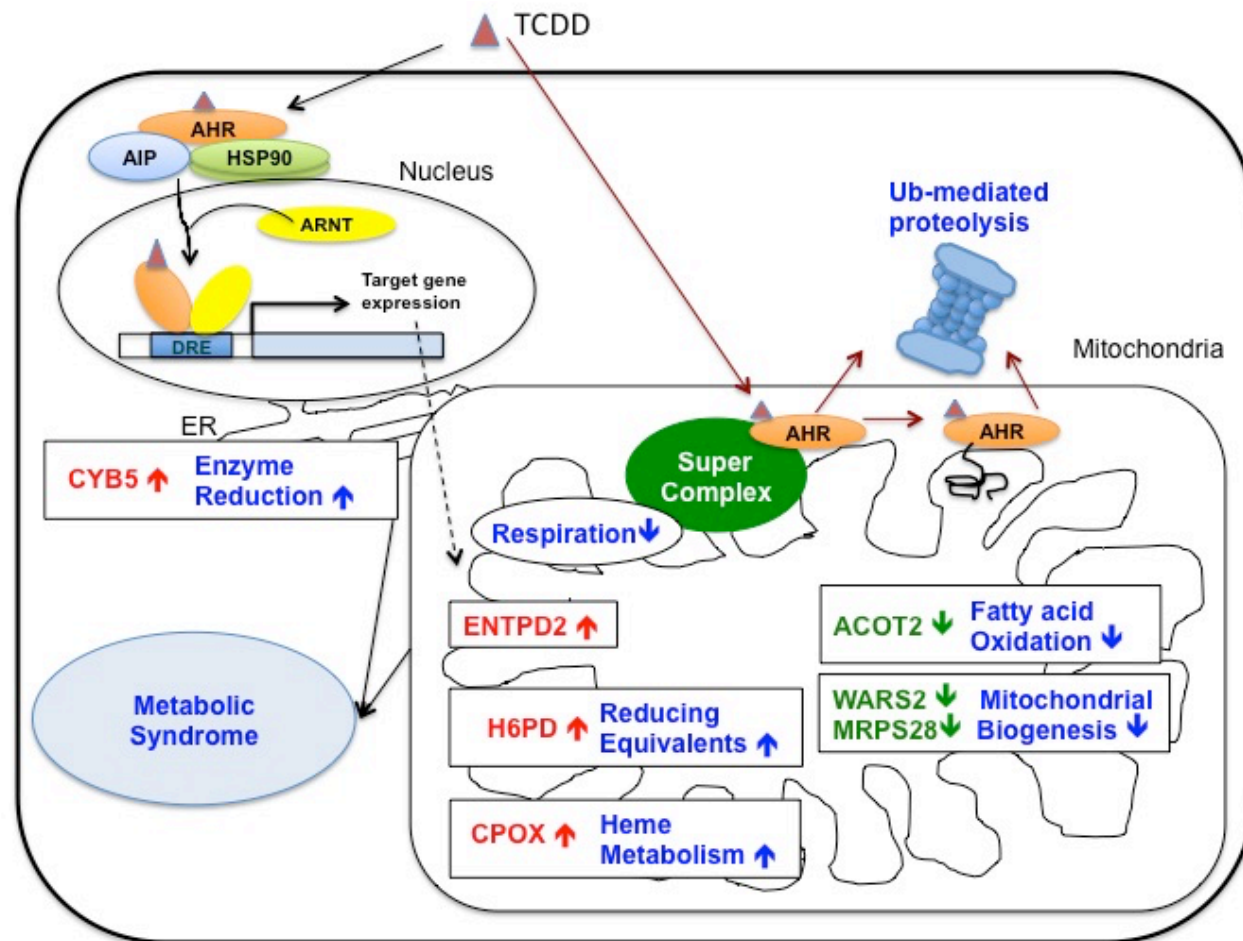


**Figure 6. Summary of AHR-mediated TCDD-induced mitochondrial dysfunction.**

Red arrows indicate the functions of TCDD-activated mitochondrial AHR. Black arrows indicate canonical TCDD-activated AHR-mediated gene expression. Red indicates upregulated proteins, green indicates down regulated proteins, and blue indicates metabolic pathways and its targets.

machinery, with the observation from the previous study, the TCDD-induced loss of AHR interaction between ATP5 $\alpha$ 1 or MRPL40. Unchanged mitochondrial coupling may cause oxidative stress due to reduced activity of the downstream factor in the ETC, oxygen consumption. This oxidative stress would cause accumulated stress and become responsible for TCDD-induced toxicity in a certain amount of time.

Finally, TCDD-induced AHR-mediated changes to the mitochondrial proteome identified the proteins which expressions were significantly changed AHR-dependently. The activities of mitochondrial ETC and ATP synthase mentioned above were measured for up to 24 h after TCDD exposure while the mitochondrial proteome was analyzed with samples exposed to TCDD for 72 h. Mitochondrial proteome was performed considering time for the effect of mitochondrial retrograde signaling to the nucleus. Identified differentially expressed proteins implicate that TCDD-induced signaling is involved in regulation of redox potential, heme biosynthesis, lipid metabolism, and mitochondrial biogenesis. These pathways are reflected in the TCDD-induced pathological effects, hepatic steatosis, antioxidant defense, and wasting syndrome. Thus, TCDD-induced metabolic dysfunction is achieved by the action of both nuclear transcription activity and mitochondrial nontranscription activity (Figure 6).

### **MITOCHONDRIAL AHR IN THE IMS**

The localization of mitochondrial AHR in the IMS by TOM20 was identified and the possible MTS was suggested. However, the role of mitochondrial AHR has not been identified and the exact AHR localization in the IMS is obscure. Whether the AHR is bound to the IM, bound to the OM or free form in the IMS still needs to be determined. Identifying the exact AHR location will provide more clues to help determine the role of mitochondrial AHR. Thus, establishing the MTS in the AHR must be achieved by a sequence deletion studies.

The limitation in studying mitochondrial AHR is that mitochondrial AHR exist as very small pool compared to cytosolic AHR. To overcome this limitation, creating cell strains that express different functional forms of the AHR would be an important first step. Once the MTS is identified, it will be possible to create mutant AHRs that are incapable of entering the mitochondria, as well as, those with inability to enter the nucleus or are engineered to increase the amount within the mitochondria. This genetic engineering would make it possible to generate AHR signaling simpler or magnify the effect from the AHR signaling more specialized. Because cytosolic AHR is observed as a complex form with molecular chaperones and destabilized without chaperones, it is assumed that AHR would exist as a bound form in the mitochondria not as a free form. Once, mitochondrial AHR can be obtained the amount enough to identify its partner proteins, clues can be found for the role of the ligand-activated AHR in mitochondria.

The hypothesis on the role of AHR mentioned above regarding mitochondrial respiration can be evaluated. To clearly examine the role of AHR in mitochondria, it is necessary to test the hypothesis in other cell types, which have differing mitochondrial respiration activity, such as skeletal muscle and heart in addition to kidney, adipose tissues and skin, which are frequently used to study TCDD-toxicity. If the existence of AHR in the mitochondria is critical for mitochondrial respiratory function especially, the AHR-mediated effect would be more clearly observed in those cells having more active mitochondria.

## **THE ROLE OF THE AHR IN MITOCHODNRIAL METABOLISM AND ITS ROLE IN TCDD-INDUCED TOXICITY**

The constant respiratory control ratio and efficiency of ETC capacity under TCDD exposure was dependent on AHR expression. The comparison of OCR and enzyme activities of OXPHOS between hepa1c1c7 and c12 cells has limitation to explain AHR-mediated effect

because hepa1c1c7 and c12 cells may have other cellular differences other than AHR dominance/deficiency. Human B cell SKW6.4 is an AHR null cell line and Dr. Kaminski's lab at the Michigan State University established SKW6.4 that overexpress the AHR. Because of identical cellular context, performing the same experiments with SKW6.4 cells with/ without expression of AHR would confirm the effect of AHR on homeostasis on respiratory control and efficiency of ETC and ATP synthase enzyme activities, which were observed in mouse hepatoma cells.

One of identified metabolic pathway from SILAC analysis was redox regulation by increased levels of H6PD, which could affect mitochondrial GSH/GSSG ratio and SOD activity. Decreased levels of ACOT2 suggested alterations in fatty acid oxidation. Gene expression analysis by other researches identified increased fatty acid uptake in liver but has not identified decreased enzyme expression levels involved in fatty acid oxidation clearly. Identification of activities of suggested metabolic pathways could advance our understanding of metabolic switches by AHR-mediated TCDD toxicity. In addition, another interesting protein identified from SILAC analysis is ENTPD2. Although mitochondrial ENTPD2 cannot be identified due to lack of a proper antibody, characterization of mitochondrial ENTPD2 against TCDD exposure would be a novel finding since a role for mitochondrial-localized ENTPD2 has not been revealed so far.

Lastly, several of the proposed endogenous ligands for the AHR, such as steroids and heme and tryptophan metabolites have direct links to mitochondria function. The role of these metabolites on modulating AHR function within the mitochondria has interesting implications. These metabolites might alter their own flux via changes in AHR signaling within the organelle that regulates their production without having a signal to the nucleus. Considering that mitochondria are central intracellular organelles for energy production and the numbers or state of mitochondria are critical factors for cellular development, proliferation, and survival, the physiological effects of AHR signaling activated by endogenous ligands linking to mitochondrial function can be studied to shed light on AHR biology.

## **APPENDICES**

## APPENDIX A. SUPPLEMENTAL TABLES

**Table A-1. Identified mitochondrial proteins differentially regulated by 10 nM TCDD exposure for 72 h in an AHR-dependent manner.**

Protein Name	Gene Name	C7(T/D) Mean	C12(T/D) Mean	P-value	Intracellular Location
Retinol-binding protein 4	Rbp4	2.859	0.926	0.001	Possibly in mitochondria
Coproporphyrinogen-III oxidase, Mitochondria	Cpox	2.433	1.229	0.001	Mitochondria
Cytochrome b5	Cyb5;Cyb5a	2.289	0.997	0.000	Mitochondria
GDH/6PGL endoplasmic bifunctional protein;Glucose 1-dehydrogenase;6-phosphogluconolactonase	H6pd	2.025	1.252	0.035	Mitochondria
Prostaglandin G/H synthase 1	Ptgs1	1.787	1.302	0.012	Possibly in mitochondria
C-Jun-amino-terminal kinase-interacting protein 4	Spag9	1.521	0.642	0.043	Possibly in mitochondria
NADPH--cytochrome P450 reductase	Por	1.447	1.095	0.004	Possibly in mitochondria
NADH-ubiquinone oxidoreductase chain 4	mt-Nd4;ND4; Mtnd4;Nd4	1.447	0.730	0.004	Mitochondria
HIG1 domain family member 1A, Mitochondria	Higd1a;Gm9790	1.428	0.965	0.018	Mitochondria
CD109 antigen	Cd109	1.378	0.813	0.006	Possibly in mitochondria
Lanosterol synthase	Lss	1.367	0.954	0.007	Possibly in mitochondria
Thioredoxin domain-containing protein 5	Txndc5	1.358	0.931	0.012	Possibly in mitochondria
Sarcoplasmic/endoplasmic reticulum calcium ATPase 2	Atp2a2	1.326	1.114	0.007	Possibly in mitochondria
Rapamycin-insensitive companion of mTOR	Rictor	1.305	0.841	0.028	Possibly in mitochondria
Cytoskeleton-associated protein 4	Ckap4	1.293	1.033	0.006	Possibly in mitochondria
Cytochrome c oxidase assembly protein COX11, Mitochondria	Cox11	1.280	1.036	0.000	Mitochondria
MAGUK p55 subfamily member 6	Mpp6	1.269	0.755	0.015	Possibly in mitochondria

**Table A-1 (cont'd).**

Protein Name	Gene Name	C7(T/D) Mean	C12(T/D) Mean	P-value	Intracellular Location
Low-density lipoprotein receptor	Ldlr	1.233	0.907	0.037	Possibly in mitochondria
[3-methyl-2-oxobutanoate dehydrogenase [lipoamide]] kinase, Mitochondria	Bckdk	1.231	0.802	0.031	Mitochondria
Peptidyl-prolyl cis-trans isomerase FKBP8	Fkbp8	1.227	0.929	0.000	Mitochondria
Proteasomal ubiquitin receptor ADRM1	Adrm1	1.208	0.748	0.003	Possibly in mitochondria
Sphingolipid delta(4)-desaturase DES1	Degs1	1.204	0.929	0.008	Mitochondria
B-cell receptor-associated protein 31	Bcap31	1.203	1.091	0.023	Possibly in mitochondria
Transmembrane emp24 domain-containing protein 10	Tmed10	1.195	0.971	0.003	Possibly in mitochondria
KN motif and ankyrin repeat domain-containing protein 2	Kank2	1.183	0.847	0.021	Mitochondria
Tensin 1	Tns1	1.176	0.858	0.015	Possibly in mitochondria
LYR motif-containing protein 4	Lym4	1.173	0.899	0.046	Mitochondria
Cystatin-B	Cstb	1.165	0.894	0.009	Possibly in mitochondria
Long-chain fatty acid transport protein 4	Slc27a4	1.155	0.933	0.047	Possibly in mitochondria
NAD kinase domain-containing protein 1, Mitochondria	Nadkd1	1.152	0.970	0.035	Mitochondria
Transmembrane protein 176A	Tmem176a	1.150	0.639	0.005	Possibly in mitochondria
EH domain-containing protein 1	Ehd1	1.145	0.890	0.002	Possibly in mitochondria
CCR4-NOT transcription complex subunit 1	Cnot1	1.137	0.976	0.039	Possibly in mitochondria
Proteasome activator complex subunit 2	Psme2	1.119	0.896	0.036	Possibly in mitochondria
Dolichyl-diphosphooligosaccharide—protein glycosyltransferase subunit DAD1	Dad1	1.116	0.866	0.027	Possibly in mitochondria
Clusterin;Clusterin;Clusterin beta chain;Clusterin alpha chain	Clu	1.100	0.538	0.012	Mitochondria

**Table A-1 (cont'd).**

<b>Protein Name</b>	<b>Gene Name</b>	<b>C7(T/D) Mean</b>	<b>C12(T/D) Mean</b>	<b>P-value</b>	<b>Intracellular Location</b>
Heat shock cognate 71 kDa protein	Hspa8	1.070	0.958	0.039	Possibly in mitochondria
Kinectin	Ktn1	1.066	1.154	0.012	Possibly in mitochondria
Fatty acid synthase;[Acyl-carrier-protein] S-acetyltransferase;[Acyl-carrier-protein] S-malonyltransferase;3-oxoacyl-[acyl-carrier-protein] synthase;3-oxoacyl-[acyl-carrier-protein] reductase	Fasn	1.063	0.855	0.003	Possibly in mitochondria
Syntaxin-4	Stx4	1.052	0.885	0.021	Possibly in mitochondria
ATP synthase subunit f, Mitochondria	Atp5j2	1.041	0.808	0.004	Mitochondria
Serine/threonine-protein phosphatase PP1-alpha catalytic subunit	Ppp1ca	1.041	0.869	0.042	Possibly in mitochondria
Mimitin, Mitochondria	Ndufaf2	1.010	0.830	0.023	Mitochondria
Succinate dehydrogenase [ubiquinone] iron-sulfur subunit, Mitochondria	Sdhb	1.006	1.095	0.010	Mitochondria
NADH dehydrogenase (ubiquinone) flavoprotein 3, 10kDa	Ndufv3	1.001	1.199	0.024	Mitochondria
Transmembrane protein 11, Mitochondria	Tmem11	0.993	0.760	0.039	Mitochondria
Cytochrome c oxidase assembly protein COX15 homolog	Cox15	0.990	0.721	0.001	Mitochondria
Hypoxia up-regulated protein 1	Hyou1	0.981	1.100	0.048	Possibly in mitochondria
NADH dehydrogenase [ubiquinone] 1 alpha subcomplex subunit 9, Mitochondria	Ndufa9	0.974	0.951	0.020	Mitochondria
Guanine nucleotide-binding protein subunit alpha-11	Gna11	0.966	0.760	0.010	Possibly in mitochondria
Cytochrome c, somatic	Cycs;Gm10108	0.966	1.344	0.045	Mitochondria
28S ribosomal protein S15, Mitochondria	Mrps15	0.966	0.749	0.040	Mitochondria
Cytochrome c oxidase subunit 7A2, Mitochondria	Cox7a2	0.964	1.100	0.012	Mitochondria
Mitochondria translocator assembly and maintenance protein 41 homolog	Tamm41	0.958	1.098	0.048	Mitochondria
Glycerol-3-phosphate dehydrogenase, Mitochondria	Gpd2	0.943	1.103	0.028	Mitochondria
Twinfilin-1	Twf1	0.942	0.687	0.030	Possibly in mitochondria

**Table A-1 (cont'd).**

<b>Protein Name</b>	<b>Gene Name</b>	<b>C7(T/D) Mean</b>	<b>C12(T/D) Mean</b>	<b>P-value</b>	<b>Intracellular Location</b>
Acetolactate synthase-like protein	Ilvbl	0.939	1.171	0.003	Possibly in mitochondria
Pyruvate dehydrogenase E1 component subunit alpha, somatic form, Mitochondria	Pdha1	0.936	1.196	0.036	Mitochondria
G-rich sequence factor 1	Grsf1	0.935	0.716	0.014	Mitochondria
Serine/threonine-protein phosphatase;Serine/threonine-protein phosphatase 2A catalytic subunit alpha isoform;Serine/threonine-protein phosphatase 2A catalytic subunit beta isoform	Ppp2cb;Ppp2ca	0.915	1.120	0.041	Mitochondria
Voltage-dependent anion-selective channel protein 2	Vdac2	0.915	1.052	0.042	Mitochondria
Saccharopine dehydrogenase-like oxidoreductase	Sccpdh	0.908	1.126	0.001	Mitochondria
Mitochondria import inner membrane translocase subunit Tim8 A	Timm8a1	0.904	1.193	0.039	Mitochondria
ATP-binding cassette sub-family B member 7, Mitochondria	Abcb7	0.893	1.102	0.003	Mitochondria
Bcl-2-like protein 1	Bcl2l1	0.884	1.128	0.005	Mitochondria
Reactive oxygen species modulator 1	Romo1	0.876	0.457	0.025	Mitochondria
Lon protease homolog, Mitochondria	Lonp1	0.874	1.036	0.024	Mitochondria
Stomatin-like protein 2, Mitochondria	Stoml2	0.870	1.055	0.016	Mitochondria
Adenylate kinase 2, Mitochondria	Ak2	0.856	1.338	0.033	Mitochondria
ATPase family AAA domain-containing protein 3	Atad3	0.847	1.098	0.001	Mitochondria
Monofunctional C1-tetrahydrofolate synthase, Mitochondria	Mthfd1l	0.844	0.963	0.013	Mitochondria
GTPase Era, Mitochondria	Eral1	0.840	0.610	0.029	Mitochondria
DnaJ homolog subfamily C member 5	Dnajc5	0.838	1.106	0.007	Mitochondria
Apoptosis-inducing factor 1, Mitochondria	Aifm1	0.837	1.032	0.032	Mitochondria
GTP:AMP phosphotransferase AK4, Mitochondria	Ak4	0.823	1.116	0.018	Mitochondria
Alpha-enolase;Enolase	Eno1	0.806	0.958	0.008	Possibly in mitochondria
Mitochondria genome maintenance exonuclease 1	Mgme1	0.805	1.049	0.024	Mitochondria
Estradiol 17-beta-dehydrogenase 8	Hsd17b8;H2-Ke6	0.783	1.116	0.008	Mitochondria

**Table A-1 (cont'd).**

<b>Protein Name</b>	<b>Gene Name</b>	<b>C7(T/D) Mean</b>	<b>C12(T/D) Mean</b>	<b>P-value</b>	<b>Intracellular Location</b>
Thioredoxin-like protein 1	Txn1l	0.778	0.936	0.011	Possibly in mitochondria
4F2 cell-surface antigen heavy chain	Slc3a2	0.743	0.937	0.015	Possibly in mitochondria
Amine oxidase [flavin-containing] A	Maoa	0.734	1.042	0.046	Mitochondria
Mitochondria 10-formyltetrahydrofolate dehydrogenase	Aldh1l2	0.703	0.973	0.003	Mitochondria
Bcl-2-like protein 11	Bcl2l11	0.682	0.978	0.002	Mitochondria
Retinal dehydrogenase 1	Aldh1a1	0.680	0.919	0.011	Possibly in mitochondria
Mitochondria 2-oxodicarboxylate carrier	Slc25a21	0.673	0.917	0.001	Mitochondria
Vesicle-associated membrane protein 4	Vamp4	0.664	1.178	0.018	Possibly in mitochondria
Formin-like protein 2	Fmn12	0.654	0.471	0.034	Possibly in mitochondria
Bifunctional methylenetetrahydrofolate dehydrogenase/cyclohydrolase, Mitochondria;NAD-dependent methylenetetrahydrofolate dehydrogenase;Methenyltetrahydrofolate cyclohydrolase	Mthfd2	0.642	0.926	0.012	Mitochondria
Acyl-coenzyme A thioesterase 2, Mitochondria;Acyl-coenzyme A thioesterase 1	Acot2;Acot1	0.581	1.266	0.038	Mitochondria
Tumor necrosis factor receptor type 1-associated DEATH domain protein	Tradd	0.566	1.046	0.049	Possibly in mitochondria
Mitochondria import inner membrane translocase subunit Tim17-B	Timm17b	0.543	2.026	0.005	Mitochondria
Adenine phosphoribosyltransferase	Aprt	0.530	0.785	0.022	Possibly in mitochondria
Thioredoxin reductase 1, cytoplasmic	Txnrd1	0.401	0.704	0.045	Possibly in mitochondria
Leukocyte surface antigen CD47	Cd47	0.334	1.042	0.001	Possibly in mitochondria
Myosin-14	Myh14	0.262	1.007	0.049	Possibly in mitochondria

**Table A-2. Identified nonmitochondrial proteins differentially regulated by 10 nM TCDD exposure for 72 h in an AHR-dependent manner.**

Protein Name	Gene Name	C7(T/D) Mean	C12(T/D) Mean	P-value	Intracellular Location
Ectonucleoside triphosphate diphosphohydrolase 2	Entpd2	7.413	1.196	0.027	ER
Tenascin XB	Tnxb	3.416	1.273	0.016	Extracellular
Poly (ADP-ribose) polymerase family, member 3	Parp3	1.945	0.934	0.029	Cytoskeletal
Myoferlin	Myof	1.813	1.043	0.024	Plasma membrane
Tetraspanin-8	Tspan8	1.758	1.182	0.037	Lysosome
Endophilin-B2	Sh3glb2	1.594	1.079	0.007	Nucleus
Protein MON2 homolog	Mon2	1.533	1.000	0.033	
cDNA sequence BC094435	ENSMUSG0000 0073624; BC094435	1.501	0.891	0.004	
IST1 homolog	Ist1	1.498	0.845	0.016	ER
Peroxisomal 2,4-dienoyl-CoA reductase	Decr2	1.357	0.841	0.038	Peroxisome
UDP-glucose 6-dehydrogenase	Ugdh	1.353	1.009	0.002	Cytosol
ER membrane protein complex subunit 7	Emc7	1.345	0.973	0.025	
Laminin subunit beta-2	Lamb2	1.307	1.025	0.004	
Cartilage-associated protein	Crtap	1.300	1.100	0.012	
Unconventional myosin-XVIIIa	Myo18a	1.264	1.030	0.012	
Putative RNA-binding protein 3	Rbm3	1.258	0.749	0.010	Nucleus
SEC23-interacting protein	Sec23ip	1.249	1.035	0.036	ER
Protein SEC13 homolog	Sec13	1.246	0.683	0.045	ER
Surfeit locus protein 4	Surf4	1.237	1.081	0.023	ER
Nicalin	Ncln	1.216	0.957	0.027	ER
Dynactin subunit 4	Dctn4	1.184	0.819	0.041	

**Table A-2 (cont'd).**

<b>Protein Name</b>	<b>Gene Name</b>	<b>C7(T/D) Mean</b>	<b>C12(T/D) Mean</b>	<b>P-value</b>	<b>Intracellular Location</b>
caldesmon 1	Cald1	1.174	0.804	0.007	Cytoskeletal
Laminin subunit gamma-1	Lamc1	1.155	0.998	0.006	Extracellular
Triple functional domain protein	Trio	1.153	0.871	0.041	Cytosol
60S acidic ribosomal protein P0	Rplp0;Gm8730	1.148	0.953	0.020	
Baculoviral IAP repeat-containing protein 6	Birc6	1.139	0.976	0.009	
Protein VAC14 homolog	Vac14	1.132	0.932	0.048	ER
Guanine nucleotide-binding protein G(q) subunit alpha	Gnaq	1.130	0.837	0.028	
Dynammin-2	Dnm2	1.106	0.896	0.004	
Protein RER1	Rer1	1.104	0.933	0.014	Golgi
Proteasome subunit beta type-6	Psmb6	1.099	0.858	0.020	Cytosol
ADP-ribosyl cyclase 2	Bst1	1.090	0.900	0.047	Plasma membrane
CD9 antigen	Cd9	1.047	0.868	0.000	
CD2-associated protein	Cd2ap	1.046	0.719	0.008	Cytoskeletal
26S proteasome non-ATPase regulatory subunit 11	Psmd11	1.036	0.887	0.048	
Tetraspanin-9	Tspan9	1.031	0.660	0.026	Plasma membrane
Protein FAM49B	Fam49b	1.029	0.745	0.027	
Beta-2-microglobulin	B2m	1.025	0.545	0.000	Extracellular
GPI transamidase component PIG-S	Pigs	1.001	1.468	0.005	ER
40S ribosomal protein S20	Rps20	0.996	0.692	0.024	
Stress-induced-phosphoprotein 1	Stip1	0.995	0.856	0.026	Golgi, Nucleus
Integrin alpha-3;Integrin alpha-3 heavy chain;Integrin alpha-3 light chain	Itga3	0.988	0.804	0.020	
Proteasome subunit alpha type-6	Psma6	0.979	0.829	0.042	
Collectin-12	Colec12	0.970	0.478	0.008	Extracellular

**Table A-2 (cont'd).**

Protein Name	Gene Name	C7(T/D) Mean	C12(T/D) Mean	P-value	Intracellular Location
Transmembrane protein 126A	Tmem126a	0.967	0.672	0.026	
60S ribosomal protein L29	Gm17669;Rpl29 ;Gm10709;Gm5 218	0.964	0.695	0.024	
Basal cell adhesion molecule	Bcam	0.962	0.718	0.031	
BAG family molecular chaperone regulator 2	Bag2	0.946	1.263	0.039	Cytosol
X-ray repair cross-complementing protein 5	Xrcc5	0.944	1.295	0.032	Nucleus
Kalirin	Kalrn	0.939	1.065	0.027	Cytoskeletal
Peroxisomal membrane protein PEX14	Pex14	0.939	1.197	0.001	Nucleus/Peroxisome
40S ribosomal protein S15	Rps15	0.925	0.674	0.032	
60S ribosomal protein L27a	Rpl27a	0.894	0.777	0.036	
Multidrug resistance-associated protein 5	Abcc5	0.892	1.055	0.019	Plasma membrane
Histone H1.4	Hist1h1e	0.873	1.339	0.034	Nucleus
60S ribosomal protein L36	Rpl36	0.868	0.682	0.001	
Vasodilator-stimulated phosphoprotein	Vasp	0.855	0.659	0.024	Cytoskeletal
Heterogeneous nuclear ribonucleoprotein A/B	Hnrnpab	0.852	1.090	0.006	Nucleus
Vacuolar ATPase assembly integral membrane protein VMA21	Vma21	0.839	0.518	0.030	ER
Reticulon 4	Rtn4	0.817	1.167	0.019	ER
WASH complex subunit strumpellin	Kiaa0196; E430025E21Rik	0.799	1.057	0.000	Endosome
Lactadherin	Mfge8	0.783	1.044	0.026	Extracellular
Annexin;Annexin A3	Anxa3	0.734	0.970	0.041	Plasma membrane
Integrin alpha-6;Integrin alpha-6 heavy chain;Integrin alpha-6 light chain	Itga6	0.734	0.838	0.039	Extracellular

**Table A-2 (cont'd).**

<b>Protein Name</b>	<b>Gene Name</b>	<b>C7(T/D) Mean</b>	<b>C12(T/D) Mean</b>	<b>P-value</b>	<b>Intracellular Location</b>
High affinity cationic amino acid transporter 1	Slc7a1; SLC7A1	0.650	0.814	0.004	Plasma membrane
Protein phosphatase 1 regulatory subunit 7	Ppp1r7	0.649	1.028	0.024	Cytosol
Dimethylaniline monooxygenase [N-oxide-forming] 1	Fmo1	0.632	2.507	0.029	ER
Collagen alpha-1(XII) chain	Col12a1	0.448	0.989	0.031	Extracellular

**APPENDIX B. HYPOXIA INDUCIBLE FACTORS (HIFs) MODULATE MITOCHONDRIAL  
OXYGEN CONSUMPTION AND TRANSCRIPTIONAL REGULATION OF NUCLEAR-  
ENCODED ELECTRON TRANSPORT CHAIN GENES**

**Authors: Hye Jin Hwang, Scott G. Lynn, Ajith Vengellur, Yogesh Saini, Elizabeth A. Grier,  
Shelagh M. Ferguson-Miller, and John J. LaPres**

This chapter is adapted with permission from *Biochemistry*, 2015, 54 (24), 3739–3748.

Copyright 2015 American Chemical Society.

## **Abstract**

Hypoxia inducible factor-1 (HIF1) is a stress-responsive nuclear transcription factor that is activated with a decrease in oxygen availability. HIF1 regulates the expression of genes involved in a cell's adaptation to hypoxic stress, including those with mitochondrial specific function. To gain a more comprehensive understanding of the role of HIF1 in mitochondrial homeostasis, we studied the link between hypoxia, HIF1 transactivation, and electron transport chain (ETC) function. We established immortalized mouse embryonic fibroblasts (MEFs) for HIF1 $\alpha$  wild-type (WT) and null cells and tested whether HIF1 $\alpha$  regulates mitochondrial respiration by modulating gene expressions of nuclear encoded ETC components. High-throughput quantitative real-time polymerase chain reaction was performed to screen nuclear encoded mitochondrial genes related to the ETC to identify those whose regulation was HIF1 $\alpha$ -dependent. Our data suggest that HIF1 $\alpha$  regulates transcription of cytochrome c oxidase (CcO) heart/muscle isoform 7a1 (*Cox7a1*) under hypoxia where it is induced 1.5-2.5 fold, whereas *Cox4i2* hypoxic induction was HIF1 $\alpha$ -independent. We propose that adaptation to hypoxic stress of CcO as the main cellular oxygen consumer is mediated by induction of hypoxia-sensitive tissue-specific isoforms. We suggest that HIF1 plays a central role in maintaining homeostasis in cellular respiration during hypoxic stress via regulation of CcO activity.

## **Introduction**

Hypoxia is defined as a state in which the level of oxygen drops below normal in cells or tissues.<sup>211</sup> Hypoxia causes stress within a cell that disrupts homeostasis and these hypoxia-induced disruptions are associated with all of the leading causes of death in the United States, including cardiovascular disease, strokes, and cancer.<sup>169, 212</sup> Because of the detrimental effects of decreased oxygen tension, primarily at the level of energetics, organisms have developed a programmed response to this condition.<sup>213</sup> This response is predominantly aimed at increasing the level of glucose utilization at the cellular level and the stimulation of erythropoiesis and angiogenesis at organismal levels.<sup>212</sup> This occurs primarily through the transcriptional regulation of genes involved in these processes, such as those for glycolytic enzymes and transporters (*Gapdh* and *Slc2a1*), erythropoietin (*Epo*), and vascular endothelial growth factor (*Vegfa*). The transcriptional response to hypoxia is primarily regulated by a subset of the PAS superfamily of proteins, the hypoxia inducible factors.<sup>211, 212</sup>

Hypoxia inducible factors (HIFs), which include HIF1 $\alpha$ , HIF2 $\alpha$ , HIF3 $\alpha$ , aryl hydrocarbon receptor nuclear translocator (ARNT, also known as HIF1b) and ARNT2, are transcriptional regulators whose activity is sensitive to decreases in oxygen availability.<sup>169, 212</sup> HIF1 $\alpha$ , HIF2 $\alpha$ , and HIF3 $\alpha$  are primarily cytoplasmic and, under normal oxygen tension conditions, are quickly degraded by the ubiquitin pathway. This degradation is dependent upon protein motifs, termed oxygen-dependent degradation domains (ODDs), found near the carboxy terminus of the protein.<sup>212</sup> The hydroxylation of conserved residues within the ODD by oxygen-requiring prolyl hydroxylase domain-containing proteins (PHDs) targets HIFs for proteasomal degradation. Under hypoxic conditions, HIFs are stabilized and translocate to the nucleus where they are free to form dimers with ARNT or ARNT2. These heterodimers bind genomic DNA at sites called hypoxia response elements (HREs) to modulate transcription.<sup>212</sup> Though HIFs are the primary mediators of the cellular response to hypoxic stress, HIF-independent signaling pathways also play a significant role following exposure to low levels of oxygen.<sup>214, 215</sup>

Hypoxia directly impacts mitochondrial function by limiting the availability of oxygen necessary to complete the electron transport chain (ETC). Mitochondria utilize approximately 90% of cellular oxygen and, in return, generate approximately 90% of the total cellular energy (ATP) in normal tissues.<sup>216, 217</sup> Aerobic respiration involves three distinct phases: oxidation of substrates (e.g., glucose), electron transport, and oxidative phosphorylation (OXPHOS). In this process, reducing equivalents, primarily derived from the tricarboxylic acid (TCA) cycle, are transferred to the ETC and ultimately to O<sub>2</sub>. The energetically favorable movement of electrons within the ETC is coupled to the production of an electrochemical gradient across the inner membrane of the mitochondria, which is used to drive ATP synthesis. The critical role of oxygen in this process makes the ability to cope with changes in oxygen tension a metabolic priority. To maintain necessary energy levels under hypoxic stress, eukaryotic cells adapt by switching to anaerobic metabolism and substrate level phosphorylation. Most of the regulation necessary to make this metabolic switch is provided by HIF1 via transcriptional regulation of a battery of genes, including glycolytic enzymes, glucose transporters, and pyruvate dehydrogenase kinase.<sup>218</sup> HIF1 also impacts mitochondrial function via transcriptional regulation of Bcl-2/adenovirus E1B 19 kDa-interacting protein3 (*Bnip3*) expression.<sup>219, 220</sup> In addition, HIF1 negatively regulates mitochondrial biogenesis and O<sub>2</sub> consumption by activating the transcription of genes that regulate c-Myc and by suppressing mitochondrial gene expression nontranscriptionally.<sup>218, 221</sup>

The respiratory chain in the inner mitochondrial membrane contains four enzyme complexes (I-IV) through which electrons pass on their way to reducing O<sub>2</sub> to water. Complex IV, cytochrome c oxidase (CcO), transfers the electrons from cytochrome c to O<sub>2</sub> for the exergonic oxygen reduction reaction, which is utilized for the proton pump. Mammalian CcO crystallizes as a dimer, with each monomer containing 13 subunits, where subunits 1-3 are encoded by the mitochondrial genome. The other 10 subunits are nuclear-encoded proteins with COX4, COX6A, COX6B, COX7A, and COX8 having tissue- and species-specific

isoforms.<sup>210, 222-224</sup> COX4, specifically isoform 1 (*Cox4i1*), has been implicated in the allosteric inhibition of CcO via binding of ATP to the matrix domain.<sup>116, 225</sup> Hypoxia was shown to upregulate *Cox4i2* isoform expression in liver and lung, which can alter CcO activity, ATP levels, and ROS production and is proposed as a mechanism for protecting tissues from oxidative damage.<sup>226, 227</sup> *Cox6a* isoforms are postulated to participate in mammalian thermogenesis by decreasing H<sup>+</sup>/e<sup>-</sup> ratios and increasing respiration and heat production.<sup>116</sup> *Cox7a1* is expressed tissue-specifically in heart and skeletal muscle, and *Cox7a2*, a liver-type isoform, is expressed ubiquitously. Though it has been suggested that *Cox7a* isoforms are associated with glucose uptake, total body aerobic capacity, StAR expression, and steroidogenesis, very little is known about the function of this isoform pair.<sup>228, 229</sup>

To gain a more comprehensive understanding of the link between hypoxic stress, HIF1 $\alpha$  activation, and mitochondrial function, we generated two immortalized cell lines [*Hif1 $\alpha$* , wild-type (WT) and null] and measured extracellular oxygen levels (indicative of oxygen consumption rates) after exposure to mitochondrial modulators. Following challenge, the cells were also assessed for changes in mitochondrial function and the expression of genes that encode proteins that are important for ETC and OXPHOS via a comprehensive qPCR screen. The results revealed HIF1 $\alpha$ -responsive genes within the ETC, especially in complex IV, subunit 7a1 of cytochrome c oxidase (*Cox7a1*). Finally, the results suggest that Hif1a plays a central role in regulating the specific activity of CcO under various experimental conditions. This most likely involves various mechanisms, such as allosteric regulation, the redox status of the cell, and, in cells that express both subunits, complex composition.

## **Materials and Methods**

### **Mouse Embryonic Fibroblast (MEF) Isolation**

*Hif1a*<sup>flox/flox</sup> transgenic mice were generous gifts from R. Johnson (University of Cambridge, Cambridge, U.K.). Mice used in this study were kept at the animal housing facility under strict hygienic and pathogen-free conditions approved by the University Laboratory Animal Resource regulatory unit. All procedures were performed with the approval of the Michigan State University Committee on Animals Use and Care. Genotype-specific homozygous male and female mice were mated, and the females were kept isolated until day 14 of gestation (vaginal plug detection day was considered as day 0). Dams were anesthetized in a CO<sub>2</sub> chamber for 90 s and then sacrificed using cervical dislocation. Embryos were surgically removed from the uterine horns and processed for fibroblast isolation using a protocol adapted from previous reports.<sup>230</sup> Briefly, after surgical excision, embryos were transferred to a sterile cell culture hood, washed with 70% ethanol and PBS, cleaned (removal of liver, limbs and head), diced, incubated with trypsin/EDTA at 37 °C for 30 min and then passed through a 22 gauge needle onto a 10 cm plate and placed in a 37 °C incubator.

### **Cell Culture**

High-glucose (Glc) MEF medium was Dulbeco's modified Eagle's medium (DMEM) (#11965, Gibco, Grand Island, NY) containing glucose (4500 mg/L) supplemented with 10% heat inactivated fetal bovine serum (FBS), 100 U/mL penicillin, 100 µg/mL streptomycin, 2mM L-glutamine, 0.1 mM nonessential amino acids, and 10 mM HEPES (pH 7.8). Galactose (Gal) MEF medium was glucose-free DMEM (#11966, Gibco) supplemented with 10 mM galactose and all additives described above. All cell culture work, unless otherwise specified, was performed under standard cell culture conditions (5% CO<sub>2</sub>, 35% humidity, and 37 °C) in a NAPCO 7000 incubator (NAPCO, Winchester, VA) for normoxic conditions (21% O<sub>2</sub>) or in an O<sub>2</sub>

Controlled Glove Box (Coy Laboratory Products Inc., Grass Lake, MI) for hypoxic conditions (1% O<sub>2</sub>).

### **MEF Cell Line Generation and Genotyping**

Freshly isolated MEF cells were plated in 10 cm plates at ~70% confluency with Glc medium changed daily. Cells were then immortalized by transfection with a plasmid construct (pRNS) containing the SV-40 large T antigen (a generous gift from C.C. Chang, Michigan State University) using Lipofectamine 2000 (Invitrogen, Carlsbad, CA) following the manufacturer's instructions. Positive stable integrants were selected with 300 µg/mL of G418 (Gibco). G418 resistant cells were split and infected with either LacZ recombinant (Ad-CMV-b-Gal) or Cre recombinase (Ad-CMV-Cre) adenovirus (Vector BioLabs, Philadelphia, PA) at 4000 multiplicity of infection for 48 h. Cells were then plated at very low densities (100 cells/15 cm plate) and when individual colonies became visible, clones were isolated and genotyped. Four WT and four null clones for *Hif1α* were pooled in equal numbers to generate two cell lines, *Hif1α* WT and *Hif1α* null. For genotyping, cell lines were grown to confluency in a 6 cm plate, rinsed and scraped with cold PBS (4 °C), and collected by centrifugation. Genomic DNA extraction and genotyping were performed on the cell pellet as previously described (primers F, TTG GGG ATG AAA ACA TCT GC; primer R, GCA GTT AAG AGC ACT AGT TG).<sup>231</sup> The size of the amplified gene for *Hif1α* WT was 962 bp.

### **Nuclear Protein Preparation**

MEF cells were grown in 15 cm plates to confluency under normoxic (21% O<sub>2</sub>) or hypoxic (1% O<sub>2</sub>) conditions or with 150 µM CoCl<sub>2</sub> for 24 h, and protein extracts were prepared as described previously.<sup>169</sup> Briefly, cells were washed with cold PBS (4 °C) and removed from the plate surface by being scraped in cold (4 °C) PBS and collected by centrifugation. Nuclear

fractions were prepared by lysing the cells in 10 mM Tris (pH 7.5), 1.5 mM MgCl<sub>2</sub>, 10 mM KCl supplemented with Complete-mini EDTA-free protease inhibitor tablets (Roche Applied Science, Indianapolis, IN), 2 mM DTT, 1 mM Na<sub>3</sub>VO<sub>4</sub>, and 0.4 mM PMSF and kept on ice for 10 min. Nuclei were collected by centrifugation (12000g for 10 min) and resuspended in 20 mM Tris (pH 7.5), 0.42 M KCl, 20% glycerol, and 1.5 mM MgCl<sub>2</sub> supplemented as described above and rotated for 45 min at 4 °C. Insoluble material was removed by centrifugation (20000g for 10 min), and the protein concentrations of the supernatant were determined using the Bio-Rad (Hercules, CA) Bradford assay kit and BSA standards.<sup>178</sup> Protein samples were analyzed for HIF1α stabilization through Western blotting.

### **Mitochondrial Protein Preparation**

MEF cells were grown in 15 cm plates to confluency under normoxic (21% O<sub>2</sub>) or hypoxic (1% O<sub>2</sub>) conditions for 24 h, and mitochondria were isolated using a protocol adapted from a previous report.<sup>168</sup> Briefly, cells were washed with cold PBS (4 °C) and removed from the plate surface by being scraped in solution A (0.25 M sucrose, 20 mM HEPES, 10 mM KCl, 1.5 mM MgCl<sub>2</sub>, 1 mM EDTA, 1 mM EGTA, 1 mM DTT, and 0.1 mM PMSF). Samples were then subjected to three freeze/thaw cycles with mixing by pipet for each thaw, and insoluble material was removed by centrifugation (700g for 10 min at 4 °C). The supernatant was further cleared by centrifugation (10000g for 15 min at 4 °C) and aspirated, and the pellet was resuspended in solution A. Mitochondrial protein concentrations were determined using Bio-Rad Bradford assay kit and BSA standards.<sup>178</sup> Protein samples were analyzed for CcO enzyme activity.

### **Western Blotting**

Protein samples were separated by sodium dodecyl sulfate–polyacrylamide gel electrophoresis (SDS-PAGE) and transferred to a nitrocellulose membrane. Western blots were

performed with rabbit antibodies against HIF1 $\alpha$  (NB100-479, Novus Biologicals, Inc., Littleton, CO) and  $\beta$ -actin (SC-7210, Santa Cruz Biotechnology, Inc., Dallas, TX). Proteins were visualized with horseradish peroxidase-conjugated goat anti-rabbit IgG (sc-2004, Santa Cruz Biotechnology, Inc.) and an ECL Western blot system (Pierce, Rockford, IL).

### **Oxygen Consumption Rate (OCR) Measurements**

OCR was measured using an XF24 Extracellular Flux Analyzer (Seahorse Bioscience, Billerica, MA) as described in the manufacturer's instructions. *Hif1 $\alpha$*  WT and null cells, preadapted to medium glucose levels for 24 h, were plated in Glc or Gal medium at a density of 40000 cells/well and were allowed to adhere to the plate for 24 h. The culture medium was then replaced with specific XF24 assay medium. Glc XF24 assay medium consisted of DMEM base (#D5030, Sigma-Aldrich, St. Louis, MO) supplemented with 25 mM glucose, 31 mM NaCl, 1 mM sodium pyruvate (Atlanta Biologicals, Inc., Flowery Branch, GA), 2 mM GlutaMAX (Gibco) and 15 mg/L phenol red (Sigma-Aldrich). Gal XF24 assay medium consisted of DMEM base (#D5030, Sigma-Aldrich) supplemented with 10 mM galactose instead of glucose and all additives described above. Measurement of OCR was started 90 min after switching XF24 assay medium and the inhibitors of ETC and OXPHOS system were injected in the following order: oligomycin A (1  $\mu$ M), CCCP (1.5  $\mu$ M for WT and 0.75  $\mu$ M for null cells), and rotenone (0.5  $\mu$ M)/antimycin A (0.5  $\mu$ M). The concentration of CCCP for each cell line was optimized by measuring OCR in different nutrient environments, Glc or Gal XF24 assay medium. After OCR had been measured, cells were washed with cold PBS and lysed in buffer [10 mM Tris-HCl (pH 7.5) and 0.1% Triton X-100] by being frozen and thawed. The total protein amounts in each well were determined using a Bio-Rad Bradford assay kit and BSA standards.<sup>178</sup> The OCR (picomoles per minute) was divided by total protein amounts for each well, and spare respiratory capacity was calculated by manufacturer's software, the XF Mito Stress Test Report Generator.

## **RNA Isolation and Quantitative Real-Time PCR (qPCR)**

RNA was isolated from the two different cell strains cultured in different carbon sources and at different oxygen tensions using TRIzol reagent via the manufacturer's instructions (Invitrogen). RNA pellets were resuspended in ddH<sub>2</sub>O and quantified spectrophotometrically (260 nm). Total RNA (2 μg) was reverse transcribed by SuperScript III using an anchored oligo-(dT)<sub>20</sub> primer as described by the manufacturer (Invitrogen). The resulting cDNA was diluted in ddH<sub>2</sub>O and used as a template for high-throughput qPCR (HTP qPCR) and manual qPCR. Primer pairs were designed to amplify 104 nuclear genes that encode specific mitochondrially related proteins (table B-1). In total, 40 ETC complex I, 4 ETC complex II, 16 ETC complex III, 15 ETC complex IV, and 19 ETC complex V genes were assayed. Five uncoupling proteins, three chaperone, three housekeeping reference, and five control genes (one stress responsive gene and four HIF1α-responsive genes) were also examined.

HTP qPCR mixtures consisting of 2 μL of cDNA, 0.3 μM of each primer and 2X Power SYBR Green PCR Master Mix (Applied Biosystems, Foster City, CA) were aliquoted into 384-well plates using a Biomeck 2000 Laboratory Automation Workstation (Beckman Coulter Inc., Fullerton, CA). Amplification was conducted using an Applied Biosystems PRISM 7900HT Sequence Detection System. Quantification was determined using the comparative C<sub>T</sub> method ( $\Delta\Delta C_T$ ) (Applied Biosystems). The geometric mean of the expression of three housekeeping genes (*Actb*, *Hprt*, and *Ppia*) was used to control for differences in RNA loading, quality, and cDNA synthesis. Fold changes in expression were calculated with HTP qPCR results using the  $\Delta\Delta C_T$  method with the WT Glc control (WT Glc Ctrl) group for each time point (4 and 24 h) being scaled to equal 1. Cluster version 3.0 software was used to generate average linkage files, and Maple Tree version 0.2.3.2 BETA (<http://sourceforge.net/projects/mapletree/>) was used to create colored dendrograms from the linkage files, where red indicates upregulation and green indicates downregulation.<sup>232</sup>

Manual qPCR was performed with 25  $\mu\text{L}$  reactions (5  $\mu\text{L}$  of cDNA template, each primer at 0.3  $\mu\text{M}$ , 3 mM  $\text{MgCl}_2$ , 200  $\mu\text{M}$  dNTPs, 0.6 unit of AmpliTaq Gold and 10X SYBR Green PCR Buffer) and amplified using an Applied Biosystems PRISM 7000 Sequence Detection System. The *Hprt* housekeeping gene was a reference and expression levels of key genes (*Slc2a1*, *Vegfa*, *Cox4i1*, *Cox4i2*, *Bnip3*, *Cox6a1*, *Cox6a2*, *Cox7a1*, and *Cox7a2*) were calculated using the  $\Delta\Delta C_T$  method. Fold changes of *Slc2a1*, *Vegfa*, and *Bnip3* were calculated compared to the WT Glc control group (WT Glc Ctrl) for 24 h being scaled to equal 1. Fold changes of *Cox4i1*, *Cox4i2*, *Cox6a1*, *Cox6a2*, *Cox7a1*, and *Cox7a2* were expressed compared to the WT Glc Ctrl of one isoform of each Cox subunit for 24 h being scaled to equal 1.

### **Measurement of CcO Enzyme Activity**

CcO activity was determined as previously described with slight modifications.<sup>233</sup> Bovine heart cytochrome c was dissolved in assay buffer (40 mM phosphate buffer and 0.5% Tween 80) at 0.4 mg/mL and was reduced using sodium dithionite. The fully reduced cytochrome c was confirmed by the ratio of absorbance at 550 and 565 nm, and the change in absorbance at 550 nm was recorded as a function of time for the CcO assay. After the absorbance at 550 nm of reduced cytochrome c ( $A_{\text{red}}$ ) had been recorded, isolated mitochondria were added and the absorbance at 550 nm was recorded every 5 s for 3 min. The CcO activity was calculated using the expression

$(\Delta\text{Abs}_{550}/\text{min}) \times (\text{total assay volume})$

$/ [19.6 \text{ mM}^{-1} \times (\text{mitochondrial volume}) \times (\text{mitochondrial concentration})]$

with units of micromoles per min per milligram. The specific activity was calculated as a turnover number in inverse minutes, dividing CcO activity in micromoles per min per milligram protein by mitochondrial CcO concentration in micromoles per milligram protein. The

absorbance for CcO activity was measured using a SpectraMax M2 spectrophotometer (Molecular Devices, Sunnyvale, CA).

### **Mitochondrial CcO Measurement**

The concentration of cytochrome *aa*<sub>3</sub> (CcO) was determined as previously described<sup>234</sup> by measuring the visible difference spectra (dithionite-reduced minus ferricyanide-oxidized) of the detergent solubilized mitochondria from 500 to 700 nm. The peak at 605 nm represented the reduced minus oxidized peak of cytochrome *a*. The concentration of CcO was calculated using the extinction coefficient for reduced-oxidized CcO of 24 mM<sup>-1</sup>cm<sup>-1</sup> at 605-630 nm.

### **Statistical Analysis**

The result of spare respiratory capacity was analyzed for significant differences by analysis of variance (ANOVA) followed by Tukey's post hoc test.

## ***Results***

### **Creation of Hif1α WT and Null Cells**

The genotype of the *Hif1α* WT and *Hif1α* null cells was confirmed by PCR, and the extent of recombination was approximately 100% in the nulls (Figure B-1A). To confirm the functional deletion of the *Hif1α* gene, HIF1α protein levels following exposure to control conditions (Ctrl), 150 μM CoCl<sub>2</sub> (Co) or hypoxia (1% O<sub>2</sub>, Hyp) for 24 h were examined by Western blot analysis (Figure B-1B). *Hif1α* null cells did not express HIF1α protein under CoCl<sub>2</sub> or hypoxia, confirming that recombination-induced functional deletion of *Hif1α* gene was approximately 100%.

### **Cellular Respiration in Hif1 $\alpha$ WT and Null Cells under Different Energy Sources**

To determine the role of HIF1 $\alpha$  in cellular respiration, the extracellular oxygen flux of each cell line in different nutrients was measured to calculate OCR (Figure B-2). OCR was monitored in the presence of ETC and OXPHOS inhibitors, oligomycin (a), CCCP (b), and rotenone/antimycin (c), in *Hif1 $\alpha$*  WT and null cells in Glc and Gal media (Figure B-2A). It is important to note that spare respiratory capacity was described as maximal respiration [i.e., the OCR in presence of CCCP (44.9 min in Figure B-2A)] divided by a basal respiration (OCR at 9.9 min in Figure B-2A) times 100 (Figure B-2B). The *Hif1 $\alpha$*  WT cells in both Glc and Gal media had spare respiratory capacities significantly higher than those of *Hif1 $\alpha$*  null cells in the Gal media (WT Glc, 182%; WT Gal, 222 %; null Gal, 100 %). The *Hif1 $\alpha$*  null cells in the Glc media showed a spare respiratory capacity of 158 %, but this was not significant when compared to that of null cells in the Gal media. Similar results were also observed in the two cell types and under different conditions when pericellular oxygen consumption was measured using a SensorDish<sup>®</sup> Reader (PreSens Precision Sensing GmbH, Regensburg, Germany)<sup>235</sup> (data not shown).

### **Screening HIF1-Dependent mRNA Expression of Nuclear-Encoded Mitochondrial Genes**

The oxygen consumption data suggest that the cellular respiration efficiency in the two cell types is inherently different. To further elucidate the role of HIF1 $\alpha$  in mitochondrial function, HTP qPCR was utilized to screen the expression levels of 104 nuclear-encoded genes associated with the ETC and mitochondrial function. *Hif1 $\alpha$*  WT and null cells were exposed to control (Ctrl) conditions or 1% O<sub>2</sub> (Hyp) in both Glc and Gal media for 4 and 24 h (Figure B-3A). Compared to the 24 h time point, the 4 h time point showed a high percentage of downregulated genes. Five groupings of differentially expressed genes are indicated in Figure B-3A. Group 1 has many genes that were upregulated at 4 h and downregulated at 24 h, including the complex

I genes *Ndufc2*, *Ndufs4*, and *Ndufb3*. Group 2 contains the positive control HIF1 $\alpha$ -regulated genes (*Bnip3*, *Slc2a1*, and *Vegfa*) along with *Cyb5r2*, *Cox6a2*, and *Cox7a1*, which, in particular, show a classic HIF1 $\alpha$ -regulated expression pattern (Figure B-3B). Most of the group 3 genes were downregulated at 4 h and upregulated at 24 h without showing a distinct HIF1 $\alpha$ -regulated expression pattern, such as *Lonp1*, *Cox4i2*, and *Cyb5r1*. There was a small group of genes (group 4) that showed greater upregulation in the null than in the WT cell line at both 4 and 24 h time points. This group includes the mitochondrial uncoupling protein (UCP4) gene, *Slc25a27*, and ATP synthase subunits *Atp5j2* and *Atp5c1*. Finally, group 5 is primarily composed of genes whose expression was downregulated at both 4 and 24 h regardless of cell type, in particular the ETC complex II genes *Sdha*, *Sdhc*, and *Sdhd*.

#### **HIF1-Dependent Gene Expression of Nuclear-Encoded Mitochondrial CcO Genes**

Manual qPCR was performed on select genes that were dependent upon HIF1 $\alpha$ -mediated regulation in HTP qPCR. Classic HIF1 $\alpha$  regulated genes *Slc2a1*, *Vegfa*, and *Bnip3* showed the expected higher level of expression in the *Hif1 $\alpha$*  WT cells in response to a 24 h hypoxia treatment compared to control and *Hif1 $\alpha$*  null cells (Figure B-4A). Several genes associated with CcO showed differential patterns of gene expression among the different isoforms (Figure B-4B-D). *Cox4i1* had a higher level of expression when cells were exposed to Gal media and hypoxia. *Cox4i2* had a higher level of expression in *Hif1 $\alpha$*  null cells under hypoxia than in WT cells regardless of sugar sources. The level of *Cox6a1* expression was higher in *Hif1 $\alpha$*  null cells regardless of nutrient type, while the level of *Cox6a2* expression was higher in Gal media regardless of cell type (WT and null cells). In agreement with Figure 3, *Cox7a1* displayed a classic HIF1 $\alpha$ -dependent expression pattern being upregulated by hypoxia in the *Hif1 $\alpha$*  WT, especially an increase in Glc media, but not the *Hif1 $\alpha$*  null cells. *Cox7a2* expression did not change between cell types or in response to treatments.

### **HIF1 $\alpha$ -Dependent Regulation of CcO Activity**

The results of transcriptional CcO subunit expressions suggest that HIF1 $\alpha$  plays a role in modulating the expression of *Cox7a1* and, potentially, other critical subunits. A biochemical assessment of the CcO activity was performed to determine if its activity was influenced by changes in *Hif1 $\alpha$*  genotype. *Hif1 $\alpha$*  WT and null cell lines were exposed to control conditions and 1% O<sub>2</sub> for 24 h in both Glc and Gal media, and mitochondria were isolated. CcO activity and quantity were assessed in these isolated mitochondria (Table B-2). The specific activity of CcO remained fairly constant in both cell strains and different treatment paradigms, with two exceptions. The WT cells showed a decrease in CcO activity following hypoxic exposure in Glc-containing media that was not evident in Gal-containing media. In addition, the null cells grown in Gal media showed an almost 3-fold increase in CcO specific activity under hypoxic stress. This increase reflects both an increase in enzyme activity and a decrease in enzyme concentration under these conditions. These data suggest that loss of HIF1 $\alpha$  signaling removes the cell's ability to regulate CcO activity under hypoxic stress and that maintenance of this activity below a given threshold is important for mitochondrial viability. However, the observed changes in CcO activity under some conditions may not be explained by changes in CcO isoform composition because *Cox7a1* transcripts constitute <1% of total subunit 7a transcripts in our cell lines (Figure B-4D) even after hypoxic induction (see Discussion).

### **COX7A Subunit and CcO Protein Structure**

The hypoxia-induced expression of *Cox7a1* appears to be HIF1a-dependent, and loss of HIF1a signaling affects the capacity of mitochondria to regulate oxygen consumption and CcO specific activity following hypoxic stress. In cells that express significant amounts of both isoforms, HIF1a might alter subunit composition of CcO upon hypoxia exposure to maintain

CcO activity within acceptable limits to sustain mitochondrial viability. To begin to gain a mechanistic understanding of this role, protein sequence alignment and structural visualization were performed. COX7A1 and COX7A2 are highly conserved across multiple species (e.g., human, 59.7% identical and 79.1% similar; mouse, 58.4% identical and 72.7% similar). The structure of bovine CcO, a 13-subunit enzyme that is highly homologous to that of the mouse, shows the location of the L-shaped COX7A subunit in blue and an associated cardiolipin molecule in green (Figure B-5). This membrane-embedded face of CcO is an area that appears to interact with complex III (cytochrome *bc<sub>1</sub>*) when they associate with complex I to form a supercomplex.<sup>236</sup> Part of the interaction appears to be mediated by cardiolipin and COX7A, and thus, the sequence variation between the 7A1 and 7A2 isoforms might well be expected to influence this interaction. The region of most sequence divergence is the N-terminus, at the bottom of the L and not completely resolved in the crystal structure. In addition, the protein sequences show distinct differences at specific residues along the surface of the helix comprising most of the subunit (i.e., R<sub>127</sub>K<sub>2</sub>, A<sub>129</sub>P<sub>2</sub>, N<sub>152</sub>A<sub>2</sub>, V<sub>157</sub>A<sub>2</sub>, C<sub>162</sub>T<sub>2</sub>, C<sub>169</sub>A<sub>2</sub>, and C<sub>172</sub>E<sub>2</sub>). COX4, COX6A, COX7A, and COX8 are also rendered and these subunits impact the conformation for interaction with *cytochrome bc<sub>1</sub>* (not shown). Given these sequence differences and hypoxic-responsive gene COX4 localization at the same side with COX7A, switching COX7A subunits under hypoxic stress might allow CcO to alter its interactions with other ETC complexes during the formation of supercomplexes.<sup>237, 238</sup> In addition, because a number of these residues are cysteines, the switch from COX7A2 to COX7A1 might render the CcO more redox sensitive or serve to protect it from oxidative damage while under hypoxic stress.<sup>224, 239</sup>

## **Discussion**

In this study, we demonstrate a role of HIF1 $\alpha$  in the basal oxygen utilization rate and the ETC function of MEF cells and establish HIF1 $\alpha$  regulation of genes associated with cytochrome *c* oxidase (CcO). Gene expression changes for CcO components occur in response to hypoxia, and the extracellular oxygen concentrations (oxygen consumption rate data) support an apparent constitutive modulation of mitochondrial function by HIF1 $\alpha$ . This study adds to the growing body of evidence that the hypoxia signaling system (especially HIF1 $\alpha$ ) regulates ETC biogenesis and processes associated with mitochondrial function, such as energy production, reactive oxygen species homeostasis, autophagy/apoptosis, and oxygen consumption.

Addition of exogenous glucose to cultured cells will increase the rate of glycolysis and inhibit OXPHOS, a phenomenon known as the Crabtree effect.<sup>240</sup> A change from Glc to Gal in culture media increases the respiration rate and cytosolic pH, increases the rate of cellular oxygen consumption and results in mitochondrial remodeling.<sup>240, 241</sup> In human primary myotubes, Gal medium enhances aerobic metabolism and decreases the rate of anaerobic glycolysis.<sup>242</sup> Our results support these observations with an increased spare respiratory capacity in the *Hif1 $\alpha$*  WT cells (Figure B-2B) and dramatic changes in ETC gene expression profiles in response to Gal (Figure B-3).<sup>164, 243, 244</sup> For example, after 24 h, expression profiles show genes upregulated in response to Gal only in the presence of HIF1 $\alpha$  (e.g., *Ndufa10*), in the absence of HIF1 $\alpha$  (e.g., *Atp5l*), and regardless of HIF1 $\alpha$  status (e.g., *Surf1*). *Cox8a* showed upregulation in response to glucose only when HIF1 $\alpha$  was present, while *Ucp1* conversely showed upregulation only in *Hif1 $\alpha$*  null cells. Rossignol *et al.* found no greater levels of mitochondria in HeLa cells grown with galactose than those grown with glucose; however, there were significant galactose-induced changes in mitochondrial protein expression in both HeLa and MRC5 fibroblast cells.<sup>241</sup> MRC5 fibroblast cells had significantly increased protein quantities for complex I, II, and IV subunits, while complex III protein levels were not increased. In our 24 h study, the complex III genes were almost all downregulated in the HIF1 $\alpha$  null cells

with mixed responses in regard to Gal (e.g., *Uqcrc1*, *Uqcrh*, and *Uqcrg*). The uniqueness of the complex III response to Gal is a point of interest as the role of ROS generated at complex III has been implicated in HIF stabilization and signaling, though this is debated.<sup>217, 245, 246</sup> Clearly, there is a complex interaction between HIF1 $\alpha$  and carbon substrate availability on mitochondrial function, OXPHOS, and gene expression of ETC components.

There is ample evidence that hypoxia alters mitochondrial function and oxygen utilization.<sup>217, 218, 247</sup> HIF1 influences mitochondrial function by suppressing both the TCA cycle and respiration and controls mitochondrial biogenesis and autophagy.<sup>217, 247</sup> Few studies, however, have examined HIF1-dependent changes in the expression of specific ETC genes. A Cox4 isoform exchange (*Cox4i1* to *Cox4i2*) in response to hypoxia was reported to be coordinated by HIF1. HIF1 upregulates *Cox4i2* mRNA expression and concurrently increases the level of *Cox4i1* degradation through an increased level of expression of *Lonp1*, a mitochondrial protease.<sup>227</sup> Our results show an upregulation of *Lonp1* and *Cox4i2*, but the increased level of *Cox4i2* was observed in *Hif1 $\alpha$*  null, as well as, WT cells (Figures B-3 and B-4). These results are in agreement with a previously published report that also found that *Cox4i2* is upregulated under hypoxia via a novel oxygen-responsive element (ORE) separate from an HRE.<sup>226, 248</sup> We observed a higher level of expression of *Cox4i1* in both WT and *Hif1 $\alpha$*  null cells grown with Gal, supporting the idea that *Cox4i1* expression is independent of HIF1 $\alpha$ . There is some indication that *Cox4i2* is expressed in only certain tissues, while *Cox4i1* is ubiquitously expressed and is the isoform responsible for ATP regulation of CcO activity.<sup>116, 210,</sup>

225

Our results indicate that *Cox7a1* is a HIF1-regulated gene (Figures B-3 and B-4), and the 5000 bp sequence on the mouse *Cox7a1* gene (NC\_00073.5: 30964250 to 30969250 bp) prior to the start codon reveals at least six possible HREs.<sup>227</sup> One of these HREs (5'-GCGTG-3') occurs within the 92 bp segment immediately upstream of the major transcription start site (-80 bp), which in the bovine *Cox7a1* gene is considered to be the basal promoter region

responsible for most of the gene expression and activity.<sup>249</sup> Evidence indicates that the level of *Cox7a1* mRNA expression in human skeletal muscle decreases significantly with age and is positively related with glucose uptake, total body aerobic capacity, and PGC-1 $\alpha$  mRNA expression.<sup>228</sup> *Cox7a1* knockout male mice displayed tissue-specific differences in resting ATP levels and reduced CcO specific activity and respiratory control ratio in skeletal muscle from WT mice.<sup>239, 250</sup> In addition, a significant increase in ROS production has been observed in response to *Cox7a2* overexpression similar to the increased ROS production observed with the *Cox4i2* replacement of *Cox4i1* under nonhypoxic conditions.<sup>227</sup> Because ROS is produced by the transfer of an electron to O<sub>2</sub> at complex I or complex III, changes in CcO structure that produce ROS are most probably manifested by limitations in CcO activity.<sup>251</sup> Moreover, cardiolipin, which interacts with COX7A near the site of the cytochrome *bc*<sub>1</sub> interface, is critical for CcO assembly and organizing components in supercomplexes and consequently improves CcO function.<sup>116</sup> Taken together, this information shows a potential link among *Cox7a* subunits, CcO activity, and hypoxia, but further experimentation is needed to determine the impact of *Cox7a* subunit switching on supercomplex formation, ETC efficiency, and cellular energetics under various oxygen tensions in cell systems that express measurably levels of both *Cox7a* isoforms.

The CcO activity (Table B-2) and cellular respiration (Figure B-2) in *Hif1 $\alpha$*  null cells suggest that HIF1 $\alpha$  stabilization under hypoxia is necessary to maintain homeostasis in cellular oxidative metabolism. As previously described, cellular respiration was measured under non-hypoxic condition and the respiration capacity in *Hif1 $\alpha$*  null cells was not changed by a mitochondrial uncoupler with either carbon source while WT cells adapted to each nutrient type. CcO activity, however, was increased almost three-fold in *Hif1 $\alpha$*  null cells grown in Gal media following hypoxic stress. This increase was not observed in *Hif1 $\alpha$*  WT cells. These results suggest two things. First, the *Hif1 $\alpha$*  null cells are at maximal respiration normally. This inability to maintain spare respiratory capacity suggests the *Hif1 $\alpha$*  null cells are partially uncoupled or lack the necessary regulatory mitochondria-to-nuclear signaling to maintain reserve respiratory

capacity. This might be partially explained by the upregulation of UCP4 in the null cells (Figure 2). This loss of spare respiratory capacity might also help explain why these cells lose mitochondrial mass under stress (i.e., hypoxia + GAL media). Second, HIF1 $\alpha$  plays a role in regulating overall CcO activity to maintain optimal efficiency and limit ROS generation. Galactose forces the cells to become more reliant on oxidative phosphorylation to meet energy demands, and hypoxia limits the cell's ability to produce ATP through complex IV. Under these conditions (i.e., hypoxia + GAL media), cells must modulate the efficiency of oxidative phosphorylation to maintain cellular energetics and limit oxidative stress. The results suggest that this adaptation is dependent upon HIF1 $\alpha$ , and in its absence, CcO activity becomes unregulated and damages the mitochondria. This is evident from the increase in specific activity and the decrease in mitochondrial mass under these conditions. This might stem from the cell's inability to upregulate glycolytic capacity in the absence of HIF1 $\alpha$ . Therefore, the higher CcO activity in *Hif1 $\alpha$*  null cells in Gal media under hypoxia shows an adapted response to cope with a stronger dependence on energy production via oxidative phosphorylation.

In conclusion, our study indicates a significant difference in oxygen utilization by *Hif1 $\alpha$*  WT and *Hif1 $\alpha$*  null MEF cells in response to a mitochondrial uncoupler. These cell lines show differences in ETC gene expression profiles under different nutrient types and oxygen concentrations. Most importantly, we have identified HIF1 $\alpha$  as a regulator of CcO activity and *Cox7a1* gene expression. Given their location within the crystal structure, we suggest a possible role for these hypoxia-induced isoform changes to translate into structural changes in a supercomplex formation depending on redox state or oxidative stress. Altogether, this study indicates that HIF1 $\alpha$  is critical for mitochondrial respiration control and transcriptional regulation of CcO components to achieve cellular adaptation in an oxygen-limiting environment.

**Table B-1. Primer pairs.**

Gene name	ETC complex	Gene ID	Reference sequences	Forward primer	Reverse primer	Amp size
Ndufa1	Complex I	54405	NM_019443	catccacaaattccaacg	caggcccttgacacatagt	124
Ndufa10	Complex I	67273	NM_024197	ccaaccaaggtgtagagga	ccggaatggtcgtgtaattc	139
Ndufa11	Complex I	239760	XM_358948	ccagatgacccccgaacta	agcttgccgatcttgaacag	140
Ndufa12	Complex I	66414	NM_025551	accgatgggtcatctacacc	gcagtcggtgattatgctg	139
Ndufa12l	Complex I	75597	XM_001476048	ctcccccactatggaggaa	tgcatgaggtgaaggcaaga	134
Ndufa13	Complex I	67184	NM_023312	tctccaggcagagaaggac	cccatcgtgtgattggaac	129
Ndufa2	Complex I	17991	NM_010885	aggtaccagagccatgcag	gacccaaagcacacatttcc	125
Ndufa3	Complex I	66091	NM_025348	catgatcaacaaggccacac	gttctcagccagccaagc	121
Ndufa4	Complex I	17992	NM_010886	cagatgtcagctgggacaga	gtctgggctcttcttctca	122
Ndufa4l2	Complex I	407790	NM_001098789	cctgagtcccaatgaccagt	gcagggagcagaaagatga	122
Ndufa5	Complex I	68202	NM_026614	ttgcttcagggtggtgaagt	tattggcacttccactggt	138
Ndufa6	Complex I	67130	NM_025987	gtcacagaccccagagtgg	agaaatccttggccttgg	139
Ndufa7	Complex I	66416	NM_023202	gttgctcctccatcat	gacagctcccactcttcat	134
Ndufa8	Complex I	68375	NM_026703	catgcagctgttctgact	tctctggcaaggacgatct	140
Ndufa9	Complex I	66108	NM_025358	caaaccggtactctcttc	tggtactagccaaagaggt	125
Ndufab1	Complex I	70316	NM_028177	gatccagaaaagctccgtaa	tcaggaattcaaacccaaa	116
Ndufaf1	Complex I	69702	NM_027175	ggaagggtacagagtcca	gggctgatcagtaaacaca	133
Ndufb10	Complex I	68342	NM_026684	tgtagcagttcaccaaagtg	gccttcttcttccagcat	121
Ndufb11	Complex I	104130	NM_019435	tttccatcgtcctgtctt	aggccattgactctcggtg	119
Ndufb2	Complex I	68198	NM_026612	tcaccgctcgtgaccttc	tgtaccgggctgaatagt	123
Ndufb3	Complex I	66495	NM_025597	agaaacgggtcagaagaagc	acccccattgactcctttt	137
Ndufb4	Complex I	68194	NM_026610	ttcagtacaacgacccccaaa	cctggcacagctcctaaaag	116
Ndufb5	Complex I	66046	NM_025316	accctggtatcctccagat	cctttcagggttggaaat	124
Ndufb6	Complex I	230075	NM_001033305	tcgctgttctcatgtgctt	tctccagctccagaattgtatca	136
Ndufb7	Complex I	66916	NM_025843	ctgaagtgaagcgagacag	cgctcagctcaaacctctt	119
Ndufb8	Complex I	67264	NM_026061	ggccgccaagaagtataaca	tgataccaggtaccctctc	123
Ndufb9	Complex I	66218	NM_023172	gtggaagaagctgaggatgg	gcaagtaccttccctctg	119
Ndufc1	Complex I	66377	NM_025523	cctcggtttcatgtggatt	tccagaggaaggactgtgat	137
Ndufc2	Complex I	68197	NM_024220	ttgtatgctgtgaaggacca	tgaaaactcaacgcactgg	129
Ndufs1	Complex I	227197	NM_145518	cttcaggaggcattcattc	gttggacacagctgcaagaa	119
Ndufs2	Complex I	226646	NM_153064	cacatgttgcagatgtcgt	ttgtctcccaccagacacag	140
Ndufs3	Complex I	68349	NM_026688	ttatggcttcgaggacatc	attctgtgccagctccact	119
Ndufs4	Complex I	17993	NM_010887	ttctgacctcagtgccaaa	tccaagaaaagttgccacca	126
Ndufs5	Complex I	595136	NM_001030274	gcgaaaaggagtgcaagat	tgaggtgaggtgtgattt	137
Ndufs6	Complex I	407785	NM_010888	cacaacagcctgtgaacgag	catgtccccgtttgtttc	118
Ndufs7	Complex I	75406	NM_029272	ggcgggtggtactaccacta	cagctgcaagatgccataaa	126
Ndufs8	Complex I	225887	NM_144870	cgacacgctatgacatcgac	cagcaactcctcgtgtgtct	128
Ndufv1	Complex I	17995	NM_133666	gactccctgtgggagatcag	aatcgttgcacccgatcct	131
Ndufv2	Complex I	72900	NM_028388	ctggaaaagttcccaacca	caagtaaaggcctgcttgc	126
Ndufv3	Complex I	78330	NM_030087	gacagcaaagaagccaggct	cgcttcttctctgcttg	127
Sdha	Complex II	66945	NM_023281	acatgcagaagtcgatgcag	cattcccctgtcaatgtct	128
Sdhb	Complex II	67680	NM_023374	agctactggtggaacggaga	gcagcggtagacagagaagg	138
Sdhc	Complex II	66052	NM_025321	cctttgggaaccacagctaa	acggacagtgccataggaag	122
Sdhd	Complex II	66925	NM_025848	ggtcagacccgcttatgtgt	gagagatgcagccttggaa	118
Cyb5a	Complex III	109672	NM_025797	gggcagtcagacaaggatgt	ttctcccaggatgctctt	138
Cyb5b	Complex III	66427	NM_025558	gtcacctactaccggctgga	gctgttccagcagaaacctc	140
Cyb5r1	Complex III	72017	NM_028057	ccttacaccctgtcaccag	ccaatcttcaggctatcca	135
Cyb5r2	Complex III	320635	NM_177216	aatgagccaggaaccctttt	agctgtagcattggcgtaat	116
Cyb5r3	Complex III	109754	NM_029787	acatcctggccttctatt	ttgaccaccaagtcacaaa	127
Cyb5r4	Complex III	266690	NM_024195	ggcctcagttctccaagcta	ggagtcacctggaggtaaa	120
Cyc1	Complex III	66445	NM_025567	gcatcagaaccagagcatga	ccagcttccgactctcagg	130

**Table B-1 (Cont'd).**

Gene name	ETC complex	Gene ID	Reference sequences	Forward primer	Reverse primer	Amp size
Rieske	Complex III	66694	NM_025710	ccacctgttctggatgtgaa	aaaaacggacagaagcaggaa	117
Ucrc	Complex III	66152	NM_197979	gcgatctacgagcacatcaa	actccaggcaaacagctgac	129
Uqcc	Complex III	226849	NM_018888	agaagccatgggattcactg	tgaatgatcgggcatctga	140
Uqcr	Complex III	66594	NM_025650	gccttacatcaacggcaagt	ctccagtgccagcttctctc	136
Uqcrb	Complex III	432822	XM_484346	taagagagcctggacctga	gcccactctctctctctt	138
Uqcrc1	Complex III	22273	NM_025407	aagctttgccagagttcca	ggfcatatggcgcatccact	138
Uqcrc2	Complex III	67003	NM_025899	ccacctctaccgtcctca	actcgtcgagaaaaggcgta	136
Uqcrh	Complex III	66576	NM_025641	tactctgggtgcgctgttg	gggggtccactagttctcc	123
Uqcrq	Complex III	22272	NM_025352	cgcttcccaagctatttc	gccccatgtgatcaggt	115
Cox10	Complex IV	70383	NM_178379	gatgatctgcctggcatttt	gaagcaggaccagtcgaaag	117
Cox11	Complex IV	69802	NM_199008	gagaacatggtgcctgtcaa	atgccagtgagctctctct	133
Cox15	Complex IV	226139	NM_144874	cagtctgtggacctccctgt	cacaaaagcccctgagagag	136
Cox4i1	Complex IV	12857	NM_009941	agtgttgtaagatgaagac	gcggtacaactgaactttctc	173
Cox4i2	Complex IV	84682	NM_053091	gttgactgtacgccagcgc	ccggtacaaggccacctctc	143
Cox5b	Complex IV	12859	NM_009942	cagaagggactggaccata	ttcacagatgcagcccacta	117
Cox6a1	Complex IV	12861	NM_007748	gagggttcagctcggatgt	ggggctctctgctcttc	115
Cox6a2	Complex IV	12862	NM_009943	ttcctagctccctttgaca	gaagagccagcacaaggctc	132
Cox6b1	Complex IV	110323	NM_025628	ccccaccagaaccagacta	gacttgatcacacgccggta	126
Cox6c	Complex IV	12864	NM_053071	cacagatgcgtggtctctg	gcatacgcctctttcttg	124
Cox7a1	Complex IV	12865	NM_009944	ccgacaatgacctccagta	ccagcccaagcagataagc	116
Cox7a2	Complex IV	12866	NM_009945	aagatggtgcggaatctgct	gcattcccattatcctctga	127
Cox7b	Complex IV	66142	NM_025379	ctaagcgtctccaagttcg	aagatggctccacctgctaa	119
Cox7c	Complex IV	12867	NM_007749	ccagagtatccggaggttca	ggfcatatagccagcaacc	118
Cox8a	Complex IV	12868	NM_007750	atgtctgtcctgacgccact	gaagtgcagccaatggtgat	137
Atp5a1	Complex V	11946	NM_007505	ttatccccgaatctctgtg	gcaatcgatgtttcccagt	130
Atp5b	Complex V	11947	NM_016774	gaggtcttcacgggtcacat	atgggtcccaccatgtagaa	125
Atp5c1	Complex V	11949	NM_001112738	acaatctggccaacctcatc	gtgcygtgaaagtaaggt	139
Atp5d	Complex V	66043	NM_025313	aggggttcacacagaagacg	agcatgtccagtgctacagc	120
Atp5e	Complex V	67126	NM_025983	ccggtttgaggctactctga	cctcactgctttgcacaga	134
Atp5f1	Complex V	11950	NM_009725	atcgctggactaccacatc	ttggcaatggtctcctttc	130
Atp5g1	Complex V	11951	NM_007506	aaaaatgcagaccaccaagg	caggaaggctgcttagatgg	129
Atp5g2	Complex V	67942	NM_026468	tgggactgttttgggagtc	tgagaaggccaccattagg	137
Atp5g3	Complex V	228033	NM_175015	cccagaatggtgtgtgtcag	caccagaaccagcaactcct	126
Atp5h	Complex V	71679	NM_027862	gaaaccacctgcgattgact	gtccaccagggtgtgtatt	133
Atp5i	Complex V	27425	NM_013795	actacgccaaggtgagctg	aaccattcagcacagcttcc	138
Atp5j	Complex V	11957	NM_016755	gtccttcggtcagcagctctc	agatgcctgtcgtttgatt	138
Atp5j2	Complex V	57423	NM_020582	tggataatgatcgggattt	ctgccaggaccatgctaatac	130
Atp5k	Complex V	11958	NM_007507	cggttcaggctctctccactc	cttctttcctccgctgcta	137
Atp5o	Complex V	28080	NM_138597	ctatgcaaccgcctgtact	gtgcgctgtatgagggatt	138
Atp5s	Complex V	68055	NM_026536	ccatggatctgtactccag	cacaccgaagtagccactca	124
Atpaf1	Complex V	230649	NM_181040	agacaaaactgcggaggaaa	aaatgtgggcaggactgag	130
Atpaf2	Complex V	246782	NM_145427	ggtgcttaccagccactgt	gaagcacagctgttccaca	137
LOC100040708	Complex V	100040708	NM_001111335	agaccatggccaagttcatc	aaccagctcaacctgtgtgt	123
Ucp1	UCP	22227	NM_009463	ggcctctacgactcagttcca	ccttcacgacctctgtaggc	136
Ucp2	UCP	22228	NM_011671	ctcaaagcagcctccagaac	acatctgtggccttgaacc	140
Ucp3	UCP	22229	NM_009464	cggtggatgtgtaagacc	aaaggagggcacaatcctt	131
Ucp4	UCP	74011	NM_028711	aggtcggatgtcacctatg	gtcagtggggttgctaaaa	139
Ucp5	UCP	20523	NM_011398	ggaatgctgggagacacaat	gtcccactattgcctctga	130

**Table B-1 (Cont'd).**

<b>Gene name</b>	<b>ETC complex</b>	<b>Gene ID</b>	<b>Reference sequences</b>	<b>Forward primer</b>	<b>Reverse primer</b>	<b>Amp size</b>
Sco1	Chaperone	52892	NM_001040026	ccaccctgttcagagacggt	ttccttgacctagcgcagt	121
Sco2	Chaperone	100126824	NM_001111288	ctgctcaaccctgatggct	acagggcctaggcaatagg	139
Surf1	Chaperone	20930	NM_013677	acttgggagtcaccatcctg	gggcttcctgtttctgtga	137
Actb	Reference	11461	NM_007393	ctaaggccaaccgtgaaaag	ccatcacaatgcctgtggta	126
Hprt	Reference	15452	NM_013556	gccccaaaatgggtaagggt	caagggcatatccaacaaca	120
Ppia	Reference	268373	NM_008907	agcatacaggctcctggcatc	ttcacctcccaaagaccac	127
Lonp1	Control	74132	NM_028782	acacatccaaggagggtgctc	gaggggtcaaggcgatgata	132
Vegfa	Control	22339	NM_001025257	caggctgctgtaacgatgaa	gcattcacatctgctgtgct	140
Bnip3	Control	12176	NM_009760	gcttgggatctacattgga	ccaaggaccatgtagctct	140
Gapdh	Control	14433	NM_008084	aacttggcattgtggaagg	ggatgcagggatgatgttct	132
Slc2a1	Control	20525	NM_011400	agcagctgtcgggtatcaat	acagcgacaccacagtgaag	132

Table B-2. CcO enzyme activity.

Nutrient	MEF	Oxygen	CcO activity	CcO protein concentration			Specific activity (sec <sup>-1</sup> )
			oxidation of cytochrome c ( $\mu$ mole/min/mg protein)	[CcO] mM	[Protein] mg/mL	[CcO] $\mu$ mol/mg	
Glucose	WT	Ctrl	0.0435	2.7E-04	5.7	4.71E-05	15.4
		Hyp	0.0320	3.7E-04	6.0	6.11E-05	8.7
	Hif1 $\alpha$ -/-	Ctrl	0.0409	3.1E-04	5.6	5.55E-05	12.3
		Hyp	0.0391	2.5E-04	5.2	4.80E-05	13.6
Galactose	WT	Ctrl	0.0476	2.1E-04	4.7	4.54E-05	17.5
		Hyp	0.0520	1.7E-04	3.6	4.67E-05	18.5
	Hif1 $\alpha$ -/-	Ctrl	0.0418	2.4E-04	4.4	5.49E-05	12.7
		Hyp	0.0944	9.1E-05	2.5	3.68E-05	42.7

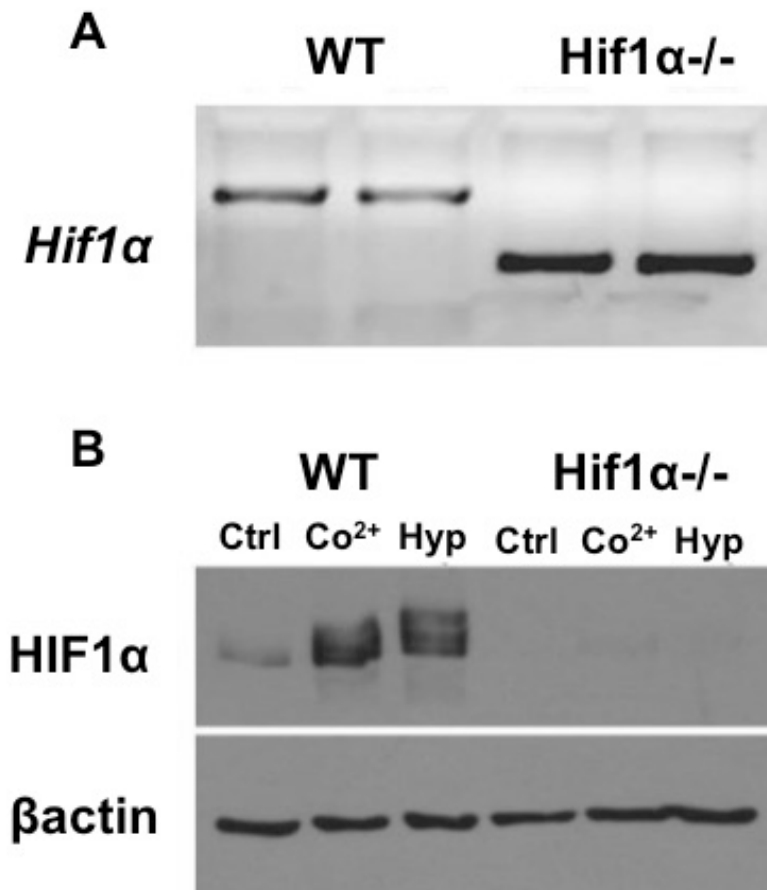


**Figure B-1. Genotype and protein comparisons of *Hif1α* WT and null cells.**

**(A)** *Hif1α* WT and null cells were harvested, DNA was extracted, and PCR-based genotyping was performed using *Hif1α* primers described in Methods and Materials. **(B)** *Hif1α* WT and null cells were exposed to control conditions (Ctrl), 150  $\mu$ M CoCl<sub>2</sub> (Co<sup>2+</sup>) or 1% O<sub>2</sub> (Hyp) for 24 h. Nuclear protein was extracted and separated by SDS-PAGE, transferred to a nitrocellulose membrane, and probed with a HIF1α-specific (top) or β-acti-specific (bottom) specific antibody (n=2).

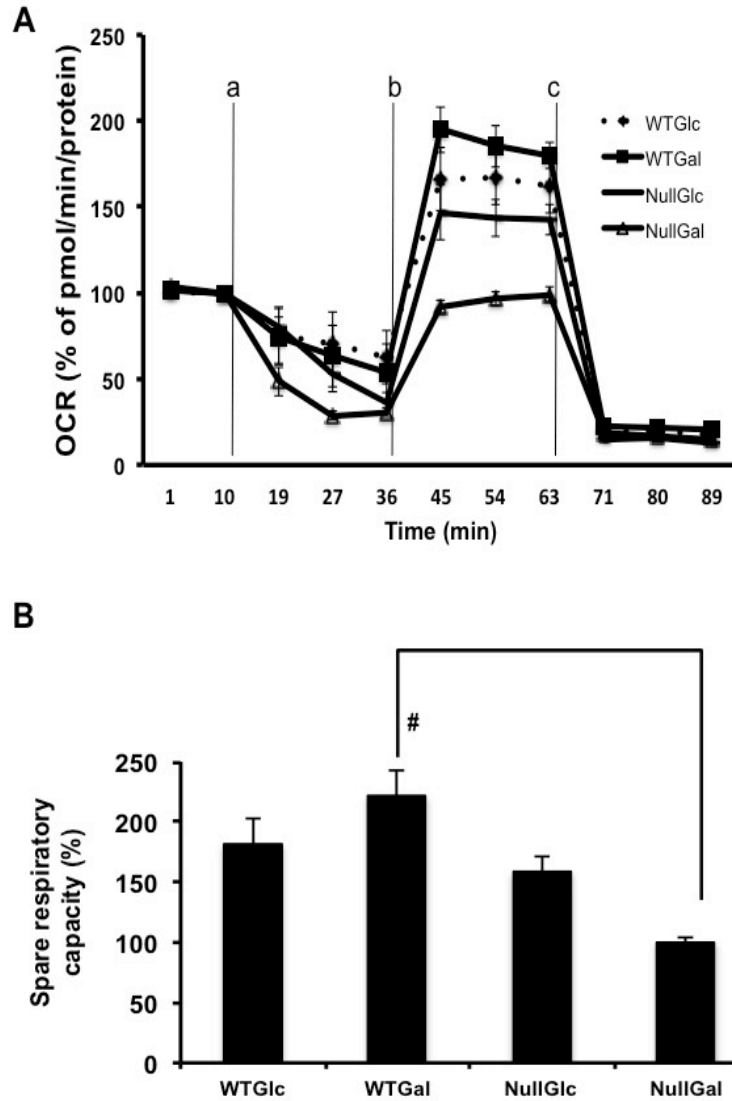


**Figure B-2. Measurement of oxygen consumption rate (OCR) from *Hif1α* WT and null cells.**

**(A)** OCR, calculated as picomoles per min per protein amount in the XF24 assay medium of *Hif1α* WT and null cells grown in Glc or Gal media, were measured exposing to (a) oligomycin (1  $\mu$ M), (b) CCCP (1.5  $\mu$ M for WT and 0.75  $\mu$ M for null cells), and (c) rotenone (0.5  $\mu$ M)/antimycin A (0.5  $\mu$ M). Lines indicate average values  $\pm$  standard errors (n=3). **(B)** Spare respiratory capacity as a percentage was calculated with maximal respiration (OCR at 44.9 min) and basal respiration (OCR at 9.9 min) by the manufacturer's software, the XF Mito Stress Test Report Generator. Data were analyzed for significant differences by ANOVA followed by Tukey's post hoc test. A number sign indicates significant differences at  $p < 0.05$ .



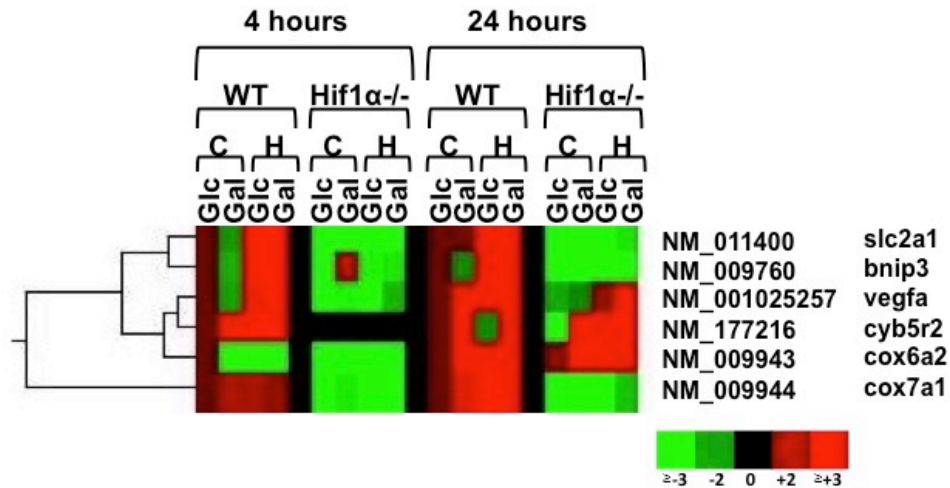


**Figure B-3B. Dendrograms.**

Gene expression fold changes calculated with HTP qPCR results using the  $\Delta\Delta C_T$  method for *Hif1α* WT and null cells exposed to control conditions (C) and 1% O<sub>2</sub> (H) in high-glucose media (Glc) or galactose media (Gal) at 4 and 24 h. The cell and medium control group (e.g., WT Glc) at each time point was scaled to 1. Red indicates upregulation, green indicates downregulation, and black indicates no data. **(A)** Genes are separated into five groups based on clustering and expression profiles. **(B)** Group 2 contains the known HIF1α-regulated genes of *Slc2a1*, *Bnip3*, and *Vegfa*.

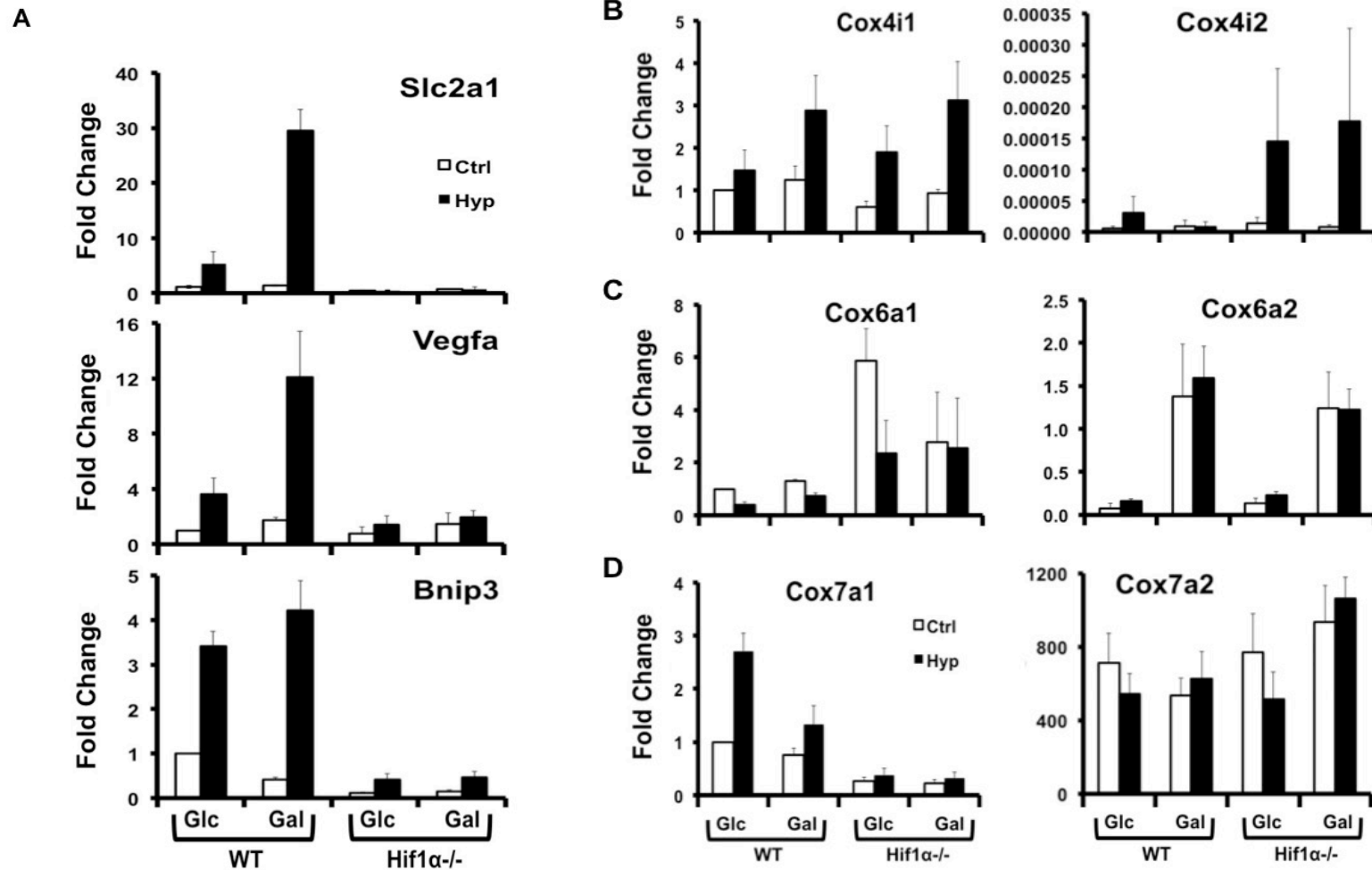


**Figure B-4. Gene expression of control and select mitochondrial genes.**

Known HIF1α target genes (A) and selected CcO subunit genes (B-D) were assessed by manual qPCR of *Hif1α* WT and null cells after exposure to treatment for 24 h. Treatment designations include high-glucose media (Glc), galactose media (Gal), control conditions (Ctrl), and 1% O<sub>2</sub> (Hyp). The y-axis indicates fold change that was calculated using the  $2^{(-\Delta\Delta CT)}$ . (A) The fold change for

**Figure B-4. (cont'd)** *Slc2a1*, *Bnip3*, and *Vegfa* was a comparison to the fold of WT Glc Ctrl being scaled to one within each gene. **(B)** The Fold change of *Cox4* was a comparison to the fold of WT Glc Ctrl of *Cox4i1* scaled to 1. **(C)** The Fold change of *Cox6* was a comparison to the fold of WT Glc Ctrl of *Cox6a1* scaled to 1. **(D)** The Fold change of *Cox7* was a comparison to the fold of WT Glc Ctrl of *Cox7a1* scaled to 1. Bars indicate average values  $\pm$  standard errors of the mean except the gene expression of *Slc2a1* (n=3 for *Vegfa*, *Cox4i1* and *Cox4i2*; n=4 for *Bnip3*, *Cox6a1*, and *Cox6a2*; n=5 for *Cox7a2*; n=7 for *Cox7a1*). Bars for *Slc2a1* expression indicate average values  $\pm$  standard deviation (n=1).

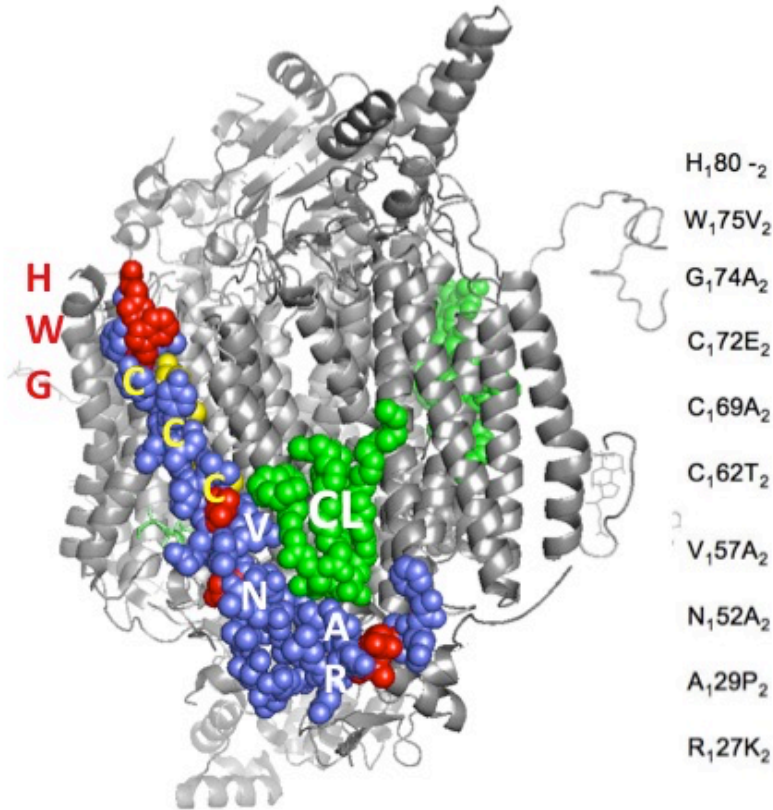


**Figure B-5. Comparative amino acid sequences for COX7A1 and COX7A2 isoforms and a 3D representation of the COX monodimer.**

The residues that are altered between 7A1 and 7A2 are listed to the right of the model, with subscripts indicating the isoform and their locations highlighted in red or yellow in the structure. The whole CcO structure is in grey and COX7A1 in purple. A molecule of cardiolipin, CL, is shown in green. The top of the figure is the inter-membrane side, the bottom is the matrix side. The COX7A1 structure is not completely resolved in the bovine crystal structure: it starts at phenylalanine 24 on the bottom (N-terminal, matrix side). The figure was made in PyMOL from the coordinates of bovine cytochrome c oxidase PDB 2dyr.

## REFERENCES

## REFERENCES

- (1) McIntosh, B. E., Hogenesch, J. B., and Bradfield, C. A. (2010) Mammalian Per-Arnt-Sim proteins in environmental adaptation, *Annu. Rev. Physiol.* 72, 625-645.
- (2) Gu, Y. Z., Hogenesch, J. B., and Bradfield, C. A. (2000) The PAS superfamily: sensors of environmental and developmental signals, *Annu. Rev. Pharmacol. Toxicol.* 40, 519-561.
- (3) Hites, R. A. (2011) Dioxins: an overview and history, *Environ. Sci. Technol.* 45, 16-20.
- (4) Linden, J., Lensu, S., Tuomisto, J., and Pohjanvirta, R. (2010) Dioxins, the aryl hydrocarbon receptor and the central regulation of energy balance, *Front Neuroendocrinol.* 31, 452-478.
- (5) Poland, A., Glover, E., and Kende, A. S. (1976) Stereospecific, high affinity binding of 2,3,7,8-tetrachlorodibenzo-p-dioxin by hepatic cytosol. Evidence that the binding species is receptor for induction of aryl hydrocarbon hydroxylase, *J. Biol. Chem.* 251, 4936-4946.
- (6) Legraverend, C., Hannah, R. R., Eisen, H. J., Owens, I. S., Nebert, D. W., and Hankinson, O. (1982) Regulatory gene product of the Ah locus. Characterization of receptor mutants among mouse hepatoma clones, *J. Biol. Chem.* 257, 6402-6407.
- (7) Reyes, H., Reisz-Porszasz, S., and Hankinson, O. (1992) Identification of the Ah receptor nuclear translocator protein (Arnt) as a component of the DNA binding form of the Ah receptor, *Science* 256, 1193-1195.
- (8) Bacsi, S. G., Reisz-Porszasz, S., and Hankinson, O. (1995) Orientation of the heterodimeric aryl hydrocarbon (dioxin) receptor complex on its asymmetric DNA recognition sequence, *Mol. Pharmacol.* 47, 432-438.
- (9) Denison, M. S., Fisher, J. M., and Whitlock, J. P., Jr. (1988) The DNA recognition site for the dioxin-Ah receptor complex. Nucleotide sequence and functional analysis, *J. Biol. Chem.* 263, 17221-17224.
- (10) Heid, S. E., Pollenz, R. S., and Swanson, H. I. (2000) Role of heat shock protein 90 dissociation in mediating agonist-induced activation of the aryl hydrocarbon receptor, *Mol. Pharmacol.* 57, 82-92.
- (11) LaPres, J. J., Glover, E., Dunham, E. E., Bungler, M. K., and Bradfield, C. A. (2000) ARA9 modifies agonist signaling through an increase in cytosolic aryl hydrocarbon receptor, *J. Biol. Chem.* 275, 6153-6159.

- (12) Carver, L. A., LaPres, J. J., Jain, S., Dunham, E. E., and Bradfield, C. A. (1998) Characterization of the Ah receptor-associated protein, ARA9, *J. Biol. Chem.* 273, 33580-33587.
- (13) Nguyen, L. P., and Bradfield, C. A. (2008) The search for endogenous activators of the aryl hydrocarbon receptor, *Chem. Res. Toxicol.* 21, 102-116.
- (14) Abel, J., and Haarmann-Stemmann, T. (2010) An introduction to the molecular basics of aryl hydrocarbon receptor biology, *Biol. Chem.* 391, 1235-1248.
- (15) Puga, A., Ma, C., and Marlowe, J. L. (2009) The aryl hydrocarbon receptor cross-talks with multiple signal transduction pathways, *Biochem. Pharmacol.* 77, 713-722.
- (16) Fukunaga, B. N., Probst, M. R., Reisz-Porszasz, S., and Hankinson, O. (1995) Identification of functional domains of the aryl hydrocarbon receptor, *J. Biol. Chem.* 270, 29270-29278.
- (17) Ikuta, T., Eguchi, H., Tachibana, T., Yoneda, Y., and Kawajiri, K. (1998) Nuclear localization and export signals of the human aryl hydrocarbon receptor, *J. Biol. Chem.* 273, 2895-2904.
- (18) Soshilov, A., and Denison, M. S. (2008) Role of the Per/Arnt/Sim domains in ligand-dependent transformation of the aryl hydrocarbon receptor, *J. Biol. Chem.* 283, 32995-33005.
- (19) Rowlands, J. C., McEwan, I. J., and Gustafsson, J. A. (1996) Trans-activation by the human aryl hydrocarbon receptor and aryl hydrocarbon receptor nuclear translocator proteins: direct interactions with basal transcription factors, *Mol. Pharmacol.* 50, 538-548.
- (20) Ramadoss, P., and Perdew, G. H. (2005) The transactivation domain of the Ah receptor is a key determinant of cellular localization and ligand-independent nucleocytoplasmic shuttling properties, *Biochemistry* 44, 11148-11159.
- (21) Bell, D. R., and Poland, A. (2000) Binding of aryl hydrocarbon receptor (AhR) to AhR-interacting protein. The role of hsp90, *J. Biol. Chem.* 275, 36407-36414.
- (22) Carver, L. A., and Bradfield, C. A. (1997) Ligand-dependent interaction of the aryl hydrocarbon receptor with a novel immunophilin homolog in vivo, *J. Biol. Chem.* 272, 11452-11456.
- (23) Ramadoss, P., Petrusis, J. R., Hollingshead, B. D., Kusnadi, A., and Perdew, G. H. (2004) Divergent roles of hepatitis B virus X-associated protein 2 (XAP2) in human versus mouse Ah receptor complexes, *Biochemistry* 43, 700-709.

- (24) Zhang, S., Rowlands, C., and Safe, S. (2008) Ligand-dependent interactions of the Ah receptor with coactivators in a mammalian two-hybrid assay, *Toxicol. Appl. Pharmacol.* 227, 196-206.
- (25) Yao, G., Craven, M., Drinkwater, N., and Bradfield, C. A. (2004) Interaction networks in yeast define and enumerate the signaling steps of the vertebrate aryl hydrocarbon receptor, *PLoS Biol.* 2, E65.
- (26) Kohle, C., and Bock, K. W. (2007) Coordinate regulation of Phase I and II xenobiotic metabolisms by the Ah receptor and Nrf2, *Biochem. Pharmacol.* 73, 1853-1862.
- (27) Nault, R., Forgacs, A. L., Dere, E., and Zacharewski, T. R. (2013) Comparisons of differential gene expression elicited by TCDD, PCB126, betaNF, or ICZ in mouse hepatoma Hepa1c1c7 cells and C57BL/6 mouse liver, *Toxicol. Lett.* 223, 52-59.
- (28) Cheng, Y., Jin, U. H., Allred, C. D., Jayraman, A., Chapkin, R. S., and Safe, S. (2015) Aryl Hydrocarbon Receptor Activity of Tryptophan Metabolites in Young Adult Mouse Colonocytes, *Drug Metab. Dispos.*
- (29) Wang, Y., Wang, Q., Wu, B., Li, Y., and Lu, G. (2013) Correlation between TCDD acute toxicity and aryl hydrocarbon receptor structure for different mammals, *Ecotoxicol. Environ. Saf.* 89, 84-88.
- (30) Pandini, A., Soshilov, A. A., Song, Y., Zhao, J., Bonati, L., and Denison, M. S. (2009) Detection of the TCDD binding-fingerprint within the Ah receptor ligand binding domain by structurally driven mutagenesis and functional analysis, *Biochemistry* 48, 5972-5983.
- (31) Ma, Q., and Baldwin, K. T. (2000) 2,3,7,8-tetrachlorodibenzo-p-dioxin-induced degradation of aryl hydrocarbon receptor (AhR) by the ubiquitin-proteasome pathway. Role of the transcription activation and DNA binding of AhR, *J. Biol. Chem.* 275, 8432-8438.
- (32) Xing, X., Bi, H., Chang, A. K., Zang, M. X., Wang, M., Ao, X., Li, S., Pan, H., Guo, Q., and Wu, H. (2012) SUMOylation of AhR modulates its activity and stability through inhibiting its ubiquitination, *J. Cell. Physiol.* 227, 3812-3819.
- (33) Ikuta, T., Kobayashi, Y., and Kawajiri, K. (2004) Phosphorylation of nuclear localization signal inhibits the ligand-dependent nuclear import of aryl hydrocarbon receptor, *Biochem. Biophys. Res. Commun.* 317, 545-550.
- (34) Hahn, M. E., Allan, L. L., and Sherr, D. H. (2009) Regulation of constitutive and inducible AHR signaling: complex interactions involving the AHR repressor, *Biochem. Pharmacol.* 77, 485-497.
- (35) Mimura, J., Ema, M., Sogawa, K., and Fujii-Kuriyama, Y. (1999) Identification of a novel mechanism of regulation of Ah (dioxin) receptor function, *Genes Dev.* 13, 20-25.

- (36) MacPherson, L., Ahmed, S., Tamblyn, L., Krutmann, J., Forster, I., Weighardt, H., and Matthews, J. (2014) Aryl hydrocarbon receptor repressor and TiPARP (ARTD14) use similar, but also distinct mechanisms to repress aryl hydrocarbon receptor signaling, *Int. J. Mol. Sci.* *15*, 7939-7957.
- (37) Evans, B. R., Karchner, S. I., Allan, L. L., Pollenz, R. S., Tanguay, R. L., Jenny, M. J., Sherr, D. H., and Hahn, M. E. (2008) Repression of aryl hydrocarbon receptor (AHR) signaling by AHR repressor: role of DNA binding and competition for AHR nuclear translocator, *Mol. Pharmacol.* *73*, 387-398.
- (38) MacPherson, L., Tamblyn, L., Rajendra, S., Bralha, F., McPherson, J. P., and Matthews, J. (2013) 2,3,7,8-Tetrachlorodibenzo-p-dioxin poly(ADP-ribose) polymerase (TiPARP, ARTD14) is a mono-ADP-ribosyltransferase and repressor of aryl hydrocarbon receptor transactivation, *Nucleic Acids Res.* *41*, 1604-1621.
- (39) Nakata, A., Urano, D., Fujii-Kuriyama, Y., Mizuno, N., Tago, K., and Itoh, H. (2009) G-protein signalling negatively regulates the stability of aryl hydrocarbon receptor, *EMBO Rep.* *10*, 622-628.
- (40) de Oliveira, S. K., Hoffmeister, M., Gambaryan, S., Muller-Esterl, W., Guimaraes, J. A., and Smolenski, A. P. (2007) Phosphodiesterase 2A forms a complex with the co-chaperone XAP2 and regulates nuclear translocation of the aryl hydrocarbon receptor, *J. Biol. Chem.* *282*, 13656-13663.
- (41) Oesch-Bartlomowicz, B., Huelster, A., Wiss, O., Antoniou-Lipfert, P., Dietrich, C., Arand, M., Weiss, C., Bockamp, E., and Oesch, F. (2005) Aryl hydrocarbon receptor activation by cAMP vs. dioxin: divergent signaling pathways, *Proc. Natl. Acad. Sci. U. S. A.* *102*, 9218-9223.
- (42) de Oliveira, S. K., and Smolenski, A. (2009) Phosphodiesterases link the aryl hydrocarbon receptor complex to cyclic nucleotide signaling, *Biochem. Pharmacol.* *77*, 723-733.
- (43) Meyer, B. K., Petrusis, J. R., and Perdew, G. H. (2000) Aryl hydrocarbon (Ah) receptor levels are selectively modulated by hsp90-associated immunophilin homolog XAP2, *Cell Stress Chaperones* *5*, 243-254.
- (44) Margineantu, D. H., Emerson, C. B., Diaz, D., and Hockenbery, D. M. (2007) Hsp90 inhibition decreases mitochondrial protein turnover, *PLoS One* *2*, e1066.
- (45) Rodriguez-Sinovas, A., Boengler, K., Cabestrero, A., Gres, P., Morente, M., Ruiz-Meana, M., Konietzka, I., Miro, E., Totzeck, A., Heusch, G., Schulz, R., and Garcia-Dorado, D. (2006) Translocation of connexin 43 to the inner mitochondrial membrane of cardiomyocytes through the heat shock protein 90-dependent TOM pathway and its importance for cardioprotection, *Circ. Res.* *99*, 93-101.

- (46) Young, J. C., Hoogenraad, N. J., and Hartl, F. U. (2003) Molecular chaperones Hsp90 and Hsp70 deliver preproteins to the mitochondrial import receptor Tom70, *Cell* 112, 41-50.
- (47) Kekatpure, V. D., Dannenberg, A. J., and Subbaramaiah, K. (2009) HDAC6 modulates Hsp90 chaperone activity and regulates activation of aryl hydrocarbon receptor signaling, *J. Biol. Chem.* 284, 7436-7445.
- (48) Lee, Y. S., Lim, K. H., Guo, X., Kawaguchi, Y., Gao, Y., Barrientos, T., Ordentlich, P., Wang, X. F., Counter, C. M., and Yao, T. P. (2008) The cytoplasmic deacetylase HDAC6 is required for efficient oncogenic tumorigenesis, *Cancer Res.* 68, 7561-7569.
- (49) Trivellin, G., and Korbonits, M. (2011) AIP and its interacting partners, *J. Endocrinol.* 210, 137-155.
- (50) Kuzhandaivelu, N., Cong, Y. S., Inouye, C., Yang, W. M., and Seto, E. (1996) XAP2, a novel hepatitis B virus X-associated protein that inhibits X transactivation, *Nucleic Acids Res.* 24, 4741-4750.
- (51) Meyer, B. K., Pray-Grant, M. G., Vanden Heuvel, J. P., and Perdew, G. H. (1998) Hepatitis B virus X-associated protein 2 is a subunit of the unliganded aryl hydrocarbon receptor core complex and exhibits transcriptional enhancer activity, *Mol. Cell. Biol.* 18, 978-988.
- (52) Jaffrain-Rea, M. L., Angelini, M., Gargano, D., Tichomirowa, M. A., Daly, A. F., Vanbellinghen, J. F., D'Innocenzo, E., Barlier, A., Giangaspero, F., Esposito, V., Ventura, L., Arcella, A., Theodoropoulou, M., Naves, L. A., Fajardo, C., Zacharieva, S., Rohmer, V., Brue, T., Gulino, A., Cantore, G., Alesse, E., and Beckers, A. (2009) Expression of aryl hydrocarbon receptor (AHR) and AHR-interacting protein in pituitary adenomas: pathological and clinical implications, *Endocr. Relat. Cancer* 16, 1029-1043.
- (53) Nukaya, M., Lin, B. C., Glover, E., Moran, S. M., Kennedy, G. D., and Bradfield, C. A. (2010) The aryl hydrocarbon receptor-interacting protein (AIP) is required for dioxin-induced hepatotoxicity but not for the induction of the Cyp1a1 and Cyp1a2 genes, *J. Biol. Chem.* 285, 35599-35605.
- (54) Fernandez-Salguero, P., Pineau, T., Hilbert, D. M., McPhail, T., Lee, S. S., Kimura, S., Nebert, D. W., Rudikoff, S., Ward, J. M., and Gonzalez, F. J. (1995) Immune system impairment and hepatic fibrosis in mice lacking the dioxin-binding Ah receptor, *Science* 268, 722-726.
- (55) Mezrich, J. D., Fechner, J. H., Zhang, X., Johnson, B. P., Burlingham, W. J., and Bradfield, C. A. (2010) An interaction between kynurenine and the aryl hydrocarbon receptor can generate regulatory T cells, *J. Immunol.* 185, 3190-3198.

- (56) Barouki, R., Coumoul, X., and Fernandez-Salguero, P. M. (2007) The aryl hydrocarbon receptor, more than a xenobiotic-interacting protein, *FEBS Lett.* **581**, 3608-3615.
- (57) Ikuta, T., Kobayashi, Y., and Kawajiri, K. (2004) Cell density regulates intracellular localization of aryl hydrocarbon receptor, *J. Biol. Chem.* **279**, 19209-19216.
- (58) Hu, Q., He, G., Zhao, J., Soshilov, A., Denison, M. S., Zhang, A., Yin, H., Fracalvieri, D., Bonati, L., Xie, Q., and Zhao, B. (2013) Ginsenosides are novel naturally-occurring aryl hydrocarbon receptor ligands, *PLoS One* **8**, e66258.
- (59) Opitz, C. A., Litzenburger, U. M., Sahm, F., Ott, M., Tritschler, I., Trump, S., Schumacher, T., Jestaedt, L., Schrenk, D., Weller, M., Jugold, M., Guillemin, G. J., Miller, C. L., Lutz, C., Radlwimmer, B., Lehmann, I., von Deimling, A., Wick, W., and Platten, M. (2011) An endogenous tumour-promoting ligand of the human aryl hydrocarbon receptor, *Nature* **478**, 197-203.
- (60) Bock, K. W., and Kohle, C. (2009) The mammalian aryl hydrocarbon (Ah) receptor: from mediator of dioxin toxicity toward physiological functions in skin and liver, *Biol. Chem.* **390**, 1225-1235.
- (61) Yang, J., Solaimani, P., Dong, H., Hammock, B., and Hankinson, O. (2013) Treatment of mice with 2,3,7,8-Tetrachlorodibenzo-p-dioxin markedly increases the levels of a number of cytochrome P450 metabolites of omega-3 polyunsaturated fatty acids in the liver and lung, *J. Toxicol. Sci.* **38**, 833-836.
- (62) Seubert, J. M., Darmon, A. J., El-Kadi, A. O., D'Souza, S. J., and Bend, J. R. (2002) Apoptosis in murine hepatoma hepa 1c1c7 wild-type, C12, and C4 cells mediated by bilirubin, *Mol. Pharmacol.* **62**, 257-264.
- (63) Rodrigues, C. M., Sola, S., Silva, R., and Brites, D. (2000) Bilirubin and amyloid-beta peptide induce cytochrome c release through mitochondrial membrane permeabilization, *Mol. Med.* **6**, 936-946.
- (64) Oakes, G. H., and Bend, J. R. (2005) Early steps in bilirubin-mediated apoptosis in murine hepatoma (Hepa 1c1c7) cells are characterized by aryl hydrocarbon receptor-independent oxidative stress and activation of the mitochondrial pathway, *J. Biochem. Mol. Toxicol.* **19**, 244-255.
- (65) Moura-Alves, P., Fae, K., Houthuys, E., Dorhoi, A., Kreuchwig, A., Furkert, J., Barison, N., Diehl, A., Munder, A., Constant, P., Skrahina, T., Guhlich-Bornhof, U., Klemm, M., Koehler, A. B., Bandermann, S., Goosmann, C., Mollenkopf, H. J., Hurwitz, R., Brinkmann, V., Fillatreau, S., Daffe, M., Tummler, B., Kolbe, M., Oschkinat, H., Krause, G., and Kaufmann, S. H. (2014) AhR sensing of bacterial pigments regulates antibacterial defence, *Nature* **512**, 387-392.

- (66) Watson, J. D., Prokopec, S. D., Smith, A. B., Okey, A. B., Pohjanvirta, R., and Boutros, P. C. (2014) TCDD dysregulation of 13 AHR-target genes in rat liver, *Toxicol. Appl. Pharmacol.* 274, 445-454.
- (67) Black, M. B., Budinsky, R. A., Dombkowski, A., Cukovic, D., LeCluyse, E. L., Ferguson, S. S., Thomas, R. S., and Rowlands, J. C. (2012) Cross-species comparisons of transcriptomic alterations in human and rat primary hepatocytes exposed to 2,3,7,8-tetrachlorodibenzo-p-dioxin, *Toxicol. Sci.* 127, 199-215.
- (68) Forgacs, A. L., Dere, E., Angrish, M. M., and Zacharewski, T. R. (2013) Comparative analysis of temporal and dose-dependent TCDD-elicited gene expression in human, mouse, and rat primary hepatocytes, *Toxicol. Sci.* 133, 54-66.
- (69) Viluksela, M., Unkila, M., Pohjanvirta, R., Tuomisto, J. T., Stahl, B. U., Rozman, K. K., and Tuomisto, J. (1999) Effects of 2,3,7,8-tetrachlorodibenzo-p-dioxin (TCDD) on liver phosphoenolpyruvate carboxykinase (PEPCK) activity, glucose homeostasis and plasma amino acid concentrations in the most TCDD-susceptible and the most TCDD-resistant rat strains, *Arch. Toxicol.* 73, 323-336.
- (70) Fong, C. J., Burgoon, L. D., and Zacharewski, T. R. (2005) Comparative microarray analysis of basal gene expression in mouse Hepa-1c1c7 wild-type and mutant cell lines, *Toxicol. Sci.* 86, 342-353.
- (71) Lin, S., Yang, Z., Liu, H., and Cai, Z. (2011) Metabolomic analysis of liver and skeletal muscle tissues in C57BL/6J and DBA/2J mice exposed to 2,3,7,8-tetrachlorodibenzo-p-dioxin, *Mol. Biosyst.* 7, 1956-1965.
- (72) Prokopec, S. D., Watson, J. D., Lee, J., Pohjanvirta, R., and Boutros, P. C. (2015) Sex-related differences in murine hepatic transcriptional and proteomic responses to TCDD, *Toxicol. Appl. Pharmacol.* 284, 188-196.
- (73) Zhang, W., Sargis, R. M., Volden, P. A., Carmean, C. M., Sun, X. J., and Brady, M. J. (2012) PCB 126 and other dioxin-like PCBs specifically suppress hepatic PEPCK expression via the aryl hydrocarbon receptor, *PLoS One* 7, e37103.
- (74) Aqil, F., Shen, H., Jeyabalan, J., Xin, X., Lehmler, H. J., Ludewig, G., Robertson, L. W., and Gupta, R. C. (2014) Sustained expression of CYPs and DNA adduct accumulation with continuous exposure to PCB126 and PCB153 through a new delivery method: Polymeric implants, *Toxicol. Rep.* 1, 820-833.
- (75) Yeager, R. L., Reisman, S. A., Aleksunes, L. M., and Klaassen, C. D. (2009) Introducing the "TCDD-inducible AhR-Nrf2 gene battery", *Toxicol. Sci.* 111, 238-246.
- (76) Boopathi, E., Srinivasan, S., Fang, J. K., and Avadhani, N. G. (2008) Bimodal protein targeting through activation of cryptic mitochondrial targeting signals by an inducible cytosolic endoprotease, *Mol. Cell* 32, 32-42.

- (77) Dong, H., Dalton, T. P., Miller, M. L., Chen, Y., Uno, S., Shi, Z., Shertzer, H. G., Bansal, S., Avadhani, N. G., and Nebert, D. W. (2009) Knock-in mouse lines expressing either mitochondrial or microsomal CYP1A1: differing responses to dietary benzo[a]pyrene as proof of principle, *Mol. Pharmacol.* 75, 555-567.
- (78) Bansal, S., Leu, A. N., Gonzalez, F. J., Guengerich, F. P., Chowdhury, A. R., Anandatheerthavarada, H. K., and Avadhani, N. G. (2014) Mitochondrial targeting of cytochrome P450 (CYP) 1B1 and its role in polycyclic aromatic hydrocarbon-induced mitochondrial dysfunction, *J. Biol. Chem.* 289, 9936-9951.
- (79) Shimada, T., and Fujii-Kuriyama, Y. (2004) Metabolic activation of polycyclic aromatic hydrocarbons to carcinogens by cytochromes P450 1A1 and 1B1, *Cancer Sci.* 95, 1-6.
- (80) Dong, H., Shertzer, H. G., Genter, M. B., Gonzalez, F. J., Vasiliou, V., Jefcoate, C., and Nebert, D. W. (2013) Mitochondrial targeting of mouse NQO1 and CYP1B1 proteins, *Biochem. Biophys. Res. Commun.* 435, 727-732.
- (81) Nebert, D. W., Roe, A. L., Dieter, M. Z., Solis, W. A., Yang, Y., and Dalton, T. P. (2000) Role of the aromatic hydrocarbon receptor and [Ah] gene battery in the oxidative stress response, cell cycle control, and apoptosis, *Biochem. Pharmacol.* 59, 65-85.
- (82) Miao, W., Hu, L., Scrivens, P. J., and Batist, G. (2005) Transcriptional regulation of NF-E2 p45-related factor (NRF2) expression by the aryl hydrocarbon receptor-xenobiotic response element signaling pathway: direct cross-talk between phase I and II drug-metabolizing enzymes, *J. Biol. Chem.* 280, 20340-20348.
- (83) Wang, L., He, X., Szklarz, G. D., Bi, Y., Rojanasakul, Y., and Ma, Q. (2013) The aryl hydrocarbon receptor interacts with nuclear factor erythroid 2-related factor 2 to mediate induction of NAD(P)H:quinoneoxidoreductase 1 by 2,3,7,8-tetrachlorodibenzo-p-dioxin, *Arch. Biochem. Biophys.* 537, 31-38.
- (84) Lu, H., Cui, W., and Klaassen, C. D. (2011) Nrf2 protects against 2,3,7,8-tetrachlorodibenzo-p-dioxin (TCDD)-induced oxidative injury and steatohepatitis, *Toxicol. Appl. Pharmacol.* 256, 122-135.
- (85) Dabir, P., Marinic, T. E., Krukovets, I., and Stenina, O. I. (2008) Aryl hydrocarbon receptor is activated by glucose and regulates the thrombospondin-1 gene promoter in endothelial cells, *Circ. Res.* 102, 1558-1565.
- (86) Ohtake, F., Takeyama, K., Matsumoto, T., Kitagawa, H., Yamamoto, Y., Nohara, K., Tohyama, C., Krust, A., Mimura, J., Chambon, P., Yanagisawa, J., Fujii-Kuriyama, Y., and Kato, S. (2003) Modulation of oestrogen receptor signalling by association with the activated dioxin receptor, *Nature* 423, 545-550.

- (87) Bock, K. W. (2012) Ah receptor- and Nrf2-gene battery members: modulators of quinone-mediated oxidative and endoplasmic reticulum stress, *Biochem. Pharmacol.* **83**, 833-838.
- (88) Hayes, C. L., Spink, D. C., Spink, B. C., Cao, J. Q., Walker, N. J., and Sutter, T. R. (1996) 17 beta-estradiol hydroxylation catalyzed by human cytochrome P450 1B1, *Proc. Natl. Acad. Sci. U. S. A.* **93**, 9776-9781.
- (89) Tsuchiya, Y., Nakajima, M., Kyo, S., Kanaya, T., Inoue, M., and Yokoi, T. (2004) Human CYP1B1 is regulated by estradiol via estrogen receptor, *Cancer Res.* **64**, 3119-3125.
- (90) Ohtake, F., Baba, A., Takada, I., Okada, M., Iwasaki, K., Miki, H., Takahashi, S., Kouzmenko, A., Nohara, K., Chiba, T., Fujii-Kuriyama, Y., and Kato, S. (2007) Dioxin receptor is a ligand-dependent E3 ubiquitin ligase, *Nature* **446**, 562-566.
- (91) Smith, B. W., Rozelle, S. S., Leung, A., Ubellacker, J., Parks, A., Nah, S. K., French, D., Gadue, P., Monti, S., Chui, D. H., Steinberg, M. H., Frelinger, A. L., Michelson, A. D., Theberge, R., McComb, M. E., Costello, C. E., Kotton, D. N., Mostoslavsky, G., Sherr, D. H., and Murphy, G. J. (2013) The aryl hydrocarbon receptor directs hematopoietic progenitor cell expansion and differentiation, *Blood* **122**, 376-385.
- (92) Stockinger, B., Di Meglio, P., Gialitakis, M., and Duarte, J. H. (2014) The aryl hydrocarbon receptor: multitasking in the immune system, *Annu. Rev. Immunol.* **32**, 403-432.
- (93) Matsumura, F. (2009) The significance of the nongenomic pathway in mediating inflammatory signaling of the dioxin-activated Ah receptor to cause toxic effects, *Biochem. Pharmacol.* **77**, 608-626.
- (94) Tian, Y., Ke, S., Denison, M. S., Rabson, A. B., and Gallo, M. A. (1999) Ah receptor and NF-kappaB interactions, a potential mechanism for dioxin toxicity, *J. Biol. Chem.* **274**, 510-515.
- (95) Harrill, J. A., Hukkanen, R. R., Lawson, M., Martin, G., Gilger, B., Soldatow, V., Lecluyse, E. L., Budinsky, R. A., Rowlands, J. C., and Thomas, R. S. (2013) Knockout of the aryl hydrocarbon receptor results in distinct hepatic and renal phenotypes in rats and mice, *Toxicol. Appl. Pharmacol.* **272**, 503-518.
- (96) Kawajiri, K., Kobayashi, Y., Ohtake, F., Ikuta, T., Matsushima, Y., Mimura, J., Pettersson, S., Pollenz, R. S., Sakaki, T., Hirokawa, T., Akiyama, T., Kurosumi, M., Poellinger, L., Kato, S., and Fujii-Kuriyama, Y. (2009) Aryl hydrocarbon receptor suppresses intestinal carcinogenesis in ApcMin/+ mice with natural ligands, *Proc. Natl. Acad. Sci. U. S. A.* **106**, 13481-13486.

- (97) Ming, M., Wang, S., Wu, W., Senyuk, V., Le Beau, M. M., Nucifora, G., and Qian, Z. (2012) Activation of Wnt/beta-catenin protein signaling induces mitochondria-mediated apoptosis in hematopoietic progenitor cells, *J. Biol. Chem.* 287, 22683-22690.
- (98) Schmidt, O., Pfanner, N., and Meisinger, C. (2010) Mitochondrial protein import: from proteomics to functional mechanisms, *Nat. Rev. Mol. Cell Biol.* 11, 655-667.
- (99) Friedman, J. R., and Nunnari, J. (2014) Mitochondrial form and function, *Nature* 505, 335-343.
- (100) Wallace, D. C. (2005) A mitochondrial paradigm of metabolic and degenerative diseases, aging, and cancer: a dawn for evolutionary medicine, *Annu. Rev. Genet.* 39, 359-407.
- (101) Fox, T. D. (2012) Mitochondrial protein synthesis, import, and assembly, *Genetics* 192, 1203-1234.
- (102) Hom, J., and Sheu, S. S. (2009) Morphological dynamics of mitochondria--a special emphasis on cardiac muscle cells, *J. Mol. Cell. Cardiol.* 46, 811-820.
- (103) Scarpulla, R. C. (2008) Transcriptional paradigms in mammalian mitochondrial biogenesis and function, *Physiol. Rev.* 88, 611-638.
- (104) Chen, X. J., Wang, X., Kaufman, B. A., and Butow, R. A. (2005) Aconitase couples metabolic regulation to mitochondrial DNA maintenance, *Science* 307, 714-717.
- (105) Matsushima, Y., and Kaguni, L. S. (2012) Matrix proteases in mitochondrial DNA function, *Biochim. Biophys. Acta* 1819, 1080-1087.
- (106) Shutt, T. E., and Shadel, G. S. (2010) A compendium of human mitochondrial gene expression machinery with links to disease, *Environ. Mol. Mutagen* 51, 360-379.
- (107) Gadir, N., Haim-Vilmovsky, L., Kraut-Cohen, J., and Gerst, J. E. (2011) Localization of mRNAs coding for mitochondrial proteins in the yeast *Saccharomyces cerevisiae*, *RNA* 17, 1551-1565.
- (108) Baker, M. J., Frazier, A. E., Gulbis, J. M., and Ryan, M. T. (2007) Mitochondrial protein-import machinery: correlating structure with function, *Trends Cell Biol.* 17, 456-464.
- (109) Gava, L. M., Goncalves, D. C., Borges, J. C., and Ramos, C. H. (2011) Stoichiometry and thermodynamics of the interaction between the C-terminus of human 90kDa heat shock protein Hsp90 and the mitochondrial translocase of outer membrane Tom70, *Arch. Biochem. Biophys.* 513, 119-125.

- (110) Budas, G. R., Churchill, E. N., Disatnik, M. H., Sun, L., and Mochly-Rosen, D. (2010) Mitochondrial import of PKCepsilon is mediated by HSP90: a role in cardioprotection from ischaemia and reperfusion injury, *Cardiovasc. Res.* **88**, 83-92.
- (111) Yano, M., Terada, K., and Mori, M. (2003) AIP is a mitochondrial import mediator that binds to both import receptor Tom20 and preproteins, *J. Cell Biol.* **163**, 45-56.
- (112) Fan, A. C., Kozlov, G., Hoegl, A., Marcellus, R. C., Wong, M. J., Gehring, K., and Young, J. C. (2011) Interaction between the human mitochondrial import receptors Tom20 and Tom70 in vitro suggests a chaperone displacement mechanism, *J. Biol. Chem.* **286**, 32208-32219.
- (113) van der Laan, M., Wiedemann, N., Mick, D. U., Guiard, B., Rehling, P., and Pfanner, N. (2006) A role for Tim21 in membrane-potential-dependent preprotein sorting in mitochondria, *Curr. Biol.* **16**, 2271-2276.
- (114) Bragoszewski, P., Gornicka, A., Sztolszterer, M. E., and Chacinska, A. (2013) The ubiquitin-proteasome system regulates mitochondrial intermembrane space proteins, *Mol. Cell. Biol.* **33**, 2136-2148.
- (115) Garesse, R., and Kaguni, L. S. (2005) A Drosophila model of mitochondrial DNA replication: proteins, genes and regulation, *IUBMB Life* **57**, 555-561.
- (116) Arnold, S. (2012) The power of life--cytochrome c oxidase takes center stage in metabolic control, cell signalling and survival, *Mitochondrion* **12**, 46-56.
- (117) Piantadosi, C. A., and Suliman, H. B. (2008) Transcriptional Regulation of SDHa flavoprotein by nuclear respiratory factor-1 prevents pseudo-hypoxia in aerobic cardiac cells, *J. Biol. Chem.* **283**, 10967-10977.
- (118) Psarra, A. M., and Sekeris, C. E. (2008) Steroid and thyroid hormone receptors in mitochondria, *IUBMB Life* **60**, 210-223.
- (119) Jenninga, E. H., Schoonjans, K., and Auwerx, J. (2010) Reversible acetylation of PGC-1: connecting energy sensors and effectors to guarantee metabolic flexibility, *Oncogene* **29**, 4617-4624.
- (120) Sena, L. A., and Chandel, N. S. (2012) Physiological roles of mitochondrial reactive oxygen species, *Mol. Cell* **48**, 158-167.
- (121) Kotiadis, V. N., Duchon, M. R., and Osellame, L. D. (2014) Mitochondrial quality control and communications with the nucleus are important in maintaining mitochondrial function and cell health, *Biochim. Biophys. Acta* **1840**, 1254-1265.
- (122) Nunnari, J., and Suomalainen, A. (2012) Mitochondria: in sickness and in health, *Cell* **148**, 1145-1159.

- (123) Brand, M. D. (2010) The sites and topology of mitochondrial superoxide production, *Exp. Gerontol.* 45, 466-472.
- (124) Bleier, L., Wittig, I., Heide, H., Steger, M., Brandt, U., and Drose, S. (2015) Generator-specific targets of mitochondrial reactive oxygen species, *Free Radic. Biol. Med.* 78, 1-10.
- (125) Drose, S., and Brandt, U. (2012) Molecular mechanisms of superoxide production by the mitochondrial respiratory chain, *Adv. Exp. Med. Biol.* 748, 145-169.
- (126) Voet, D., and Voet, J. G. (1995) *Biochemistry*, 2nd ed., J. Wiley & Sons, New York.
- (127) Denko, N. C. (2008) Hypoxia, HIF1 and glucose metabolism in the solid tumour, *Nat. Rev. Cancer* 8, 705-713.
- (128) Chin, R. M., Fu, X., Pai, M. Y., Vergnes, L., Hwang, H., Deng, G., Diep, S., Lomenick, B., Meli, V. S., Monsalve, G. C., Hu, E., Whelan, S. A., Wang, J. X., Jung, G., Solis, G. M., Fazlollahi, F., Kaweeteerawat, C., Quach, A., Nili, M., Krall, A. S., Godwin, H. A., Chang, H. R., Faull, K. F., Guo, F., Jiang, M., Trauger, S. A., Saghatelian, A., Braas, D., Christofk, H. R., Clarke, C. F., Teitell, M. A., Petrascheck, M., Reue, K., Jung, M. E., Frand, A. R., and Huang, J. (2014) The metabolite alpha-ketoglutarate extends lifespan by inhibiting ATP synthase and TOR, *Nature* 510, 397-401.
- (129) Dang, L., White, D. W., Gross, S., Bennett, B. D., Bittinger, M. A., Driggers, E. M., Fantin, V. R., Jang, H. G., Jin, S., Keenan, M. C., Marks, K. M., Prins, R. M., Ward, P. S., Yen, K. E., Liao, L. M., Rabinowitz, J. D., Cantley, L. C., Thompson, C. B., Vander Heiden, M. G., and Su, S. M. (2009) Cancer-associated IDH1 mutations produce 2-hydroxyglutarate, *Nature* 462, 739-744.
- (130) Xu, W., Yang, H., Liu, Y., Yang, Y., Wang, P., Kim, S. H., Ito, S., Yang, C., Wang, P., Xiao, M. T., Liu, L. X., Jiang, W. Q., Liu, J., Zhang, J. Y., Wang, B., Frye, S., Zhang, Y., Xu, Y. H., Lei, Q. Y., Guan, K. L., Zhao, S. M., and Xiong, Y. (2011) Oncometabolite 2-hydroxyglutarate is a competitive inhibitor of alpha-ketoglutarate-dependent dioxygenases, *Cancer Cell* 19, 17-30.
- (131) Koivunen, P., Hirsila, M., Remes, A. M., Hassinen, I. E., Kivirikko, K. I., and Myllyharju, J. (2007) Inhibition of hypoxia-inducible factor (HIF) hydroxylases by citric acid cycle intermediates: possible links between cell metabolism and stabilization of HIF, *J. Biol. Chem.* 282, 4524-4532.
- (132) King, A., Selak, M. A., and Gottlieb, E. (2006) Succinate dehydrogenase and fumarate hydratase: linking mitochondrial dysfunction and cancer, *Oncogene* 25, 4675-4682.
- (133) Benit, P., Letouze, E., Rak, M., Aubry, L., Burnichon, N., Favier, J., Gimenez-Roqueplo, A. P., and Rustin, P. (2014) Unsuspected task for an old team: succinate, fumarate and

- other Krebs cycle acids in metabolic remodeling, *Biochim. Biophys. Acta* 1837, 1330-1337.
- (134) Zhao, S., Xu, W., Jiang, W., Yu, W., Lin, Y., Zhang, T., Yao, J., Zhou, L., Zeng, Y., Li, H., Li, Y., Shi, J., An, W., Hancock, S. M., He, F., Qin, L., Chin, J., Yang, P., Chen, X., Lei, Q., Xiong, Y., and Guan, K. L. (2010) Regulation of cellular metabolism by protein lysine acetylation, *Science* 327, 1000-1004.
- (135) Schlicker, C., Gertz, M., Papatheodorou, P., Kachholz, B., Becker, C. F., and Steegborn, C. (2008) Substrates and regulation mechanisms for the human mitochondrial sirtuins Sirt3 and Sirt5, *J. Mol. Biol.* 382, 790-801.
- (136) Lin, Z. F., Xu, H. B., Wang, J. Y., Lin, Q., Ruan, Z., Liu, F. B., Jin, W., Huang, H. H., and Chen, X. (2013) SIRT5 desuccinylates and activates SOD1 to eliminate ROS, *Biochem. Biophys. Res. Commun.* 441, 191-195.
- (137) Fong, G. H., and Takeda, K. (2008) Role and regulation of prolyl hydroxylase domain proteins, *Cell Death. Differ.* 15, 635-641.
- (138) Nassir, F., and Ibdah, J. A. (2014) Role of mitochondria in nonalcoholic fatty liver disease, *Int. J. Mol. Sci.* 15, 8713-8742.
- (139) Begriche, K., Massart, J., Robin, M. A., Bonnet, F., and Fromenty, B. (2013) Mitochondrial adaptations and dysfunctions in nonalcoholic fatty liver disease, *Hepatology* 58, 1497-1507.
- (140) Mandal, P. K. (2005) Dioxin: a review of its environmental effects and its aryl hydrocarbon receptor biology, *J. Comp. Physiol. B.* 175, 221-230.
- (141) Steenland, K., Bertazzi, P., Baccarelli, A., and Kogevinas, M. (2004) Dioxin revisited: developments since the 1997 IARC classification of dioxin as a human carcinogen, *Environ. Health Perspect.* 112, 1265-1268.
- (142) Diani-Moore, S., Zhang, S., Ram, P., and Rifkind, A. B. (2013) Aryl hydrocarbon receptor activation by dioxin targets phosphoenolpyruvate carboxykinase (PEPCK) for ADP-ribosylation via 2,3,7,8-tetrachlorodibenzo-p-dioxin (TCDD)-inducible poly(ADP-ribose) polymerase (TiPARP), *J. Biol. Chem.* 288, 21514-21525.
- (143) Boverhof, D. R., Burgoon, L. D., Tashiro, C., Chittim, B., Harkema, J. R., Jump, D. B., and Zacharewski, T. R. (2005) Temporal and dose-dependent hepatic gene expression patterns in mice provide new insights into TCDD-Mediated hepatotoxicity, *Toxicol. Sci.* 85, 1048-1063.
- (144) Ikegwonu, F. I., and Jefcoate, C. R. (1999) Evidence for the involvement of the fatty acid and peroxisomal beta-oxidation pathways in the inhibition by dehydroepiandrosterone (DHEA) and induction by 2,3,7,8-tetrachlorodibenzo-p-dioxin

- (TCDD) and benz(a)anthracene (BA) of cytochrome P4501B1 (CYP1B1) in mouse embryo fibroblasts (C3H10T1/2 cells), *Mol. Cell. Biochem.* 198, 89-100.
- (145) Diani-Moore, S., Ram, P., Li, X., Mondal, P., Youn, D. Y., Sauve, A. A., and Rifkind, A. B. (2010) Identification of the aryl hydrocarbon receptor target gene TiPARP as a mediator of suppression of hepatic gluconeogenesis by 2,3,7,8-tetrachlorodibenzo-p-dioxin and of nicotinamide as a corrective agent for this effect, *J. Biol. Chem.* 285, 38801-38810.
- (146) Angrish, M. M., Jones, A. D., Harkema, J. R., and Zacharewski, T. R. (2011) Aryl hydrocarbon receptor-mediated induction of Stearoyl-CoA desaturase 1 alters hepatic fatty acid composition in TCDD-elicited steatosis, *Toxicol. Sci.* 124, 299-310.
- (147) Sato, S., Shirakawa, H., Tomita, S., Ohsaki, Y., Haketa, K., Tooi, O., Santo, N., Tohkin, M., Furukawa, Y., Gonzalez, F. J., and Komai, M. (2008) Low-dose dioxins alter gene expression related to cholesterol biosynthesis, lipogenesis, and glucose metabolism through the aryl hydrocarbon receptor-mediated pathway in mouse liver, *Toxicol. Appl. Pharmacol.* 229, 10-19.
- (148) Tanos, R., Patel, R. D., Murray, I. A., Smith, P. B., Patterson, A. D., and Perdew, G. H. (2012) Aryl hydrocarbon receptor regulates the cholesterol biosynthetic pathway in a dioxin response element-independent manner, *Hepatology* 55, 1994-2004.
- (149) Angrish, M. M., Dominici, C. Y., and Zacharewski, T. R. (2013) TCDD-elicited effects on liver, serum, and adipose lipid composition in C57BL/6 mice, *Toxicol. Sci.* 131, 108-115.
- (150) He, J., Hu, B., Shi, X., Weidert, E. R., Lu, P., Xu, M., Huang, M., Kelley, E. E., and Xie, W. (2013) Activation of the aryl hydrocarbon receptor sensitizes mice to nonalcoholic steatohepatitis by deactivating mitochondrial sirtuin deacetylase Sirt3, *Mol. Cell. Biol.* 33, 2047-2055.
- (151) Unkila, M., Pohjanvirta, R., and Tuomisto, J. (1998) Body weight loss and changes in tryptophan homeostasis by chlorinated dibenzo-p-dioxin congeners in the most TCDD-susceptible and the most TCDD-resistant rat strain, *Arch. Toxicol.* 72, 769-776.
- (152) Shen, D., Dalton, T. P., Nebert, D. W., and Shertzer, H. G. (2005) Glutathione redox state regulates mitochondrial reactive oxygen production, *J. Biol. Chem.* 280, 25305-25312.
- (153) Shertzer, H. G., Genter, M. B., Shen, D., Nebert, D. W., Chen, Y., and Dalton, T. P. (2006) TCDD decreases ATP levels and increases reactive oxygen production through changes in mitochondrial F(0)F(1)-ATP synthase and ubiquinone, *Toxicol. Appl. Pharmacol.* 217, 363-374.
- (154) Kennedy, L. H., Sutter, C. H., Leon Carrion, S., Tran, Q. T., Bodreddigari, S., Kensicki, E., Mohny, R. P., and Sutter, T. R. (2013) 2,3,7,8-Tetrachlorodibenzo-p-dioxin-

- mediated production of reactive oxygen species is an essential step in the mechanism of action to accelerate human keratinocyte differentiation, *Toxicol. Sci.* 132, 235-249.
- (155) Makay, B., Makay, O., Yenisey, C., Icoz, G., Ozgen, G., Unsal, E., Akyildiz, M., and Yetkin, E. (2009) The interaction of oxidative stress response with cytokines in the thyrotoxic rat: is there a link?, *Mediators Inflamm.* 2009, 391682.
- (156) Elmarakby, A. A., and Sullivan, J. C. (2012) Relationship between oxidative stress and inflammatory cytokines in diabetic nephropathy, *Cardiovasc. Ther.* 30, 49-59.
- (157) Chen, C. Y., Huang, Y. L., and Lin, T. H. (1998) Association between oxidative stress and cytokine production in nickel-treated rats, *Arch. Biochem. Biophys.* 356, 127-132.
- (158) Vogel, C. F., Khan, E. M., Leung, P. S., Gershwin, M. E., Chang, W. L., Wu, D., Haarmann-Stemann, T., Hoffmann, A., and Denison, M. S. (2014) Cross-talk between aryl hydrocarbon receptor and the inflammatory response: a role for nuclear factor-kappaB, *J. Biol. Chem.* 289, 1866-1875.
- (159) Senft, A. P., Dalton, T. P., Nebert, D. W., Genter, M. B., Hutchinson, R. J., and Shertzer, H. G. (2002) Dioxin increases reactive oxygen production in mouse liver mitochondria, *Toxicol. Appl. Pharmacol.* 178, 15-21.
- (160) Senft, A. P., Dalton, T. P., Nebert, D. W., Genter, M. B., Puga, A., Hutchinson, R. J., Kerzee, J. K., Uno, S., and Shertzer, H. G. (2002) Mitochondrial reactive oxygen production is dependent on the aromatic hydrocarbon receptor, *Free Radic. Biol. Med.* 33, 1268-1278.
- (161) Aly, H. A., and Domenech, O. (2009) Cytotoxicity and mitochondrial dysfunction of 2,3,7,8-tetrachlorodibenzo-p-dioxin (TCDD) in isolated rat hepatocytes, *Toxicol. Lett.* 191, 79-87.
- (162) Rico de Souza, A., Zago, M., Pollock, S. J., Sime, P. J., Phipps, R. P., and Baglole, C. J. (2011) Genetic ablation of the aryl hydrocarbon receptor causes cigarette smoke-induced mitochondrial dysfunction and apoptosis, *J. Biol. Chem.* 286, 43214-43228.
- (163) Biswas, G., Srinivasan, S., Anandatheerthavarada, H. K., and Avadhani, N. G. (2008) Dioxin-mediated tumor progression through activation of mitochondria-to-nucleus stress signaling, *Proc. Natl. Acad. Sci. U. S. A.* 105, 186-191.
- (164) Forgacs, A. L., Burgoon, L. D., Lynn, S. G., LaPres, J. J., and Zacharewski, T. (2010) Effects of TCDD on the expression of nuclear encoded mitochondrial genes, *Toxicol. Appl. Pharmacol.* 246, 58-65.
- (165) Tappenden, D. M., Lynn, S. G., Crawford, R. B., Lee, K., Vengellur, A., Kaminski, N. E., Thomas, R. S., and LaPres, J. J. (2011) The aryl hydrocarbon receptor interacts with

ATP5alpha1, a subunit of the ATP synthase complex, and modulates mitochondrial function, *Toxicol. Appl. Pharmacol.* 254, 299-310.

- (166) Tappenden, D. M., Hwang, H. J., Yang, L., Thomas, R. S., and Lapres, J. J. (2013) The Aryl-Hydrocarbon Receptor Protein Interaction Network (AHR-PIN) as Identified by Tandem Affinity Purification (TAP) and Mass Spectrometry, *J. Toxicol.* 2013, 279829.
- (167) Kang, B. H., Xia, F., Pop, R., Dohi, T., Socolovsky, M., and Altieri, D. C. (2011) Developmental control of apoptosis by the immunophilin aryl hydrocarbon receptor-interacting protein (AIP) involves mitochondrial import of the survivin protein, *J. Biol. Chem.* 286, 16758-16767.
- (168) Yang, T. T., Hsu, C. T., and Kuo, Y. M. (2009) Cell-derived soluble oligomers of human amyloid-beta peptides disturb cellular homeostasis and induce apoptosis in primary hippocampal neurons, *J. Neural Transm.* 116, 1561-1569.
- (169) Vengellur, A., and LaPres, J. J. (2004) The role of hypoxia inducible factor 1alpha in cobalt chloride induced cell death in mouse embryonic fibroblasts, *Toxicol. Sci.* 82, 638-646.
- (170) Frezza, C., Cipolat, S., and Scorrano, L. (2007) Organelle isolation: functional mitochondria from mouse liver, muscle and cultured fibroblasts, *Nat. Protoc.* 2, 287-295.
- (171) Griparic, L., and van der Bliek, A. M. (2005) Assay and properties of the mitochondrial dynamin related protein Opa1, *Methods Enzymol.* 404, 620-631.
- (172) Brand, M. D., and Nicholls, D. G. (2011) Assessing mitochondrial dysfunction in cells, *Biochem. J.* 435, 297-312.
- (173) Frazier, A. E., and Thorburn, D. R. (2012) Biochemical analyses of the electron transport chain complexes by spectrophotometry, *Methods Mol. Biol.* 837, 49-62.
- (174) Barrientos, A., Fontanesi, F., and Diaz, F. (2009) Evaluation of the mitochondrial respiratory chain and oxidative phosphorylation system using polarography and spectrophotometric enzyme assays, *Curr. Protoc. Hum. Genet. Chapter 19*, Unit19 13.
- (175) Shevchenko, A., Wilm, M., Vorm, O., and Mann, M. (1996) Mass spectrometric sequencing of proteins silver-stained polyacrylamide gels, *Anal. Chem.* 68, 850-858.
- (176) Cox, J., and Mann, M. (2008) MaxQuant enables high peptide identification rates, individualized p.p.b.-range mass accuracies and proteome-wide protein quantification, *Nat. Biotechnol.* 26, 1367-1372.
- (177) Cox, J., Neuhauser, N., Michalski, A., Scheltema, R. A., Olsen, J. V., and Mann, M. (2011) Andromeda: a peptide search engine integrated into the MaxQuant environment, *J. Proteome Res.* 10, 1794-1805.

- (178) Lowry, O. H., Rosebrough, N. J., Farr, A. L., and Randall, R. J. (1951) Protein measurement with the Folin phenol reagent, *J. Biol. Chem.* *193*, 265-275.
- (179) Claros, M. G., and Vincens, P. (1996) Computational method to predict mitochondrially imported proteins and their targeting sequences, *Eur. J. Biochem.* *241*, 779-786.
- (180) Fukasawa, Y., Tsuji, J., Fu, S. C., Tomii, K., Horton, P., and Imai, K. (2015) MitoFates: improved prediction of mitochondrial targeting sequences and their cleavage sites, *Mol. Cell. Proteomics* *14*, 1113-1126.
- (181) Sickmann, A., Reinders, J., Wagner, Y., Joppich, C., Zahedi, R., Meyer, H. E., Schonfisch, B., Perschil, I., Chacinska, A., Guiard, B., Rehling, P., Pfanner, N., and Meisinger, C. (2003) The proteome of *Saccharomyces cerevisiae* mitochondria, *Proc. Natl. Acad. Sci. U. S. A.* *100*, 13207-13212.
- (182) Diekert, K., Kispal, G., Guiard, B., and Lill, R. (1999) An internal targeting signal directing proteins into the mitochondrial intermembrane space, *Proc. Natl. Acad. Sci. U. S. A.* *96*, 11752-11757.
- (183) Huang, X., and Miller, W. (1991) A time-efficient, linear-space local similarity algorithm, *Adv. Appl. Math.* *12*, 337-357.
- (184) Pollenz, R. S., Wilson, S. E., and Dougherty, E. J. (2006) Role of endogenous XAP2 protein on the localization and nucleocytoplasmic shuttling of the endogenous mouse Ahb-1 receptor in the presence and absence of ligand, *Mol. Pharmacol.* *70*, 1369-1379.
- (185) Pollenz, R. S., and Dougherty, E. J. (2005) Redefining the role of the endogenous XAP2 and C-terminal hsp70-interacting protein on the endogenous Ah receptors expressed in mouse and rat cell lines, *J. Biol. Chem.* *280*, 33346-33356.
- (186) Azzu, V., and Brand, M. D. (2010) Degradation of an intramitochondrial protein by the cytosolic proteasome, *J. Cell Sci.* *123*, 578-585.
- (187) Azzu, V., and Brand, M. D. (2010) The on-off switches of the mitochondrial uncoupling proteins, *Trends Biochem. Sci.* *35*, 298-307.
- (188) Jaiswal, P. K., Srivastava, S., Gupta, J., and Thakur, I. S. (2012) Dibenzofuran induces oxidative stress, disruption of trans-mitochondrial membrane potential ( $\Delta\psi$ ) and G1 arrest in human hepatoma cell line, *Toxicol. Lett.* *214*, 137-144.
- (189) Forgacs, A. L., Kent, M. N., Makley, M. K., Mets, B., DelRaso, N., Jahns, G. L., Burgoon, L. D., Zacharewski, T. R., and Reo, N. V. (2012) Comparative metabolomic and genomic analyses of TCDD-elicited metabolic disruption in mouse and rat liver, *Toxicol. Sci.* *125*, 41-55.

- (190) Zhang, J., Lanham, K. A., Heideman, W., Peterson, R. E., and Li, L. (2013) Statistically enhanced spectral counting approach to TCDD cardiac toxicity in the adult zebrafish heart, *J. Proteome Res.* 12, 3093-3103.
- (191) Sarioglu, H., Brandner, S., Habeger, M., Jacobsen, C., Lichtmanegger, J., Wormke, M., and Andrae, U. (2008) Analysis of 2,3,7,8-tetrachlorodibenzo-p-dioxin-induced proteome changes in 5L rat hepatoma cells reveals novel targets of dioxin action including the mitochondrial apoptosis regulator VDAC2, *Mol. Cell. Proteomics* 7, 394-410.
- (192) Schulz, M., Brandner, S., Eberhagen, C., Eckardt-Schupp, F., Larsen, M. R., and Andrae, U. (2013) Quantitative phosphoproteomic analysis of early alterations in protein phosphorylation by 2,3,7,8-tetrachlorodibenzo-p-dioxin, *J. Proteome Res.* 12, 866-882.
- (193) Leopold, J. A., and Loscalzo, J. (2000) Cyclic strain modulates resistance to oxidant stress by increasing G6PDH expression in smooth muscle cells, *Am. J. Physiol. Heart Circ. Physiol.* 279, H2477-2485.
- (194) Mailloux, R. J., and Harper, M. E. (2010) Glucose regulates enzymatic sources of mitochondrial NADPH in skeletal muscle cells; a novel role for glucose-6-phosphate dehydrogenase, *FASEB J.* 24, 2495-2506.
- (195) Kohno, H., Furukawa, T., Yoshinaga, T., Tokunaga, R., and Taketani, S. (1993) Coproporphyrinogen oxidase. Purification, molecular cloning, and induction of mRNA during erythroid differentiation, *J. Biol. Chem.* 268, 21359-21363.
- (196) Chavan, H., and Krishnamurthy, P. (2012) Polycyclic aromatic hydrocarbons (PAHs) mediate transcriptional activation of the ATP binding cassette transporter ABCB6 gene via the aryl hydrocarbon receptor (AhR), *J. Biol. Chem.* 287, 32054-32068.
- (197) Dere, E., Lo, R., Celius, T., Matthews, J., and Zacharewski, T. R. (2011) Integration of genome-wide computation DRE search, AhR ChIP-chip and gene expression analyses of TCDD-elicited responses in the mouse liver, *BMC Genomics* 12, 365.
- (198) Lang, E., Schafer, M., Schwender, H., Neumann, N. J., and Frank, J. (2015) Occurrence of Malignant Tumours in the Acute Hepatic Porphyrias, *JIMD Rep.* 22, 17-22.
- (199) Smith, A. G., Clothier, B., Robinson, S., Scullion, M. J., Carthew, P., Edwards, R., Luo, J., Lim, C. K., and Toledano, M. (1998) Interaction between iron metabolism and 2,3,7,8-tetrachlorodibenzo-p-dioxin in mice with variants of the Ahr gene: a hepatic oxidative mechanism, *Mol. Pharmacol.* 53, 52-61.
- (200) Farombi, E. O., and Surh, Y. J. (2006) Heme oxygenase-1 as a potential therapeutic target for hepatoprotection, *J. Biochem. Mol. Biol.* 39, 479-491.

- (201) Moffat, C., Bhatia, L., Nguyen, T., Lynch, P., Wang, M., Wang, D., Ilkayeva, O. R., Han, X., Hirschey, M. D., Claypool, S. M., and Seifert, E. L. (2014) Acyl-CoA thioesterase-2 facilitates mitochondrial fatty acid oxidation in the liver, *J. Lipid Res.* 55, 2458-2470.
- (202) Masse, K., Bhamra, S., Eason, R., Dale, N., and Jones, E. A. (2007) Purine-mediated signalling triggers eye development, *Nature* 449, 1058-1062.
- (203) Vandenbeuch, A., Anderson, C. B., Parnes, J., Enjoji, K., Robson, S. C., Finger, T. E., and Kinnamon, S. C. (2013) Role of the ectonucleotidase NTPDase2 in taste bud function, *Proc. Natl. Acad. Sci. U. S. A.* 110, 14789-14794.
- (204) Yu, J., Lavoie, E. G., Sheung, N., Tremblay, J. J., Sevigny, J., and Dranoff, J. A. (2008) IL-6 downregulates transcription of NTPDase2 via specific promoter elements, *Am. J. Physiol. Gastrointest. Liver Physiol.* 294, G748-756.
- (205) Mateo, J., Kreda, S., Henry, C. E., Harden, T. K., and Boyer, J. L. (2003) Requirement of Cys399 for processing of the human ecto-ATPase (NTPDase2) and its implications for determination of the activities of splice variants of the enzyme, *J. Biol. Chem.* 278, 39960-39968.
- (206) Dere, E., Lee, A. W., Burgoon, L. D., and Zacharewski, T. R. (2011) Differences in TCDD-elicited gene expression profiles in human HepG2, mouse Hepa1c1c7 and rat H4IIE hepatoma cells, *BMC Genomics* 12, 193.
- (207) Gao, L., Dong, L., and Whitlock, J. P., Jr. (1998) A novel response to dioxin. Induction of ecto-ATPase gene expression, *J. Biol. Chem.* 273, 15358-15365.
- (208) Vlajkovic, S. M., Housley, G. D., Greenwood, D., and Thorne, P. R. (1999) Evidence for alternative splicing of ecto-ATPase associated with termination of purinergic transmission, *Brain Res. Mol. Brain Res.* 73, 85-92.
- (209) Hwang, H. J., Lynn, S. G., Vengellur, A., Saini, Y., Grier, E. A., Ferguson-Miller, S. M., and LaPres, J. J. (2015) Hypoxia Inducible Factors Modulate Mitochondrial Oxygen Consumption and Transcriptional Regulation of Nuclear-Encoded Electron Transport Chain Genes, *Biochemistry* 54, 3739-3748.
- (210) Huttemann, M., Kadenbach, B., and Grossman, L. I. (2001) Mammalian subunit IV isoforms of cytochrome c oxidase, *Gene* 267, 111-123.
- (211) Vengellur, A., Woods, B. G., Ryan, H. E., Johnson, R. S., and LaPres, J. J. (2003) Gene expression profiling of the hypoxia signaling pathway in hypoxia-inducible factor 1alpha null mouse embryonic fibroblasts, *Gene Expression* 11, 181-197.
- (212) Ratcliffe, P. J. (2013) Oxygen sensing and hypoxia signalling pathways in animals: the implications of physiology for cancer, *J. Physiol.* 591, 2027-2042.

- (213) Bunn, H. F., and Poyton, R. O. (1996) Oxygen sensing and molecular adaptation to hypoxia, *Physiol. Rev.* 76, 839-885.
- (214) Shen, C., Nettleton, D., Jiang, M., Kim, S. K., and Powell-Coffman, J. A. (2005) Roles of the HIF-1 hypoxia-inducible factor during hypoxia response in *Caenorhabditis elegans*, *J. Biol. Chem.* 280, 20580-20588.
- (215) Li, Y., Padmanabha, D., Gentile, L. B., Dumur, C. I., Beckstead, R. B., and Baker, K. D. (2013) HIF- and non-HIF-regulated hypoxic responses require the estrogen-related receptor in *Drosophila melanogaster*, *PLoS Genet.* 9, e1003230.
- (216) Taylor, C. T. (2008) Mitochondria and cellular oxygen sensing in the HIF pathway, *Biochem. J.* 409, 19-26.
- (217) Solaini, G., Baracca, A., Lenaz, G., and Sgarbi, G. (2010) Hypoxia and mitochondrial oxidative metabolism, *Biochim. Biophys. Acta* 1797, 1171-1177.
- (218) Palsson-McDermott, E. M., and O'Neill, L. A. (2013) The Warburg effect then and now: from cancer to inflammatory diseases, *Bioessays* 35, 965-973.
- (219) Bruick, R. K. (2000) Expression of the gene encoding the proapoptotic Nip3 protein is induced by hypoxia, *Proc. Natl. Acad. Sci. U. S. A.* 97, 9082-9087.
- (220) Rikka, S., Quinsay, M. N., Thomas, R. L., Kubli, D. A., Zhang, X., Murphy, A. N., and Gustafsson, A. B. (2011) Bnip3 impairs mitochondrial bioenergetics and stimulates mitochondrial turnover, *Cell Death Differ.* 18, 721-731.
- (221) Gomes, A. P., Price, N. L., Ling, A. J., Moslehi, J. J., Montgomery, M. K., Rajman, L., White, J. P., Teodoro, J. S., Wrann, C. D., Hubbard, B. P., Mercken, E. M., Palmeira, C. M., de Cabo, R., Rolo, A. P., Turner, N., Bell, E. L., and Sinclair, D. A. (2013) Declining NAD(+) induces a pseudohypoxic state disrupting nuclear-mitochondrial communication during aging, *Cell* 155, 1624-1638.
- (222) Huttemann, M., Jaradat, S., and Grossman, L. I. (2003) Cytochrome c oxidase of mammals contains a testes-specific isoform of subunit VIb--the counterpart to testes-specific cytochrome c?, *Mol. Reprod. Dev.* 66, 8-16.
- (223) Huttemann, M., Schmidt, T. R., and Grossman, L. I. (2003) A third isoform of cytochrome c oxidase subunit VIII is present in mammals, *Gene* 312, 95-102.
- (224) Pierron, D., Wildman, D. E., Huttemann, M., Markondapatnaikuni, G. C., Aras, S., and Grossman, L. I. (2012) Cytochrome c oxidase: evolution of control via nuclear subunit addition, *Biochim. Biophys. Acta* 1817, 590-597.

- (225) Acin-Perez, R., Gatti, D. L., Bai, Y., and Manfredi, G. (2011) Protein phosphorylation and prevention of cytochrome oxidase inhibition by ATP: coupled mechanisms of energy metabolism regulation, *Cell Metab.* 13, 712-719.
- (226) Huttemann, M., Lee, I., Liu, J., and Grossman, L. I. (2007) Transcription of mammalian cytochrome c oxidase subunit IV-2 is controlled by a novel conserved oxygen responsive element, *FEBS J.* 274, 5737-5748.
- (227) Fukuda, R., Zhang, H., Kim, J. W., Shimoda, L., Dang, C. V., and Semenza, G. L. (2007) HIF-1 regulates cytochrome oxidase subunits to optimize efficiency of respiration in hypoxic cells, *Cell* 129, 111-122.
- (228) Ronn, T., Poulsen, P., Hansson, O., Holmkvist, J., Almgren, P., Nilsson, P., Tuomi, T., Isomaa, B., Groop, L., Vaag, A., and Ling, C. (2008) Age influences DNA methylation and gene expression of COX7A1 in human skeletal muscle, *Diabetologia* 51, 1159-1168.
- (229) Chen, L., Xin, Z. C., Li, X., Tian, L., Yuan, Y. M., Liu, G., Jiang, X. J., and Guo, Y. L. (2006) Cox7a2 mediates steroidogenesis in TM3 mouse Leydig cells, *Asian J. Androl.* 8, 589-594.
- (230) Ryan, H. E., Poloni, M., McNulty, W., Elson, D., Gassmann, M., Arbeit, J. M., and Johnson, R. S. (2000) Hypoxia-inducible factor-1alpha is a positive factor in solid tumor growth, *Cancer Res.* 60, 4010-4015.
- (231) Saini, Y., Harkema, J. R., and LaPres, J. J. (2008) HIF1alpha is essential for normal intrauterine differentiation of alveolar epithelium and surfactant production in the newborn lung of mice, *J. Biol. Chem.* 283, 33650-33657.
- (232) de Hoon, M. J., Imoto, S., Nolan, J., and Miyano, S. (2004) Open source clustering software, *Bioinformatics* 20, 1453-1454.
- (233) Capaldi, R. A., Marusich, M. F., and Taanman, J. W. (1995) Mammalian cytochrome-c oxidase: characterization of enzyme and immunological detection of subunits in tissue extracts and whole cells, *Methods Enzymol.* 260, 117-132.
- (234) Thompson, D. A., and Ferguson-Miller, S. (1983) Lipid and subunit III depleted cytochrome c oxidase purified by horse cytochrome c affinity chromatography in lauryl maltoside, *Biochemistry* 22, 3178-3187.
- (235) Naciri, M., Kuystermans, D., and Al-Rubeai, M. (2008) Monitoring pH and dissolved oxygen in mammalian cell culture using optical sensors, *Cytotechnology* 57, 245-250.
- (236) Althoff, T., Mills, D. J., Popot, J. L., and Kuhlbrandt, W. (2011) Arrangement of electron transport chain components in bovine mitochondrial supercomplex I1III2IV1, *EMBO J* 30, 4652-4664.

- (237) Tsukihara, T., Aoyama, H., Yamashita, E., Tomizaki, T., Yamaguchi, H., Shinzawa-Itoh, K., Nakashima, R., Yaono, R., and Yoshikawa, S. (1996) The whole structure of the 13-subunit oxidized cytochrome c oxidase at 2.8 Å, *Science* 272, 1136-1144.
- (238) Cui, T. Z., Conte, A., Fox, J. L., Zara, V., and Winge, D. R. (2014) Modulation of the respiratory supercomplexes in yeast: enhanced formation of cytochrome oxidase increases the stability and abundance of respiratory supercomplexes, *J. Biol. Chem.* 289, 6133-6141.
- (239) Huttemann, M., Klewer, S., Lee, I., Pecinova, A., Pecina, P., Liu, J., Lee, M., Doan, J. W., Larson, D., Slack, E., Maghsoodi, B., Erickson, R. P., and Grossman, L. I. (2012) Mice deleted for heart-type cytochrome c oxidase subunit 7a1 develop dilated cardiomyopathy, *Mitochondrion* 12, 294-304.
- (240) Rodriguez-Enriquez, S., Juarez, O., Rodriguez-Zavala, J. S., and Moreno-Sanchez, R. (2001) Multisite control of the Crabtree effect in ascites hepatoma cells, *Eur. J. Biochem.* 268, 2512-2519.
- (241) Rossignol, R., Gilkerson, R., Aggeler, R., Yamagata, K., Remington, S. J., and Capaldi, R. A. (2004) Energy substrate modulates mitochondrial structure and oxidative capacity in cancer cells, *Cancer Res.* 64, 985-993.
- (242) Aguer, C., Gambarotta, D., Mailloux, R. J., Moffat, C., Dent, R., McPherson, R., and Harper, M. E. (2011) Galactose enhances oxidative metabolism and reveals mitochondrial dysfunction in human primary muscle cells, *PLoS One* 6, e28536.
- (243) Pulliam, D. A., Deepa, S. S., Liu, Y., Hill, S., Lin, A. L., Bhattacharya, A., Shi, Y., Sloane, L., Viscomi, C., Zeviani, M., and Van Remmen, H. (2014) Complex IV-deficient Surf1(-/-) mice initiate mitochondrial stress responses, *Biochem. J.* 462, 359-371.
- (244) Oelkrug, R., Goetze, N., Meyer, C. W., and Jastroch, M. (2014) Antioxidant properties of UCP1 are evolutionarily conserved in mammals and buffer mitochondrial reactive oxygen species, *Free Radic. Biol. Med.* 77, 210-216.
- (245) Chandel, N. S. (2010) Mitochondrial regulation of oxygen sensing, *Adv. Exp. Med. Biol.* 661, 339-354.
- (246) Chua, Y. L., Dufour, E., Dassa, E. P., Rustin, P., Jacobs, H. T., Taylor, C. T., and Hagen, T. (2010) Stabilization of hypoxia-inducible factor-1α protein in hypoxia occurs independently of mitochondrial reactive oxygen species production, *J. Biol. Chem.* 285, 31277-31284.
- (247) Papandreou, I., Cairns, R. A., Fontana, L., Lim, A. L., and Denko, N. C. (2006) HIF-1 mediates adaptation to hypoxia by actively downregulating mitochondrial oxygen consumption, *Cell Metab.* 3, 187-197.

- (248) Aras, S., Pak, O., Sommer, N., Finley, R., Jr., Huttemann, M., Weissmann, N., and Grossman, L. I. (2013) Oxygen-dependent expression of cytochrome c oxidase subunit 4-2 gene expression is mediated by transcription factors RBPJ, CXXC5 and CHCHD2, *Nucleic Acids Res.* 41, 2255-2266.
- (249) Seelan, R. S., Gopalakrishnan, L., Scarpulla, R. C., and Grossman, L. I. (1996) Cytochrome c oxidase subunit VIIa liver isoform. Characterization and identification of promoter elements in the bovine gene, *J. Biol. Chem.* 271, 2112-2120.
- (250) Lee, I., Huttemann, M., Liu, J., Grossman, L. I., and Malek, M. H. (2012) Deletion of heart-type cytochrome c oxidase subunit 7a1 impairs skeletal muscle angiogenesis and oxidative phosphorylation, *J. Physiol.* 590, 5231-5243.
- (251) Chen, Q., Vazquez, E. J., Moghaddas, S., Hoppel, C. L., and Lesnefsky, E. J. (2003) Production of reactive oxygen species by mitochondria: central role of complex III, *J. Biol. Chem.* 278, 36027-36031.